The Thesis Committee for Valerie Gono
Certifies that this is the approved version of the following thesis:

On Shaky Ground: Understanding the Correlation between Induced Seismicity and Wastewater Injection in the Fort Worth Basin

APPROVED BY
SUPERVISING COMMITTEE:

Supervisor:

Jon E. Olson

Loukas F. Kallivokas

On Shaky Ground: Understanding the Correlation between Induced Seismicity and Wastewater Injection in the Fort Worth Basin

by

Valerie Gono, B.A.; B.S.

Thesis

Presented to the Faculty of the Graduate School of

The University of Texas at Austin

in Partial Fulfillment

of the Requirements

for the Degree of

Master of Science in Engineering

The University of Texas at Austin

December 2015

Dedication

To Dr. Christopher Hart,

A mentor who instilled in me scientific curiosity,

And who believed in me all those years ago.

Without him I would not be where I am today.

Acknowledgements

First, I would like to thank my parents for all the support that they have given me throughout my academic career. Thank you for giving me the freedom to choose my field of study and for your blind faith that I will choose what is best for me.

Secondly, I would also like to thank Dr. Jon Olson for taking a chance on me by taking me on as one of his students. Thank you for all your support, without it, I would not have been able to finish this degree. Thank you for believing in me, and be the one responsible for making me fall in love with teaching. Your enthusiasm and support for your students are truly inspiring.

Thirdly, I would like to thank Dr. Julia Gale and Dr. Richard Schultz for all their guidance and encouragement throughout this process. Julia for the countless hours of discussion while I was trying to get a foothold on the topic; and Rich for all his help in trying to get me to be more organized. I am sure that I will be looking to the both of you for guidance and assistance sometime in the future.

Next, I would like to thank the Research Partnership to Secure Energy for America (RPSEA) for the funding that made this research possible. I would also like to thank the people at the Bureau of Economic Geology (BEG), David Smith and Qilong Fu in particular, for all their help in data gathering.

Furthermore, I would like to thank my office mates, Li Ji, Farrokh Sheibani, Kan Wu, Abdul Khan, Kashif Naseem, Hunjoo Lee, Weiwei Wang, Kaimin Yue, Javad Rashidi, Emad Alabbad, Nana Asiamah, Andreas Michael, and Mohsen Babazadeh for the countless hours of serious discussions and comic reliefs. Special thanks to Kashif for helping me with ECLIPSE, without his help, I would have never been able to start my research.

Additionally, I would like to thank KD, BL, and SP for the endless support and encouragement. Thank you for the countless hours of conversations that made me laugh and kept me going, and thank you all for your unwavering believe in me.

Lastly, to everyone who I cannot name individually that have helped and inspired me throughout this process; know that you all have my deepest gratitude.

Abstract

On Shaky Ground: Understanding the Correlation between Induced Seismicity and Wastewater Injection in the Fort Worth Basin

Valerie Gono, M.S.E.

The University of Texas at Austin, 2015

Supervisor: Jon E. Olson

Starting in the mid-2000s, there has been an increase in seismic activity around areas where wastewater injection was occurring in association with produced water from oil and gas development. As the rate of wastewater injection increased, so did occurrences of earthquakes in the surrounding area. There are, however, many injectors that do not spatially correlate with earthquakes, and the boundaries between safe and high risk practice have yet to be defined. The goal of the study is to understand both positive and negative correlations between seismic events and injection well locations by conducting fluid flow simulations and geomehcanical analysis.

In order to identify areas of injection with and without seismic activity, a reservoir simulation model was utilized using the Computer Modeling Group (CMG) Implicit Explicit Black Oil (IMEX) simulator for the Fort Worth Basin (FWB), including 374 wells with relevant data located in the following counties: Denton, Ellis, Erath, Hill, Hood, Jack, Johnson, Palo Pinto, Parker, Somervell, Tarrant and Wise. The model integrated formation and injection data. The formation data incorporated includes the

formation thickness and permeability; the injection data incorporated includes injection volume, time, and depth. Most of the high volume injection activities occurred in the Ellenburger formation; hence in-depth analysis of the results for the Ellenburger formation was performed. Simulation results showed that there are spatial and temporal correlations between earthquake events and areas of pore pressure increase in the Ellenburger. However, not all areas with elevated pore pressure are correlated with seismic activity.

Geomechanical analysis was performed by taking the pore pressure change results from the flow modeling and the in-situ stress data available in the literature as inputs. Earthquakes induced by wastewater injection would be predicted to occur in area where the simulated pore pressure increase met or exceeded the minimum frictional resistance of optimally oriented fault surface, given the absence of mapped faults in the area. The geomechanical strength limit for the location one of the earthquake events of interest, the DFW airport earthquakes, could be reached, however, by a 10x permeability reduction in the estimated permeability for the injection into the Ellenburger.

This research highlight the need to consider pore pressure changes, more precise earthquake locations, better estimate of the permeability values in the injection horizon, and a more accurate stress state and geomechanical strength criteria to reduce modeling uncertainty in order to better understand the correlation between induced seismicity and wastewater injection.

Table of Contents

List of Tables

List of Figures

Chapter 1: Introduction to Induced Seismicity and Wastewater Injection

1.1 MOTIVATION

Within the last few years, an increased number of earthquakes in the central and eastern United States (mostly magnitude range of 2 to 3) has occurred and has increased the visibility of induced seismic risk (Frohlich 2012b; Keranen et al. 2014; McGarr et al. 2015). The increase in number of earthquakes has been linked to oil and gas activities (Frohlich et al. 2010; Hornbach et al. 2015). One of the leading theories is that these seismic events are triggered by the increasing amount of wastewater injection, which is the result of increased produced water from oil and gas wells (Zoback 2012; Weingarten et al. 2015).

The seismic events that are continuing to occur across the central and eastern United States may not be of alarming magnitude yet, however, the sheer increase in frequency of these earthquakes has raised red flags to both operators and regulators. Regulators have begun implementing risk mitigation methods in response to the increase in induced seismicity. In Oklahoma and Kansas, the Oklahoma Corporation Commission's Oil and Gas Conservation Division (OGCD) and the Kansas Corporation Commission (KCC) respectively, have issued the "traffic light" system as a risk mitigation method (Baker 2015; KCC 2013). The "traffic light" system is a method to screen hazard and impact levels of injection wells (KCC 2013). Each well is categorize into either a green light, yellow light, or red light. Green light categorizes the well as having low hazard and impact with minimal to no seismic events recorded in the vicinity of the wells. In the case where seismic events were recorded, the magnitudes of the events were small and seismicity was not felt on the surface. Red light categorizes the well as having high hazard and impact with induced earthquake events that can be felt at

surface with possibility of distress and/or damage. When a well is categorized as red light, all injection activities must cease immediately. Yellow light categorization of the well means more assessment is needed for that particular well. Wells that are categorized as yellow light have induced earthquake events in their vicinity that were felt at the surface, but the magnitudes of the events were not damaging, hence further study needs to be performed and actions need to be taken in order to prevent the wells from being categorized as red light (KCC 2013).

In Texas, the Texas Railroad Commission (RRC), adopted new disposal well rule amendments at the end of 2014 (Texas RRC 2014). The new rules require new disposal injection well applicants to conduct seismic analysis within a radius of approximately 6 miles (10 km) of the new injection well locations. The new rules also give the RRC authority to modify and/or suspend injection permits if scientific data indicate that induced seismicity is likely. Furthermore, the RRC has the ability to request additional information to assess induced seismicity risk from permitted wells (Texas RRC 2014).

The increase in earthquake frequency can be further understood by examining data queried from the United State Geological Survey (USGS) National Earthquake Information Center (NEIC) database for the Fort Worth Basin in Texas (Figure 1.1). In the last seven years, the number of earthquake occurrences within the Fort Worth area has increased dramatically. From Figure 1.1, it can be seen that prior to 2008, there were only two earthquakes within the Fort Worth area in a 23-year span. Since 2008, however, there have been 164 earthquake events of magnitude 2 and larger, which is a significant increase in number of earthquake events. Furthermore, there is at least one event of magnitude 4 that has recently occurred in the area. An increase in earthquake frequency since 2008 was also evident in Oklahoma (Walsh & Zoback 2015). Based on the increased of earthquakes frequency of all magnitudes in Oklahoma, Walsh and Zoback

concluded that these earthquake events are correlated to injection of produced saltwater and are not an artifact from an increased availability of seismic monitoring equipment in the recent years. The same observation can also be made for the Fort Worth Basin. Examining earthquake events that occurred after 1995 in the Fort Worth area, it can be observed that between 1995 and 2008, there were no magnitude 3 or magnitude 4 events. However, since 2008, there have been 30 magnitude 3 events, and one magnitude 4 event. In the last 20 years, the likelihood of missing magnitude 3 and magnitude 4 events in Texas is negligible (Coppersmith et al. 2012). Hence, the evidence suggests that the recent earthquake events in the Fort Worth area are related to injection of produced saltwater and not due to the increase of seismic monitoring equipment in the region.

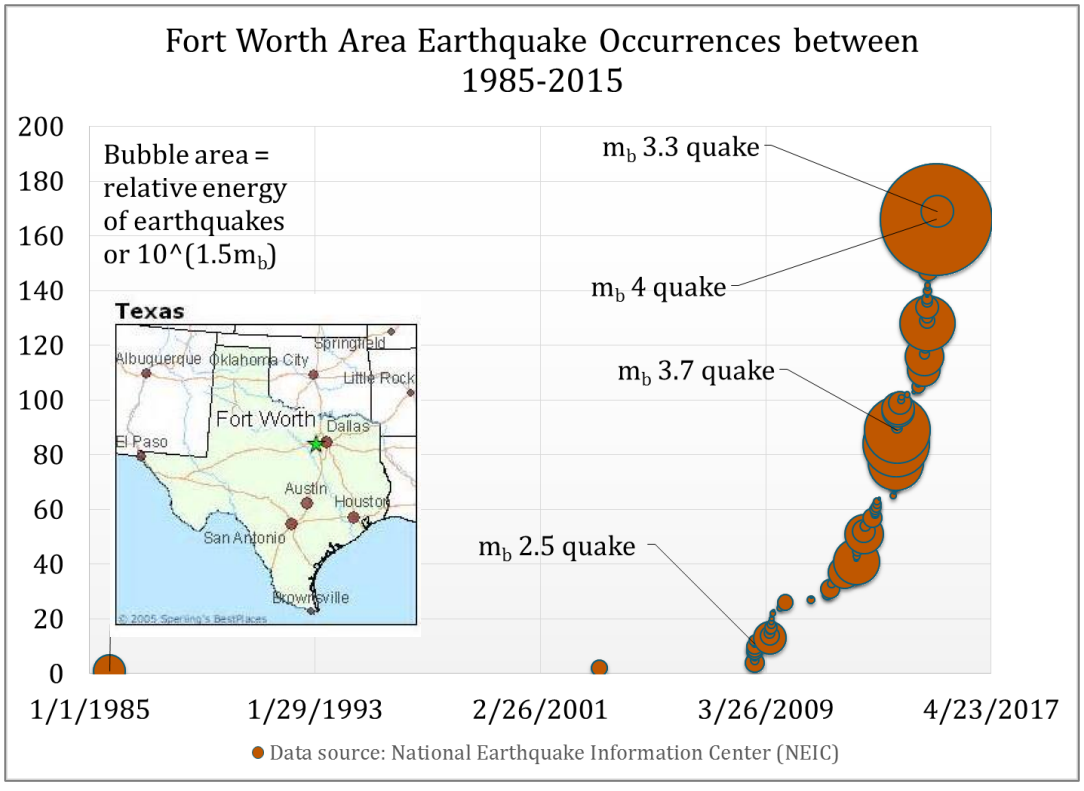

Figure 1.1: Fort Worth area earthquake occurrences between 1985 - 2015.

Over the years, many studies have been done to correlate the location of the earthquakes to their proximity to injection wells in the Fort Worth Basin (Frohlich 2012b; Justinic et al. 2013). These studies concluded that there are spatial and temporal correlation between earthquakes and injection wells and that there is a possibility that the earthquake events were induced by wastewater injection. However, since no pore pressure modeling was performed, no geomechanical correlation can be determined from these studies. Pore pressure modeling provides input data required for in-depth geomechanical analysis to better understand whether the earthquake events were induced by wastewater injection.

In Figure 1.2, the map-view locations of earthquakes were plotted together with the locations of injection wells. The bubble plots show the magnitude of the earthquakes, the maximum rates of the injection wells, and the location of cities in the Fort Worth Basin. From the figure, it can be seen that in some cases, such as the wells located northwest of Cleburne, wells with larger maximum injection rates qualitatively correlate spatially to larger magnitude earthquakes. However, in some other wells, such as the ones located to the northwest of Dallas and northwest of Weatherford, this is not the case. The large magnitude earthquakes are not spatially correlated to the larger maximum injection rate. As can be observed, correlation between maximum injection rates and earthquake magnitudes are difficult to categorize without further analysis.

In recent years, in-depth pore pressure simulations have been performed to correlate fluid injection and seismic events on a localized scale after unexpected seismic events have occurred (Keranen et al. 2014; Hornbach et al. 2015). In this work, the scope of the study is expanded and a basin-wide model of wastewater injection for the Fort Worth Basin is developed in order to gain a better understanding of how pore pressure increase on a basin-wide scale may affect seismicity. The goal is to understand both

positive and negative correlation between earthquakes and injection wells. Furthermore, the areal extent of the pore pressure front is also of interest, since there is a possibility that the pore pressure front will extent farther than the region in the proximity of the injection well (Shapiro et al. 2006). Understanding the areal extent and the magnitude of pore pressure response from fluid injection is a key factor in correlating induced seismicity and wastewater injection.

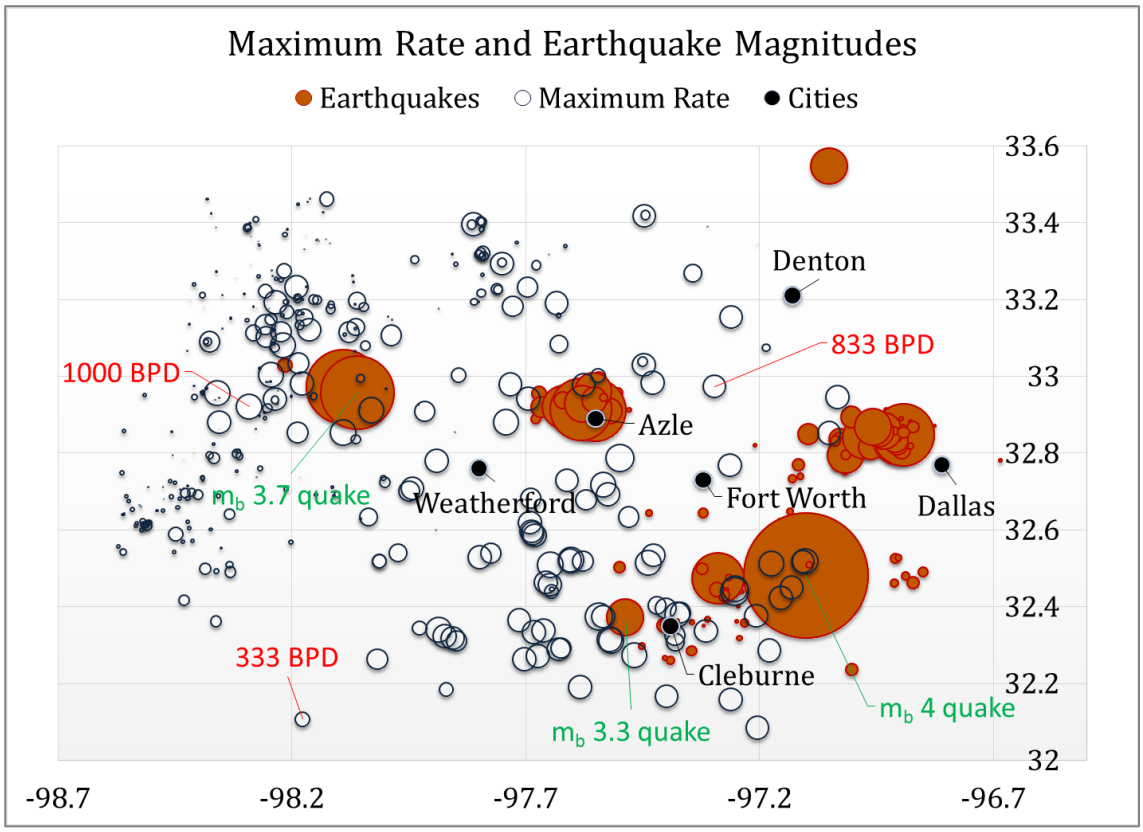

Figure 1.2: Correlation between maximum injection rates and earthquake magnitudes.

1.2 Background on Induced Seismicity

The correlation between wastewater injection and induced seismicity has been studied extensively since the 1960s (Healy et al. 1968; Raleigh et al. 1976; Hsieh &

Bredehoeft 1981). The physics behind injection-induced seismicity is reasonably well understood, yet this does not yet permit accurate predictions on the timing of seismic events post-injection.

One of the first studies on induced seismicity due to fluid injection was performed on the Denver earthquakes that occurred in the 1960's. These events were interpreted to have been caused by injection into a deep disposal well at the Rocky Mountain Arsenal (RMA) (Healy et al., 1968). The disposal well was completed in 1961 for the United States Army at the depth of approximately 11,800 ft (3.60 km) (Healy et al. 1968). It was used to dispose of fluid wastes from chemical-manufacturing operations. Injection continued intermittently for 5 years between 1962 and 1967, and in that period of time, 35 earthquakes with a body wave magnitude (m_b) of 3 and larger were observed (Healy et al. 1968). One key observation from the RMA sequence was that during the period where injection ceased, earthquakes continued to occur, albeit at a lower frequency than when injection was occurring.

In 1969, an experiment was conducted in Rangely, Colorado to test the hypothesis that the RMA earthquake sequence was triggered by the increase of fluid pressure, and hence may also be controllable (Raleigh et al. 1976). The experiment conducted in the Rangely Oil Field was designed such that there were on and off periods of injection throughout the duration of experiment. As a result, the experiment showed that it is possible to control earthquake events that are induced by fluid injection (Raleigh et al. 1976). From the experiment it was shown that fluid pressure plays a crucial role in inducing seismic events, since an increase in pore pressure is needed to trigger slip in faults which in turn cause the earthquake events.

A sequence of induced earthquakes was also observed in Cogdell Oil Field in west Texas from 1974 to 1982 (Davis & Pennington 1989). The largest earthquake that

occurred was of m_b 4.3. Furthermore, there was a delay between the start of injection and the onset of the earthquake sequence. Davis and Pennington examined the sequence and built models under different constraints to determine whether seismic failure would occur under the history of fluid pressure in the field. Their work concluded that the earthquake sequence was induced due to the combination of both high fluid pressure and stress loading from injection-induced failure. Furthermore, they concluded that on sites where earthquake should have occurred but didn't, failure was either aseismic or the seismic events were of inconsequential magnitudes (Davis & Pennington 1989).

In 1993, Davis and Frohlich published a paper on profiling seismic sequences (Davis & Frohlich 1993). The paper presented two lists of yes-no questions that would help determine whether or not the current deep-well injection regime has caused earthquakes, or if a proposed deep-well injection project will cause earthquakes (Davis & Frohlich 1993). This qualitative analysis provided an easy checklist-type method to assess any correlation between induced seismicity and injection well.

Within the last decade, the discovery and exploitation of shale gas and tight oil reservoirs necessitated mass adoption of hydraulic fracturing across the oil and gas industry, which led to an increase in the production of wastewater and as a result, it increased the amount of wastewater injected into wells (Zoback 2012). In the last five years, much work have been done with regards to earthquake sequences and their proximity to injection wells (Kim 2013; Justinic et al. 2013; Frohlich 2012a; Keranen et al. 2014; Hornbach et al. 2015). All of the current work concluded that the earthquake sequences that occurred could potentially be induced by fluid injection. While many positive correlation studies have been performed, no negative correlation study has been done. This is because areas of no earthquake events are not the focus of spatial and temporal correlation studies between earthquake events and injection wells. In this study,

pore pressure modeling was performed, and negative correlation can be made and will provide further insights into the state of the basin.

While studies correlating induced seismicity and injection wells have been ongoing in the scientific community for over 50 years, however, it has yet to attract much of the public's attention until recently. In the past couple of years, more and more prominent newspapers and magazines, such as The New York Times, The Los Angeles Times, and the New Yorker began covering the issue (Perez-Pena 2015; Lin II et al. 2015; Galchen 2015). With the recent surge of earthquake events in areas that historically have little to no seismicity, the amount of research performed by the state geological surveys (especially in states where oil and gas is a big part of the economy) has increased drastically. With the increase of interest in understanding induced seismicity, it is hopeful that there will be more studies performed and data gather to build more robust and realistic models. Some of the important information needed to fully understand the seismic response due to wastewater injection include detailed formation permeability and porosity data, and knowing the in-situ stress state in the areas of interest.

1.3 Background on Wastewater Injection

Injection of any fluid into the ground in the United States is regulated by the Environmental Protection Agency (EPA). The EPA's Underground Injection Control (UIC) program categorizes fluid injection into seven different classes. All wells disposing of wastewater from oil and gas production are classified and regulated as Class II injection wells (Environmental Protection Agency 2015). According to the EPA inventory, there are currently a total of 172,068 Class II injection wells across the United States (Environmental Protection Agency 2015).

The main purpose of the UIC program is to protect underground sources of drinking water (USDWs) from contamination; as such, the EPA has published a code of federal regulation on construction requirements for Class II injection wells under Title 40, Part 146, Subpart C, Section 146.22. Furthermore, Section 146.22 part g) under EPA's federal regulation also required the determination of the following for the injection formation: fluid pressure, estimated fracture pressure, and physical and chemical characteristics of the injection zone. While this information is required to be collected and reported, almost all operators requested the agency to withhold the information from being publicly disclosed citing it as proprietary information.

In terms operation of Class II injection wells, under Title 40, Part 146, Subpart C, Section 146.23 part b) dictates that the minimum requirements should include weekly monitoring of injection pressure, flow rate, and cumulative volume for fluid disposal operations. However, Section 146.23 part (c) only requires annual reporting of monthly records of the required monitoring for fluid disposal operations.

Wastewater injected into Class II injection wells is the produced water that is the byproduct of oil and gas production. In general, for every barrel of oil produced, 7.5 – 15 barrels of water are also produced (Kemp 2014; Grinberg 2014). A 2009 report from Argonne National Laboratory estimated that the annual United States produced wastewater volume is between 15 to 20 billion barrels (Clark & Veil 2009). In 2007, the five states with the greatest produced wastewater volumes were Texas, California, Wyoming, Oklahoma, and Kansas (Figure 1.3).

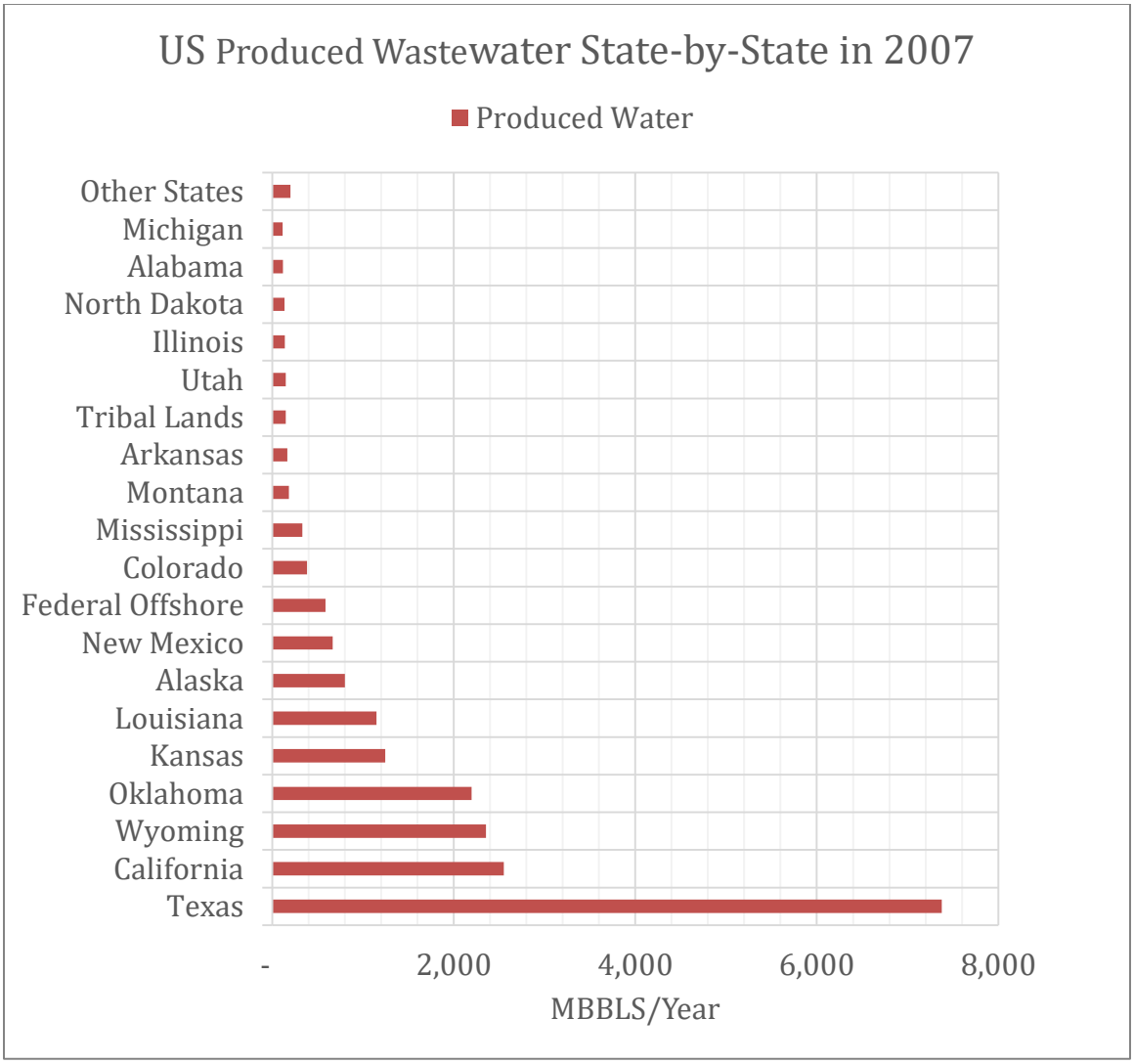

Figure 1.3: US produced water state-by-state in 2007, data from Argonne National Laboratories (Clark & Veil 2009).

Furthermore, from Figure 1.3, the total produced water for each oil and gas producing state can be observed. Texas, California, and Wyoming are the three states with the highest produced water. The most common method to discard of produced wastewater is by injection for enhanced oil recovery (EOR), injection for disposal, and surface discharge (Clark & Veil 2009).

From Figure 1.4, it can be seen that most of the produced wastewater in 2007 was reinjected for enhanced oil recovery, and approximately a third of the total produced wastewater was injected into Class II disposal wells. 80% of the produced wastewater discarded through the surface discharge method was from the Federal Offshore production.

Even though the EPA regulates the Class II disposal wells on a federal level, each state determine its own requirements for operating, monitoring, and reporting of injection wells that has to, at the very least, fall within the minimum regulation set forth by the EPA. In Texas, for example, oil and gas activities are regulated by the Railroad Commission of Texas (RRC) on the state level. The RRC further categorize injection wells into two categories, disposal into a non-productive zone (W-14) and disposal into a productive zone (H-1). On the application to dispose into either a productive zone or a non-productive zone, the information required are different. For example, in the permitting of H-1 wells, information of the average horizontal permeability and porosity are required. These information are not required in the permitting of W-14 wells.

Furthermore, in addition to providing general information on the type of fluid to be injected into the disposal wells, the RRC also require operators to specify the source of each type of wastewater by formation or depths. It should be noted however, the specifics of disposal well permitting differ from state to state.

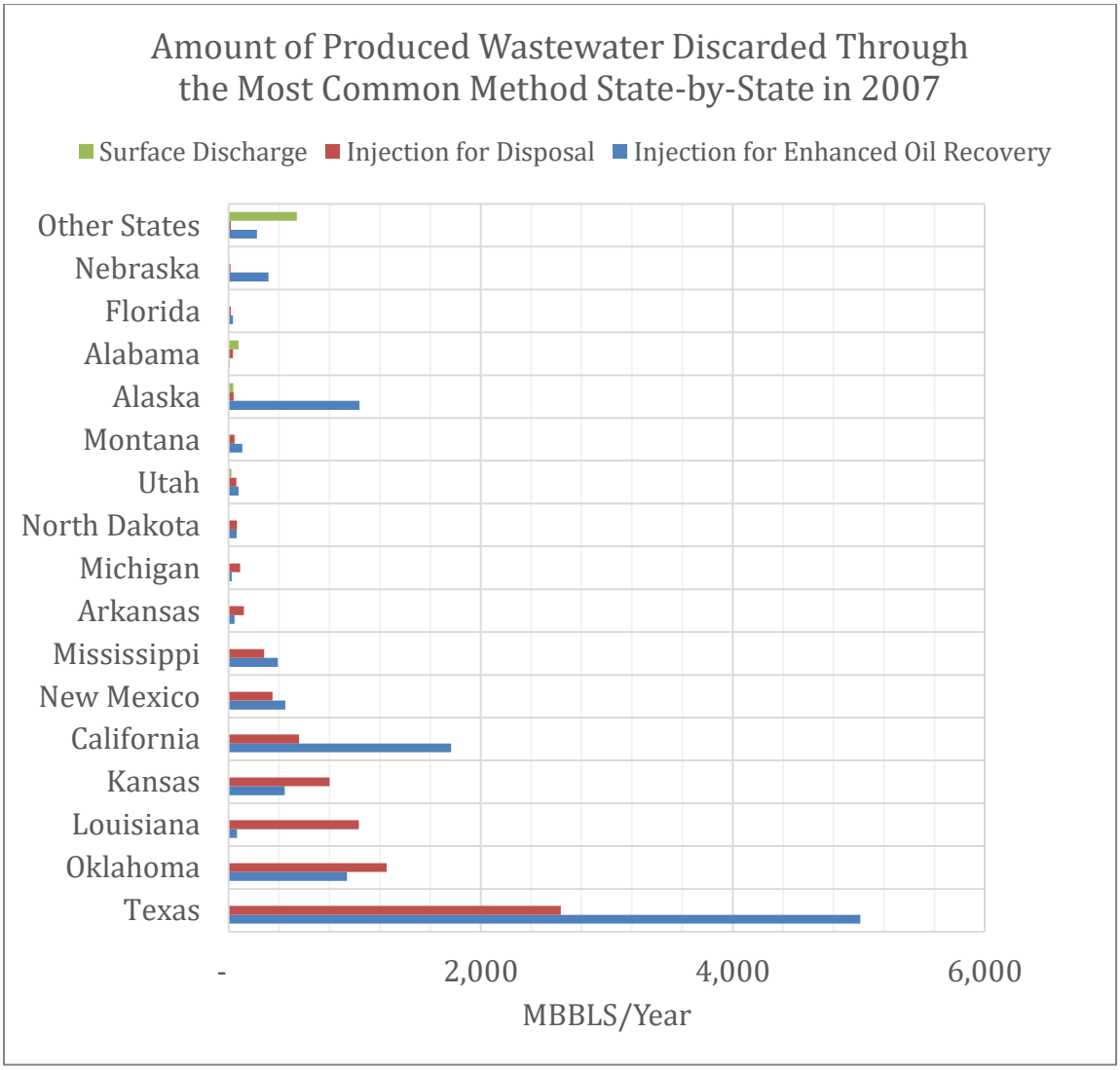

Figure 1.4: Amount of produced wastewater discarded through the three most common method state-by-state in 2007, data from Argonne National Laboratories (Clark & Veil 2009).

Chapter 2: Modeling Method and Data Sources

Most studies in the literature of induced seismicity have focused on single wells or small regions. Here we have undertaken a basin-wide simulation study of the pore pressure response of injection wells, in order to assess both positive and negative correlations between seismic events and injectors. We hope this approach will better illuminate the risk factors controlling the likelihood of induced earthquakes.

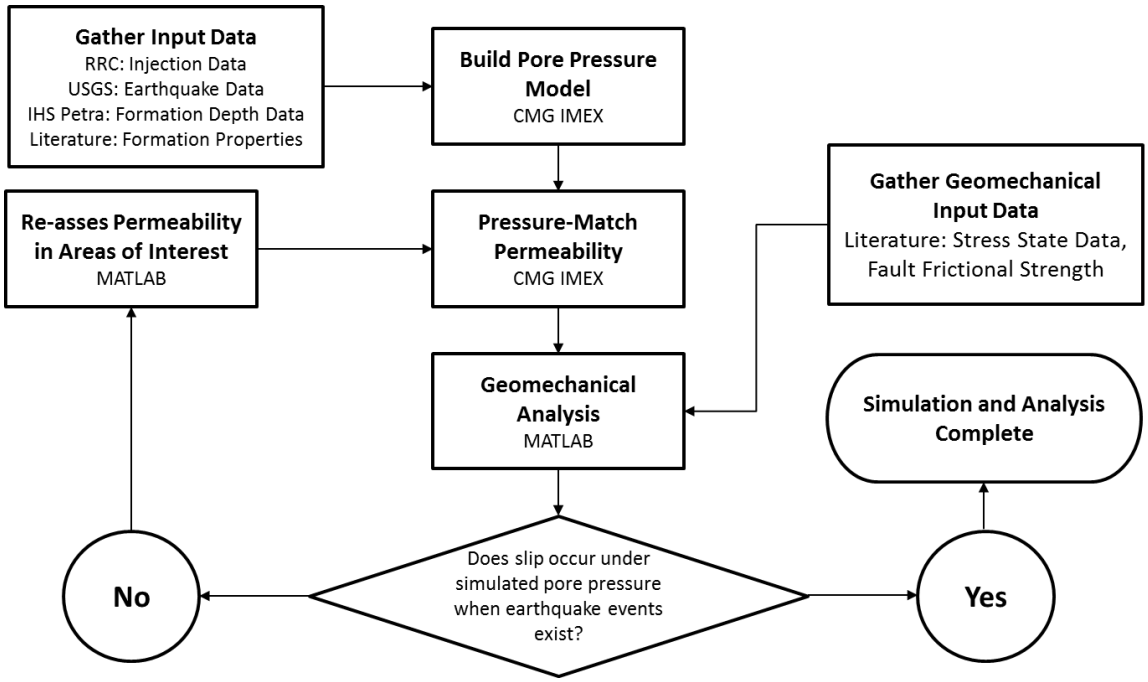

Figure 2.1: Workflow diagram of simulation.

In this study, a pore pressure model was built using commercial reservoir simulation software distributed by Computer Modeling Group (CMG). For the pore pressure simulation, the input data needed was injection data and formation data. Earthquake data is needed for the analysis of the pore pressure simulation results. A further constraint of layer permeability was determined by comparing the simulated and observed wellbore pressure responses. The history-matched reservoir simulations were

then used as input data for geomechanical analysis. Furthermore, stress state and fault friction data from the literature provided additional input values in the geomechanical analysis. A detailed simulation workflow is shown in Figure 2..

2.1 PORE PRESSURE SIMULATION DOMAIN

Simulations were performed using CMG's Implicit Explicit Black Oil (IMEX) finite difference simulator to understand pore pressure disturbances in the Fort Worth Basin due to wastewater injection. The area of interest consists of 12 counties: Denton, Ellis, Erath, Hill, Hood, Jack, Johnson, Palo Pinto, Parker, Somervell, Tarrant, and Wise. The region is bounded by the following structural elements: on the west, the Bend Arch; on the north, the Red River and Muenster Arches; and on the east, the Ouachita Thrust (Pollastro et al. 2003).

The areal extent is approximately 130 miles by 125 miles with variable depths up to 14,000 ft (4.27 km) thick. Using a Cartesian coordinate system, there were 342 cells at 2,000 ft (0.61 km) spacing in the x-direction, 330 cells at 2,000 ft (0.61 km) spacing in the y-direction, and 9 layers of variable thicknesses in the z-direction. Injection began in December 1997 and continued for approximately 16.5 years (199 time steps). The discretized well placement map can be seen in Figure 1.1. The initial pressure in this study was assumed to be hydrostatic at 0.433 psi/ft (9.79 MPa/km) (Townend & Zoback 2000; Bowker 2007). Hydrostatic initial pore pressure was chosen since no detailed pore pressure study was available for the various layers in the basin.

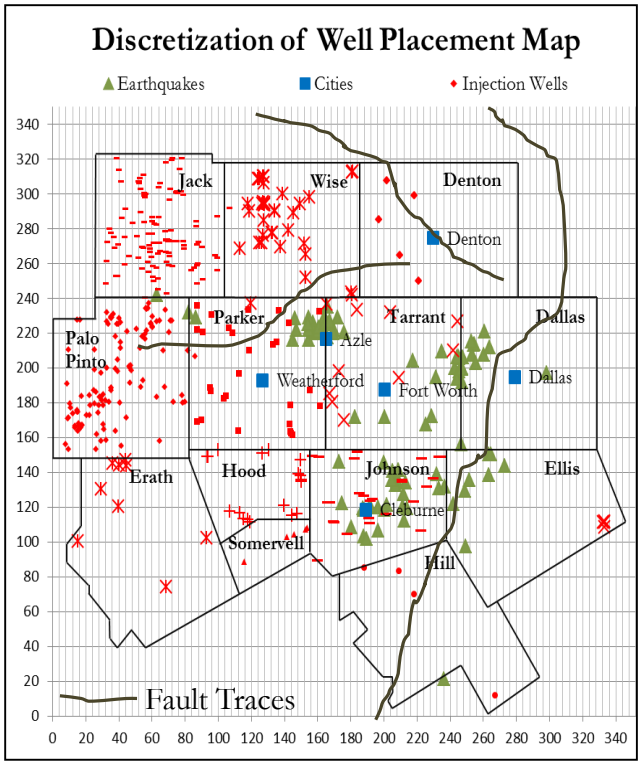

Figure 2.2: Discretized well placement map.

2.2 Data Sources

The accuracy of the simulation results is dependent on the quality of the data used in building the model. All the data used in the simulation has been acquired through public access or through subscription to a database catalogue. The stress state data has been compiled from the literature. The description of the data used in the simulation as well as the data sources are explained in detail in the following subsections.

2.2.1 Formation Data

Formation tops data was used to constrain the vertical height of the model for the different layers. The data tops for the Strawn, Marble Falls, Barnett, and Ellenburger formations were queried from IHS Petra[1]. As can be seen from Figure 2.3, most of the

[1] https://www.ihs.com/products/petra-geological-analysis.html

formation tops are concentrated in the middle part of the basin. To encompass the outer reaches of the simulation area, the available data was extrapolated. The tops for the Strawn, Marble Falls, Barnett, and Ellenburger formations correspond to the top of layers 2, 4, 6, and 8, respectively. The top of layer 1 is taken to be 0 ft, and the tops of layer 3, 5, and 7 are computed by taking the average between the two layers that sandwich the odd-numbered layers. Furthermore, layer 9 was assumed to be 4,000 ft (1.22 km) thick below layer 8 (McDonnell et al. 2007).

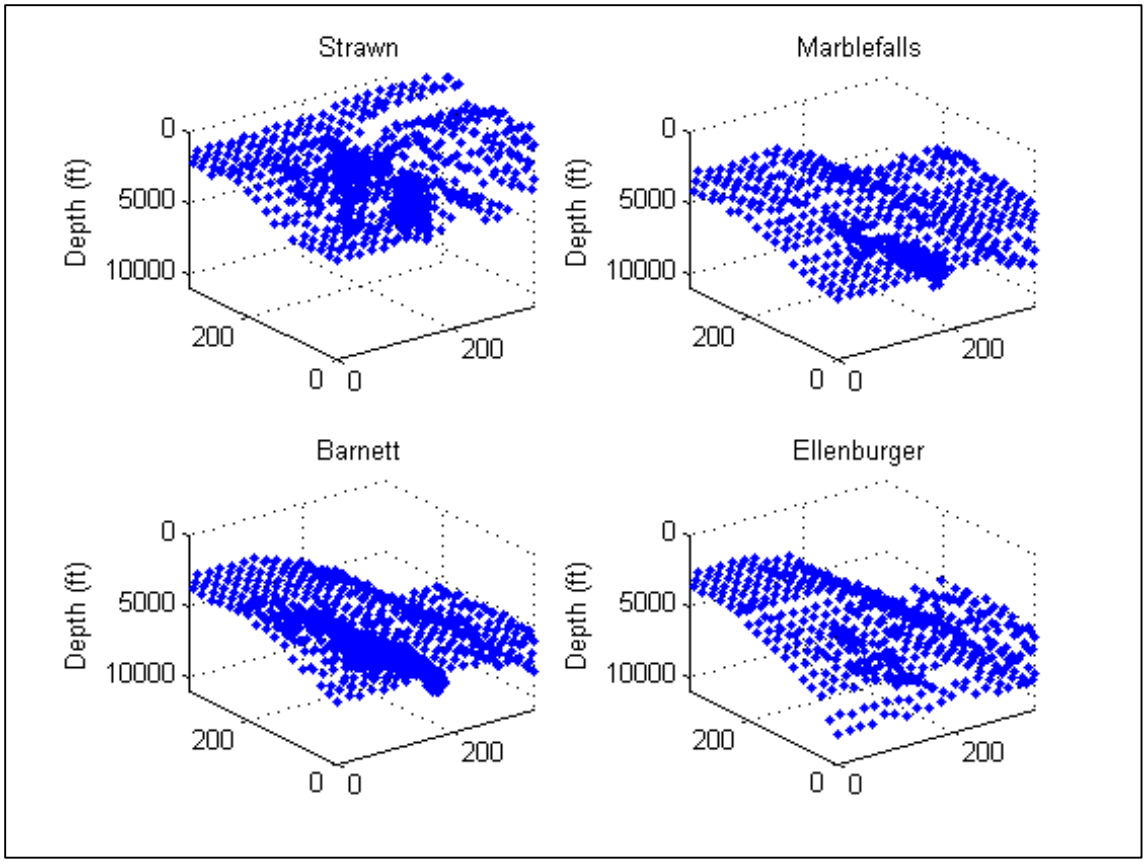

Figure 2.3: IHS Petra extrapolated formation tops data.

Once the region was populated with tops from the well data, the surface was smoothed using the cubic spline method (Figure 2.4) (The Mathworks, Inc. 2013). The

formation tops increased in depth as they move from the western part of the basin to the eastern part of the basin. These steep changes in depth are especially prominent in the Barnett and Ellenburger formations, which is consistent with published structure contour maps (Pollastro et al. 2007).

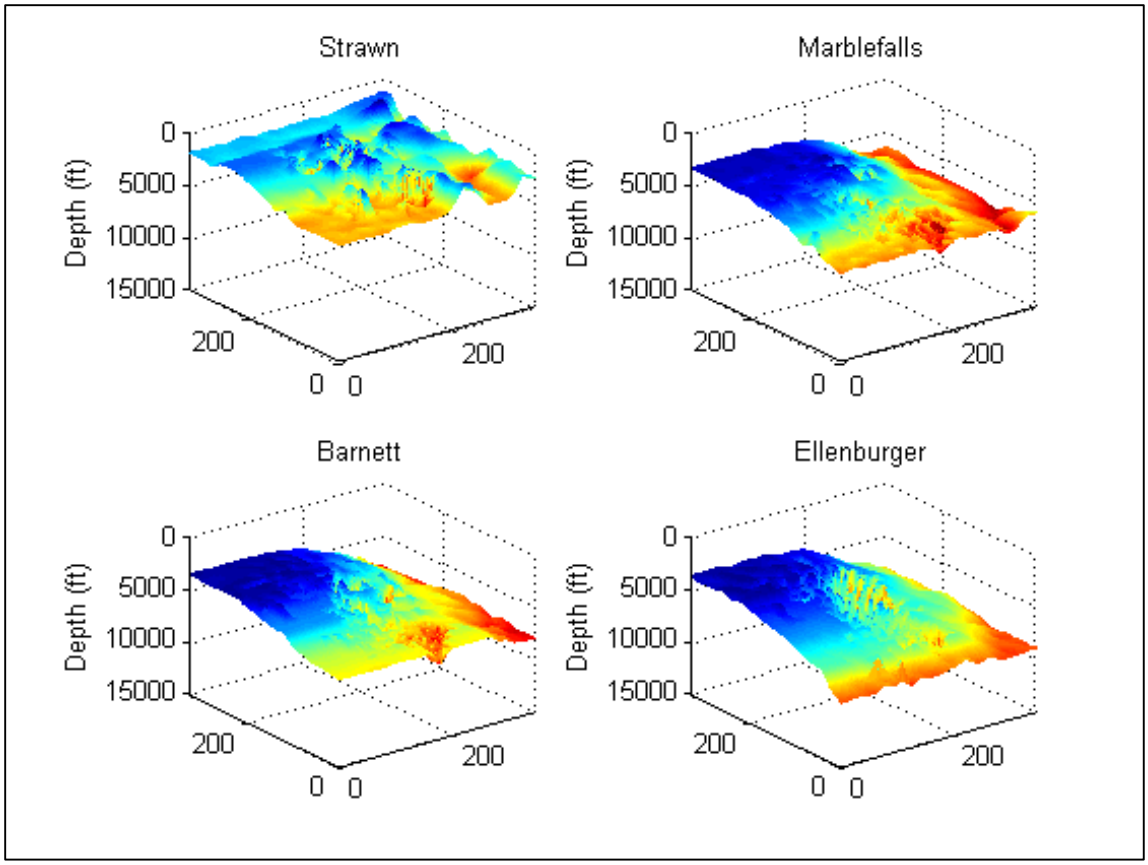

Figure 2.4: Interpolated formation tops utilizing the cubic spline interpolation method.

2.2.4 Seismic Data

Seismic data was compiled from the United States Geological Survey (USGS) National Earthquake Information Center (NEIC) database[2] for the region bounded by the coordinates N = 34º, S = 31.467º, E = -96.354º, and W = -98.625º. The associated data

[2] http://earthquake.usgs.gov/earthquakes/search/

available for each earthquake event included the date, latitude, longitude, and magnitude (Figure 1.1). The magnitude of these earthquakes in relation to their locations can be seen in Figure 1.2, while the temporal correlation of the earthquakes magnitude can be observed in Figure 1.1.

2.2.3 Injection Data

The wastewater injection data was queried from the Railroad Commission of Texas (RRC). For the wells located in the area of interest, the following information was obtained: well locations[3], injection depths[3], injection volumes[4], and injection pressures[5].

The well locations and injection depths were queried by the counties using the Injection & Disposal Query[3] form by the county. Each injection well in the RRC database was given an American Petroleum Institute (API) well number and an Underground Injection Control (UIC) number. The API number is unique to each well and is used as a numerical identifier of the well, while the UIC number is a unique number issued for a specific well each time an injection permit is issued for the well. Hence, it is possible for one API number to be associated with multiple UIC numbers, for example, if multiple injection permits have been issued over the years. The well API and UIC numbers are the identifiers in the Injection & Disposal Query.

The injection volume for each well was queried using the UIC number in the H10 Injection Volume Query. The H10 Injection Volume Query can also be used to query total injection volumes for a specific county, a specific district, or a specific injection category (W–14 or H–1).

---

[3] http://webapps2.rrc.state.tx.us/EWA/uicQueryAction.do

[4] http://webapps.rrc.state.tx.us/H10/searchVolume.do;jsessionid=DwynW1Fp28Qx145vwbK91LL2N1jxPQ2xR1VK8LwFxyRMqTTlmcsL!-936114876?fromMain=yes&sessionId=144636447836735

[5] http://webapps.rrc.state.tx.us/H10/searchH10.do?fromMain=yes&sessionId=144636553474136

The injection pressure for each well was queried using either the API or the UIC number in the Search for H10s Query. The pressure data is available through the operator submitted H10 forms in Hypertext Markup Language (HTML) format.

In general, the operator of the wells is required to submit injection data on a yearly basis, and depending on the original month the well was permitted, the updated injection data may not be available until the end of a specific calendar year.

2.2.4 Layer Permeability and Porosity

The permeability and porosity for each layer is based on published data. When no permeability and porosity data is available, an average between the known values was taken to represent the unknown values. Vertical permeability was assumed to be 0.1 of the horizontal permeability value (Kasap 2001; Elfenbein et al. 2005) The permeability and porosity values can be seen in Table 2.1.

In Table 2.1, permeability for layer 8 is listed as variable in both the horizontal and vertical direction. The permeability in layer 8 was pressure-matched by comparing the injection pressure available through the RRC and the pressure response from the simulation result. The reason behind pressure matching the permeability for layer 8 was because, out of all of the injected layers, layer 8 has the highest number of wells injecting into it. There are 62 wells injecting into layer 8 at various time steps during the injection period. Furthermore, based on preliminary modeling, the pressure differential is greatest in layer 8.

Layer	k_{horiz} (mD)	k_{vert} (mD)	Porosity
1	75 (Ball & Perry 1990)	7.5	0.20 (Ball & Perry 1990)
2	40	4.0	0.13
3	1 (Herkommer & Denke 1982)	0.1	0.05 (Hentz et al. 2012)
4	5	0.5	0.07
5	9 (Pollastro et al. 2007)	0.9	0.06 (Fu et al. 2015)
6	13	1.3	0.11
7	16 (Holtz & Kerans 1992)	1.6	0.09 (Holtz & Kerans 1992)
8	Variable	Variable	0.07
9	0.001 (Hornbach et al. 2015)	0.0001	0.09 (Holtz & Kerans 1992)

Table 2.1: Layer permeability and porosity.

From the 62 wells injecting into layer 8, simulated pressure data from 39 wells were matched to within an average of 10% of the actual pressure data. An example of the pressure-matching plot can be seen in Figure 2.5. The blue curve is the recorded surface

injection pressure data queried from the RRC, and the red curve is the surface pressure for a simulated average layer-permeability that best matched the recorded data. The pressure matching plots for all individual wells are presented in Appendix A. The individual well's permeability data was grouped by counties, averaged, and assigned as indicated in Figure 2.6. For counties with no injection activities, the average permeability of the whole layer, 29.64 mD, was used. Except for Jack and Wise counties, the average permeability for the rest of the counties is within 15% of the average permeability of the whole layer.

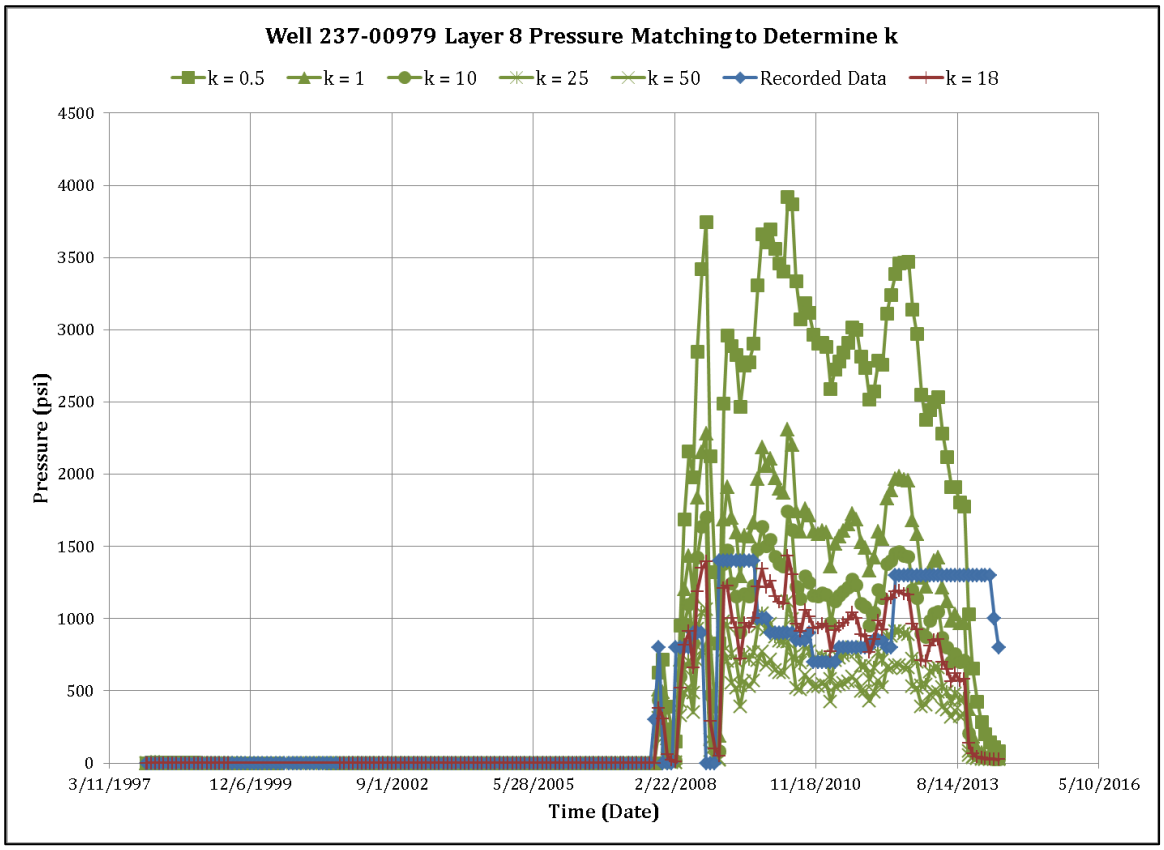

Figure 2.5: Example of pressure matching to determine permeability at a specific well.

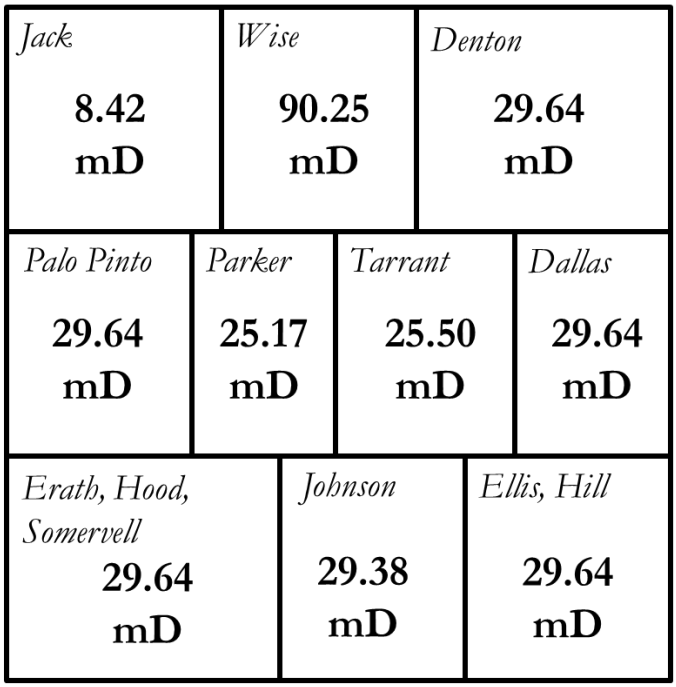

Figure 2.6: Pressure-matched permeability of layer 8 assigned by counties.

2.2.5 Ellenburger Stress State

As previously mentioned, based on the preliminary fluid flow modeling result, the maximum pore pressure changes occurred in layer 8, which corresponds to the Ellenburger formation. In order to perform geomechanical analysis to correlate the area of increased pore pressure and the possibility of fault slip associated with it, an in-depth understanding of the geologic setting of the Ellenburger formation is needed.

The Ellenburger formation in the Fort Worth Basin has depths ranging between approximately 4,000 ft (1.22 km) and 10,000 ft (3.05 km). The lithology primarily consists of dolomitic limestone (Herkommer & Denke, 1982), which is karst-modified in some sections (Baruch et al. 2012). Karst-modified areas were observed in the southwest corner of Parker County, and are surrounded by circular fault systems on top of the Ellenburger group (Baruch et al. 2012). While this is true locally, seismic mapping has

confirmed that the faults in the Ellenburger and the Precambrian Group below it are generally trending northeast-southwest (Elebiju et al. 2010).

From seismic analysis, it was shown that for the Ellenburger Group, the maximum horizontal stress is oriented northeast-southwest at 045°, while the minimum horizontal stress, S_{hmin}, trends northwest-southeast (Baruch et al. 2008). Furthermore, the Ellenburger formation is under the normal faulting stress regime (Baruch et al. 2008). Since no log data was available for the analysis of stress state, values for the stress gradients were obtained from the literature, and were assumed to be isotropic throughout the Ellenburger formation in the basin. A gradient of 0.84 psi/ft (19.00 MPa/km) was used for S_{hmin} (Waters et al. 2011). Based on a log analysis performed on a well in Somervell County, a gradient of 1.1 psi/ft (24.88 MPa/km) was used for the vertical stress, S_v, and the calibrated maximum horizontal stress, S_{Hmax}, is very close to the value of the vertical stress (Rathje & Olson 2007). For the purpose of this study, a gradient of 1.05 psi/ft (23.75 MPa/km) was used for S_{Hmax} (Rathje & Olson 2007). It should be noted, however, that the value of S_{Hmax} is not used in the geomechanical analysis, since the Ellenburger formation is under the normal faulting stress regime (Baruch et al. 2008).

2.3 GEOMECHANICAL ANALYSIS

In addition to understanding how pore pressure changes, an understanding of the geomechanical limit to injection pressures is an integral part in understanding how seismicity may be induced through wastewater injection. Earthquakes can be induced during fluid injection if an increase in pore pressure reduces the effective confining stress sufficiently to allow frictional sliding on pre-existing faults (Miller et al. 1996; Hubbert & Rubey 1959). The Mohr-Coulomb Failure Criterion can be utilized to understand the

mechanics of induced seismicity. The Mohr – Coulomb failure envelope is given by the following equation (Healy et al. 1968) and is presented below.

$$\tau = \tau_o + \mu\sigma_n \tag{2.1}$$

where τ is the shear stress, τ_o is the fracture cohesion, μ is the coefficient of friction, and σ_n is the normal stress. A Mohr circle for the Mohr-Coulomb failure criterion can be seen in Figure 2.7.

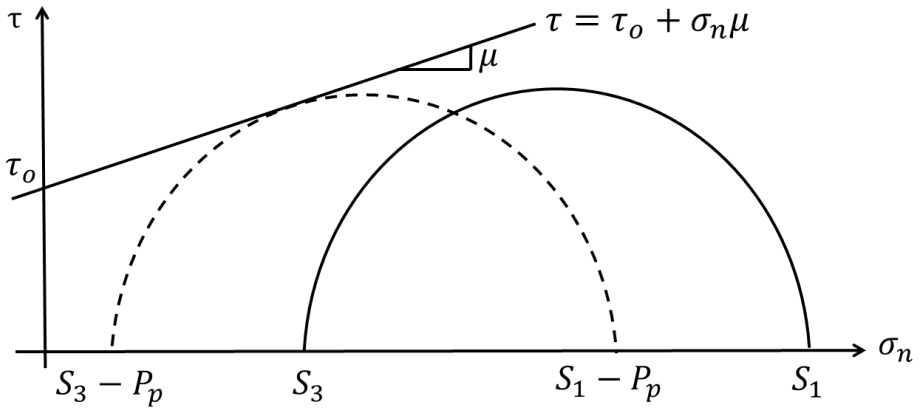

Figure 2.7: Mohr circle for general Mohr-Coulomb failure criterion.

For pre-existing faults, the fracture cohesion, τ_o, at the fault plane is taken to be zero (Zoback & Healy 1984), and therefore the failure criterion is simplified to be the following (Zoback 2007).

$$\tau = \mu\sigma_n \tag{2.2}$$

Due to the limited amount of fault data on the Ellenburger formation and the pre-Cambrian basement in the Fort Worth Basin, geomechanical analysis was performed under the assumption that the faults are critically oriented. Critically oriented faults are faults with strike that is parallel to the maximum horizontal stress, S_{Hmax}, and have a dip angle of 60°, therefore a lower pore pressure limit is required for fault slip (Zoback 2007). When the faults become more unfavorably oriented, the pore pressure required to

cause fault slip will increase (Zoback 2007). Since no in-situ stress data is available for the basement, the in-situ stress data from the Ellenburger formation is extrapolated downwards and used for the geomechanical analysis of the basement. Based on these assumptions, for favorably oriented faults, the frictional limit is given by the following equation for a normal faulting regime (Zoback 2007).

$$\frac{S_v - P_p}{S_{hmin} - P_p} \leq \left[(\mu^2 + 1)^{\frac{1}{2}} + \mu\right]^2 \tag{2.3}$$

The coefficient of friction, μ, for relatively deep wells with crystalline rock ranges between 0.6 and 1.0 (Zoback & Townend 2001). Using the lower limit of μ = 0.6, Equation 2.3 simplifies to

$$\frac{S_v - P_p}{S_{hmin} - P_p} \leq 3.12 \tag{2.4}$$

Based on the simplified equation, and given the vertical stress and the minimum horizontal stress, the pore pressure change from the initial pore pressure needed to slip the fault can be determined. Geomechanical analysis helps to build a better understanding of induced seismicity by giving an explanation for why pre-existing faults may or may not slip based on the results from the pore pressure simulation. If the pore pressure result from the simulation were below the initial pore pressure needed to slip the fault, then no earthquake event would be triggered. However, if the pore pressure result from the simulation is above the initial pore pressure needed to slip the fault, then earthquake events should be observed. The results and analysis for this study are presented in the next chapter.

Chapter 3: Results and Discussions

3.1 Pore Pressure Modeling

The three main areas of interest where earthquake swarms have occurred in the Fort Worth Basin are highlighted by different color circles in Figure 3.1. The first area is the Dallas Fort-Worth (DFW) Airport marked by the red circle. The DFW Airport earthquake swarm occurred in November 2008. In 2011, Frohlich et al. performed a spatial and temporal correlation study between the earthquakes and wastewater injection. They concluded that it is likely that the DFW Airport earthquake sequence was induced by fluid injection.

The second area of interest is located in Cleburne and is marked by the green circle in Figure 3.1. The Cleburne earthquake swarm occurred between June and August 2012. An earlier earthquake cluster that occurred in the area from June 2009 to June 2010 was previously studied by Justinic et al. (2013). Similar to the study performed by Frohlich et al. (2011) on the DFW Airport earthquakes, Justinic et al. performed spatial and temporal correlation between earthquakes and wastewater injection, and concluded that the earthquake swarm that occurred was also likely to have been induced by fluid injection.

The third area of interest is located in Azle and is marked by the blue circle in Figure 3.1. The Azle earthquake swarm occurred between November 2013 and January 2014. The earthquake swarm was previously studied by Hornbach et al. (2015). They were the first to have included pore pressure modeling into a spatial and temporal correlation study. From their study, Hornbach et al. concluded that the Azle earthquake swarm was likely induced by not only wastewater injection, but also oil and gas production activities that occurred adjacent to a fault in the region.

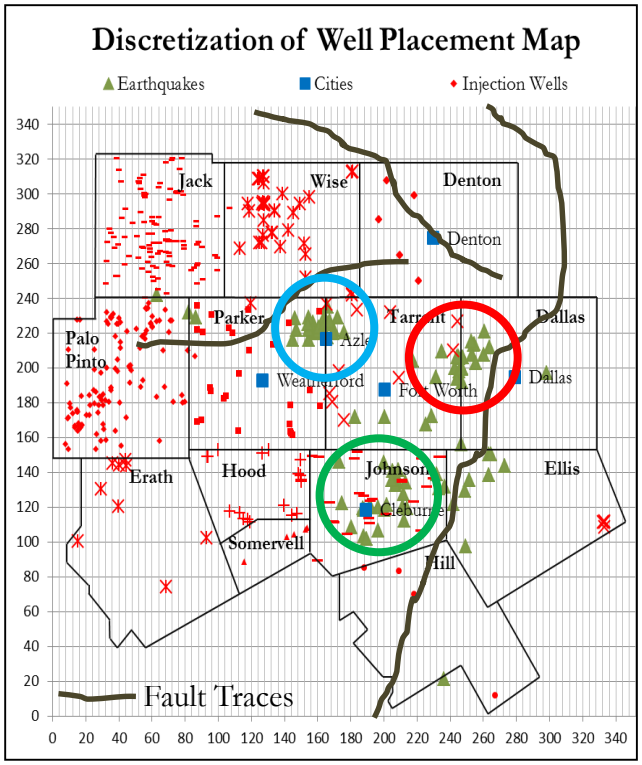

Figure 3.1: Areas of interest where clusters of earthquakes occurred.

Simulation results and discussions of the studies performed on the three areas of interest are presented in the following subchapters. Simulation results for the layers associated with the Ellenburger formation (layer 7 & 8) are presented and discussed in detail in the following subchapters. Other works (Keranen et al. 2014; Hornbach et al. 2015) suggested that a modest pore pressure increase (within 10's of psi change), assuming critically stressed or near-critically stressed faults, could cause earthquakes. Therefore, all of the results presented for this study have a truncated pore pressure distribution at 100 psi (0.70 MPa), yielding an increase in resolution that provides better visualization of the location of the pore pressure front at lower range pressure changes. For complete simulation results see Appendix B.

3.1.1 Dallas – Fort Worth (DFW) Airport Earthquakes

The Dallas – Fort Worth (DFW) Airport earthquake sequence began in October 2008 and continued intermittently until May 2009. In this study, pore pressure change at the onset of earthquake events is of interest. Pore pressure simulation results for the upper Ellenburger, lower Ellenburger, and basement layers on 1 November 2008, which is the end date of the first DFW airport earthquake swarm, are presented in Figure 3.a and Figure 3.b, respectively. From Figure 3., it can be seen that there are some areas of pore pressure increase in the vicinity of the earthquakes.

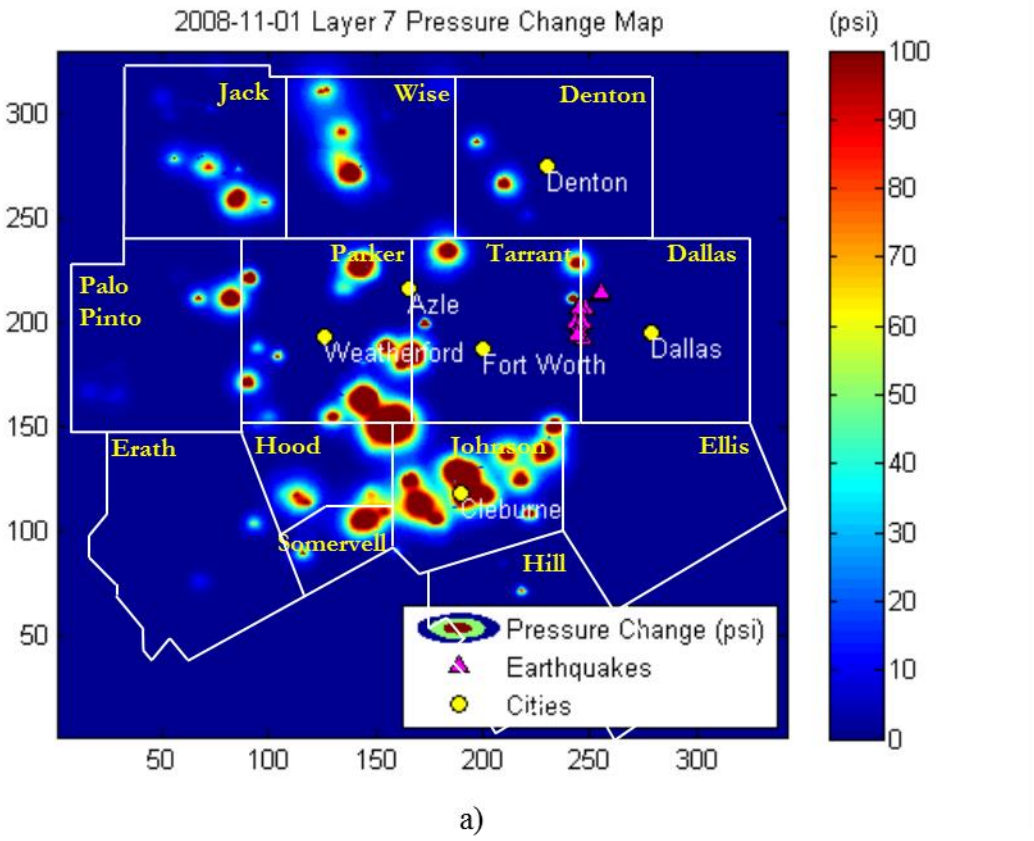

a)

Figure 3.2: a) DFW Airport earthquakes upper Ellenburger pore pressure change plot.
b) DFW Airport earthquakes lower Ellenburger pore pressure change plot.

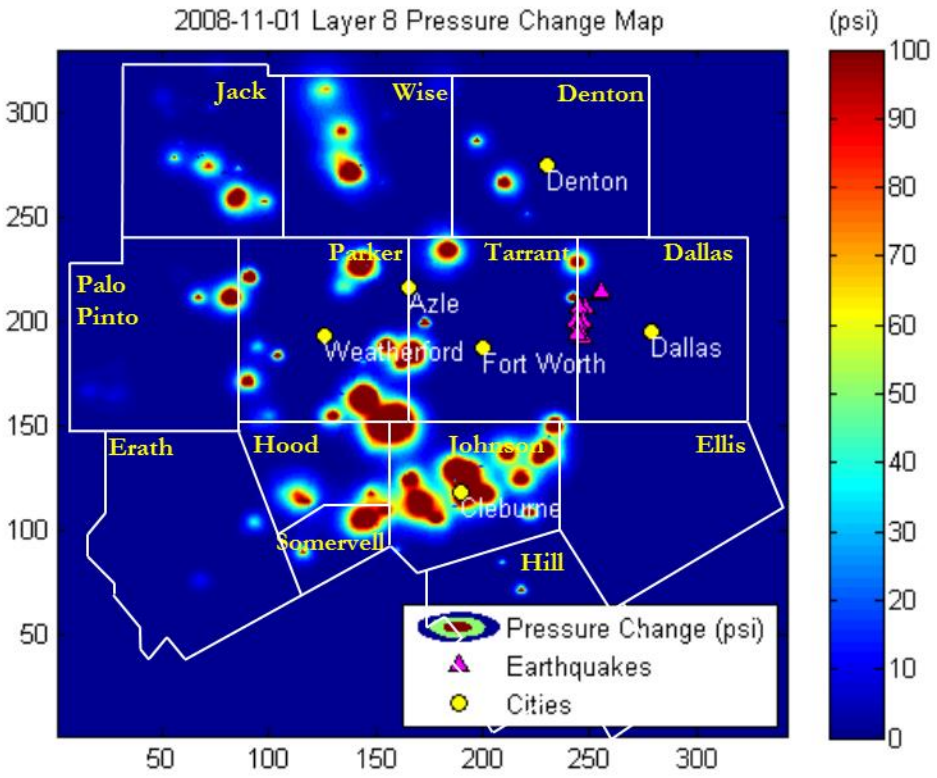

b)

Figure 3.2, cont.

However, a more in-depth analysis showed a potential spatial and temporal correlation between earthquake events and wastewater injection. A detailed pore pressure change plot for the lower Ellenburger can be seen in Figure 3.3. Looking at the DFW Airport area in more detail, it can be seen that there are at least two areas within the vicinity of the earthquake events in which localized pore pressure increases did occur by the end of September 2008. Most of the earthquake events are located within a few miles of the areas of pore pressure increase marked as the South Well on the figure, with the closest earthquake event occurring at the location of approximately 5 psi (0.03 MPa) pore pressure increase.

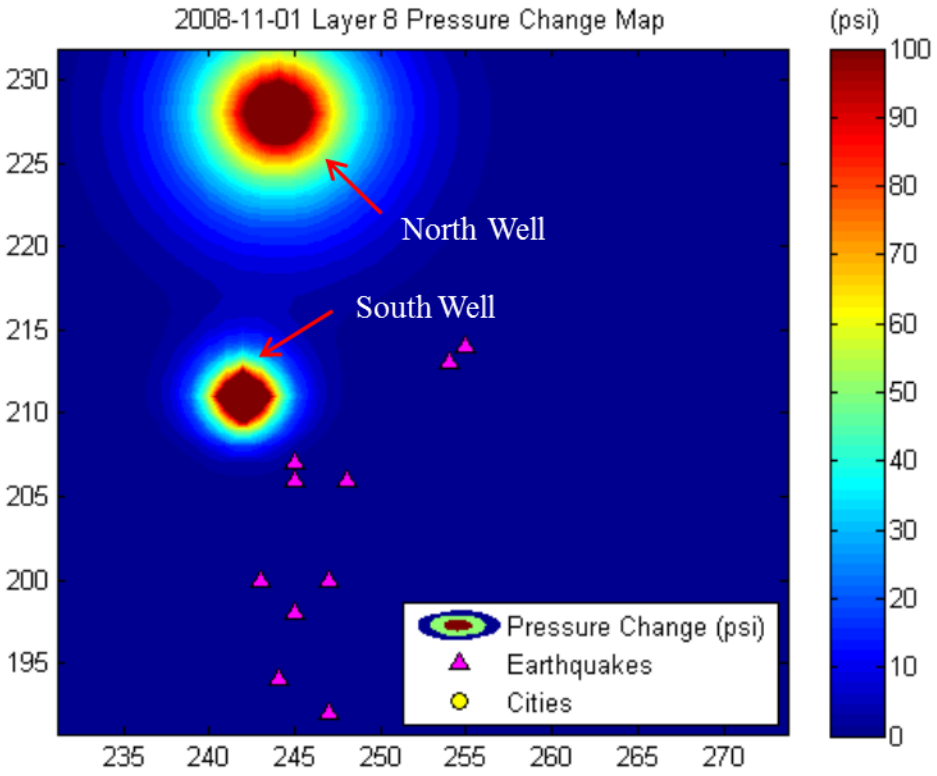

Figure 3.3: In-depth pore pressure change map in the vicinity of the DFW airport earthquakes' locations.

The pore pressure change located in the vicinity of the DFW Airport earthquake swarm has a maximum pressure change of approximately 400 psi (2.76 MPa). The change in pore pressure coincides with the coordinates of Well 439-32673, marked as South Well on Figure 3.3, which is located in the northeastern part of Tarrant County. In September 2008, the well had a total injection volume of 165,224 BPM. The monthly injection rate was 5,510 BPD (876.02 m^3/day) and the average monthly injection pressure was 1,200 psi (8.27 MPa) (Figure 3.4). The injection history of the well showed that there was no injection prior to September 2008, and injection was stopped after August 2009. In this study, the DFW Airport earthquakes of interest occurred one month after

wastewater injection into the Ellenburger formation commenced. This strongly suggests that there is a temporal correlation between the DFW Airport earthquake swarm and wastewater injection.

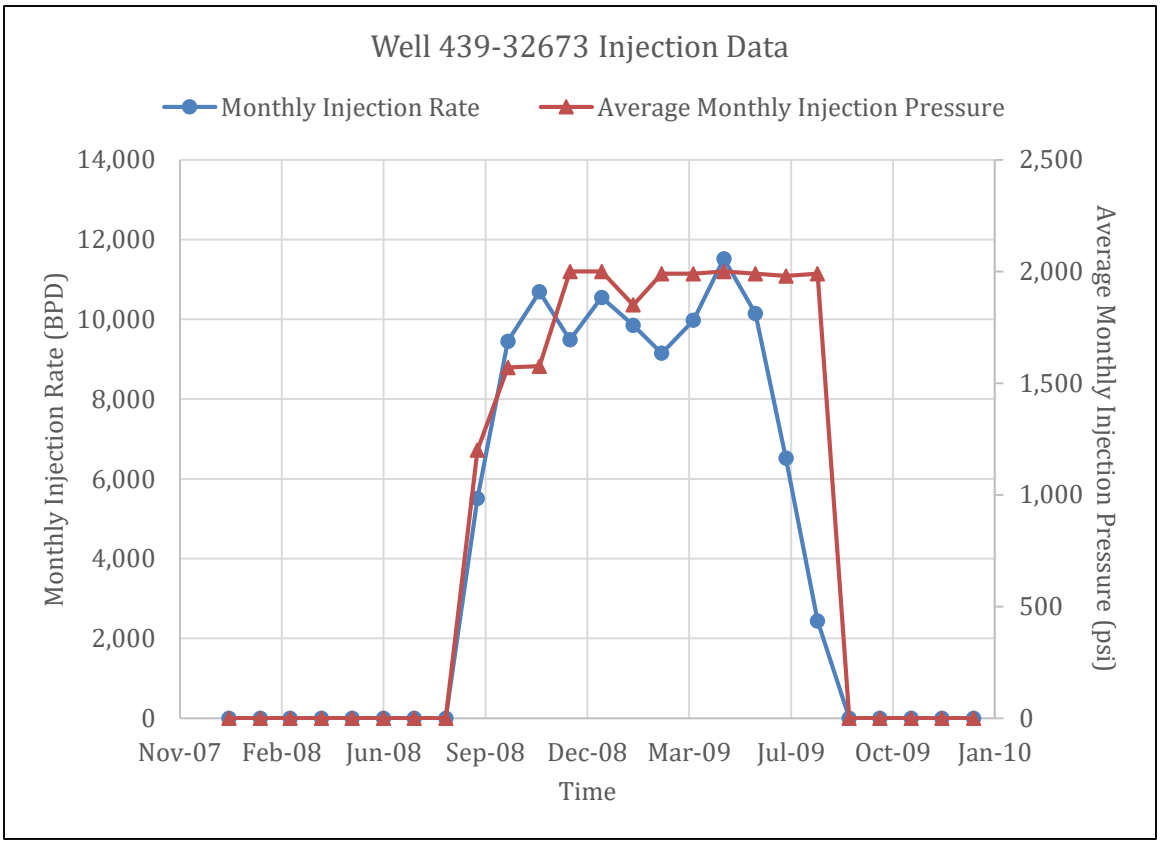

Figure 3.4: Well 439-32673 monthly injection data.

In this study, using the original USGS earthquake locations, there is no strong evidence of spatial correlation between the DFW Airport earthquakes and the local injector. However, Frohlich et al. (2011) relocated the DFW Airport earthquakes, showing that they were much closer to the injectors than previously thought, based on USGS initial locations (Figure 3.5), hence concluding that there was likely a causal relationship between the earthquakes and the injection. They were able to do this work

because after the initial earthquake swarm occurred, they deployed six temporary seismographs near the earthquake locations to gather better P and S waves arrival data in order to more accurately identify the locations of earthquakes. While only data recorded through the temporary seismographs was shown in Figure 3.5, cross-correlation analysis performed in their study asserted that the earthquake events reported by the USGS originated from hypocenters close to those of the earthquakes that they recorded with the temporary seismographs. Therefore, it is assumed that the earthquakes in this study can be relocated to the same locations as the ones that were more accurately located in the study conducted by Frohlich et al. (2011).

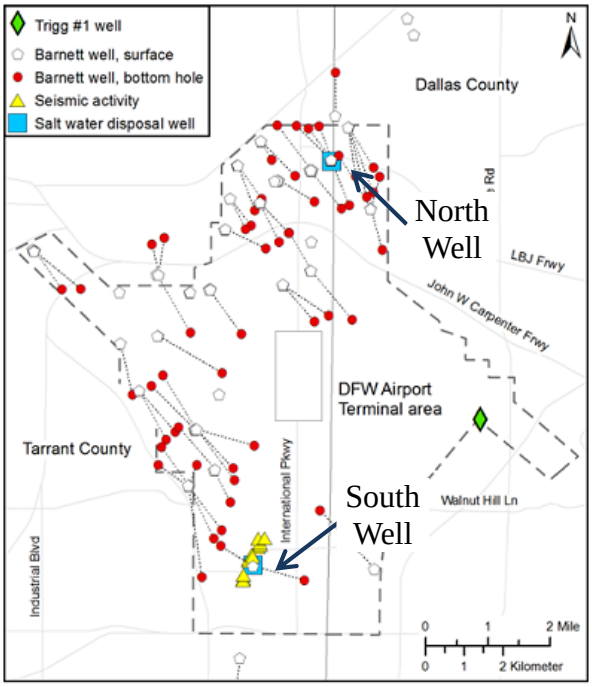

Figure 3.5: Map of the DFW airport with injection wells' locations and relocated earthquakes' locations, modified from Frohlich et al. (2011)

Furthermore, as can be observed in Figure 3.6, there is a normal fault mapped by Ewing (1990) in the area where USGS recorded earthquakes occurred (Frohlich et al. 2011). Comparing Figure 3.5 and Figure 3.6, it is evident that the earthquakes located by Frohlich et al. (2011) and the location of the South Well correspond to the location of the NE-SW trending mapped fault. As evident from the pore pressure modeling done in this study, wastewater injection in the South Well into the Ellenburger formation caused a pore pressure increase (Figure 3.3), and assuming a critically stressed fault, the pore pressure increase is likely to cause the fault to slip.

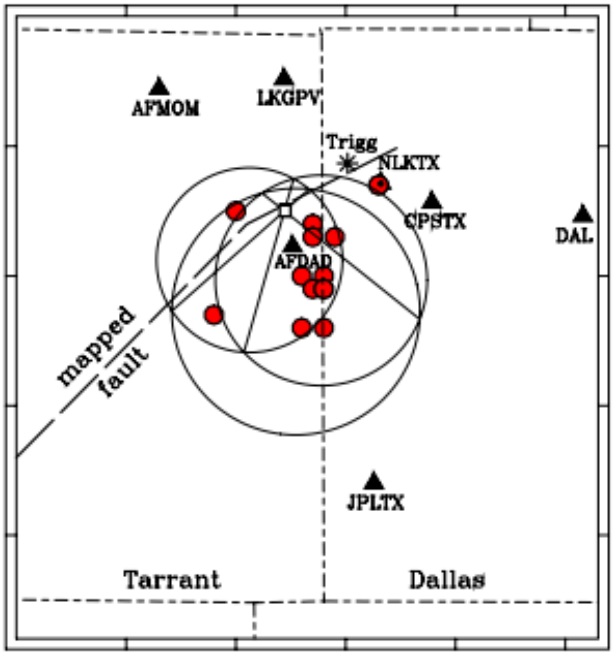

Figure 3.6: Mapped normal fault near earthquakes recorded through USGS, from Frohlich et al. (2011).

It can be concluded that there is a strong spatial and temporal correlation between the DFW Airport earthquakes and the area of increased pore pressure. The pore pressure change is confined to an area of roughly 4 miles (6.44 km) by 4 miles (6.44 km).

Furthermore, pore pressure change of 50 psi (0.34 MPa) and above is confined to an area of roughly 2 miles (3.22 km) by 2 miles (3.22 km).

3.1.2 Cleburne Earthquakes

Pore pressure simulation results for the upper Ellenburger and the lower Ellenburger layers on 1 August 2012, the end date of the Cleburne earthquake swarm, are presented in Figure 3a and Figure 3b, respectively. As can be observed from Figure 3, all of the earthquakes occurred in the areas of increased pore pressure. However, at the end of July 2012, most of the injection in Johnson County, where Cleburne is located, occurred primarily in the lower Ellenburger formation, which is the reason this layer is the focus of the discussion in this subchapter.

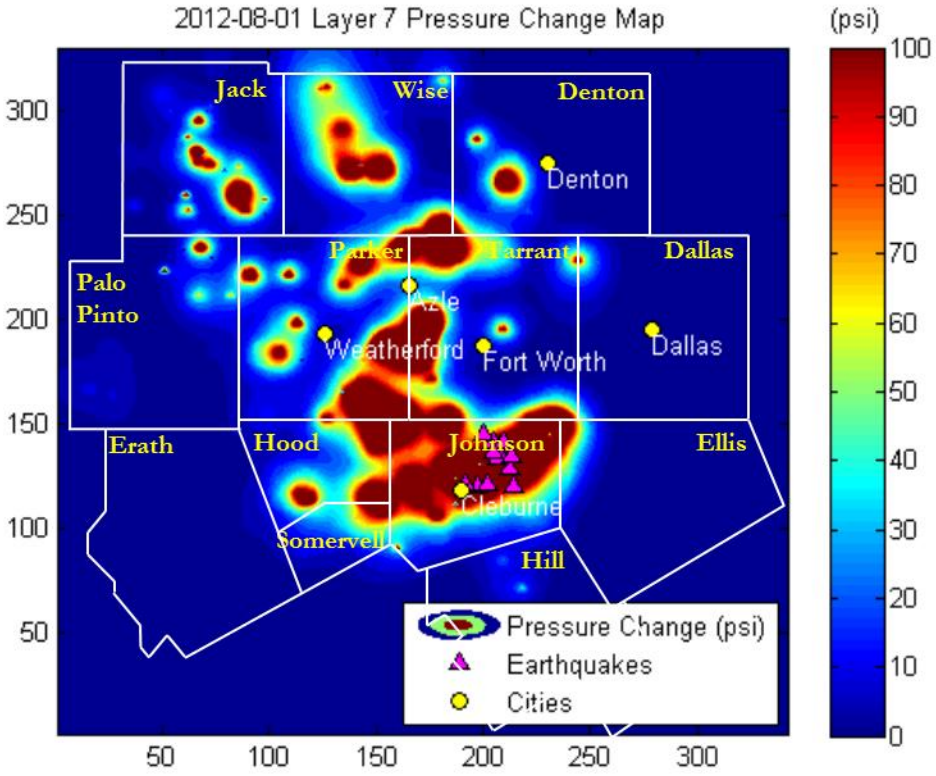

a)

Figure 3.7: a) Cleburne earthquakes upper Ellenburger pore pressure change plot. b) Cleburne earthquakes lower Ellenburger pore pressure change plot

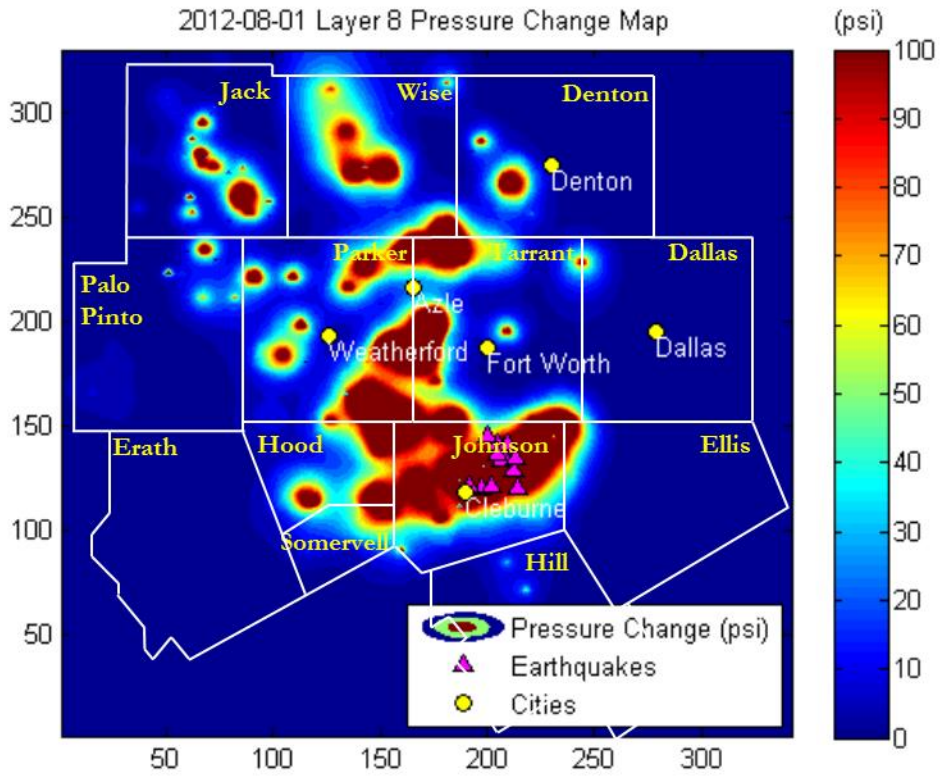

b)

Figure 3.7, cont.

To determine the temporal correlation between the Cleburne earthquakes and the location of pore pressure increase, analysis of the injection data was performed. From Figure 3.8, it can be observed that there are 10 wells injecting into the lower Ellenburger formation near the earthquakes' locations. Injection for these wells began in mid-2005 (Figure 3.9), yet USGS reported no earthquakes in the region prior to 31 October 2008 (Justinic et al. 2013). Furthermore, the first observed earthquake sequence in the Cleburne area occurred between June 2009 and June 2010. Out of the 10 wells in the area, 8 wells were fully injecting into the lower Ellenburger by mid-2007. This means there is a two-year lag between injection activities and the onset of an observable

earthquake sequence in the area. The next earthquake sequence, which occurred between June and August 2012, is the one being analyzed in this study. This is approximately a two-year lag between the end of the previous sequence and the onset of this sequence. The consistent time lag between the observed earthquakes sequences may indicate a regional signature, where it may take up to two years for significant build-up of pore pressure to occur before fault slip is triggered.

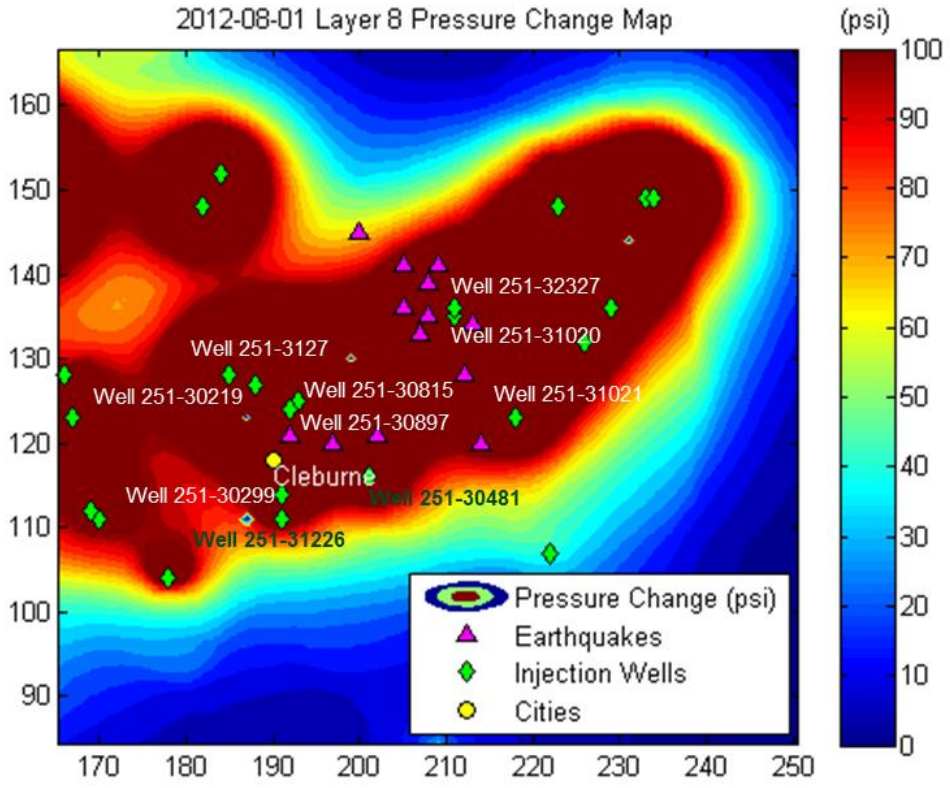

Figure 3.8: A detailed view of area of increase pore pressure that corresponds to the Cleburne earthquakes and wastewater injection wells.

From Figure 3.9, it can be observed that the monthly injection rate for the 10 wells in the vicinity of the earthquake events varies tremendously throughout time. For

example, for Well 251-3237, while the injection rate varies from month-to-month, the general injection rate trend has increased since injection began for the well in May 2008. Conversely, for Well 251-30481, the general injection rate trend has been declining since December 2008. Furthermore, examining the cumulative injection volume for each well, it can be observed that high cumulative injection volume does not outwardly correlate to occurrence of earthquakes. It was difficult to determine whether the earthquake events and the injection activities themselves are correlated, due to the complicated nature of injection patterns.

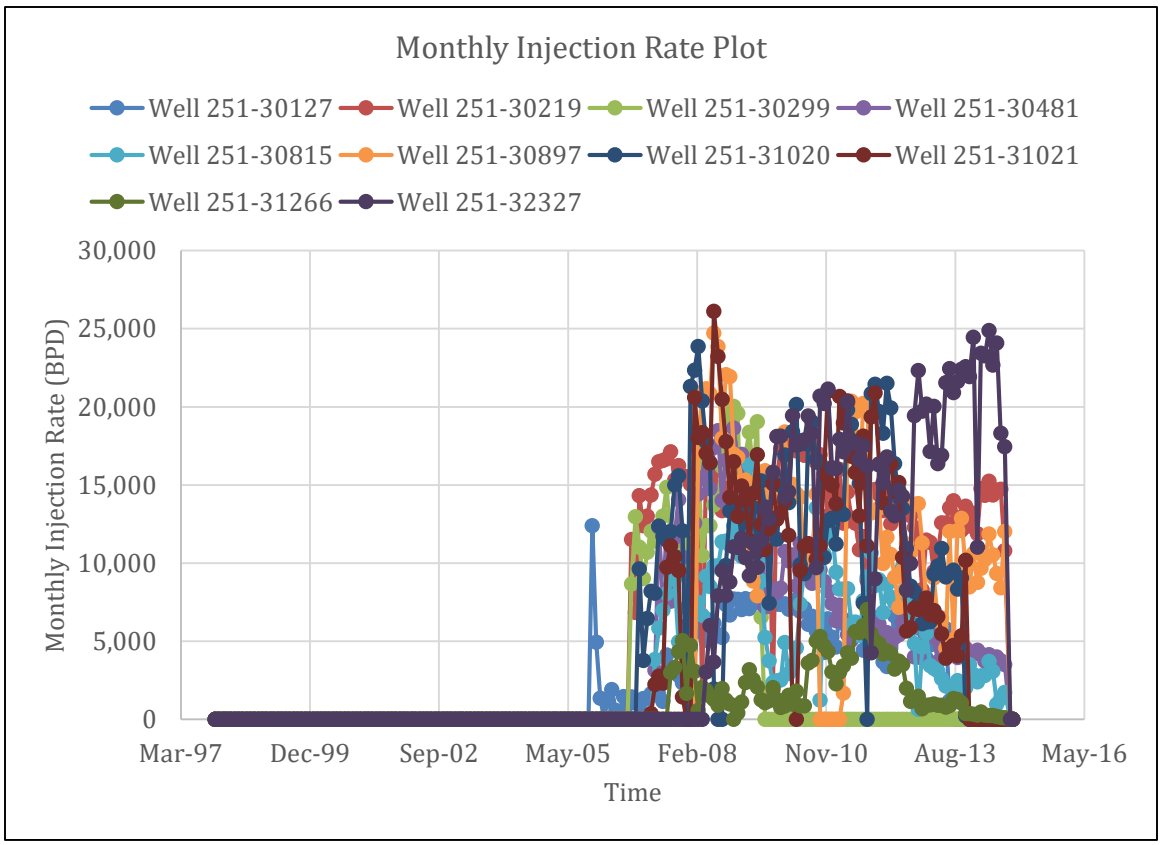

Figure 3.9: Monthly injection rate for wells located near the Cleburne earthquake swarm.

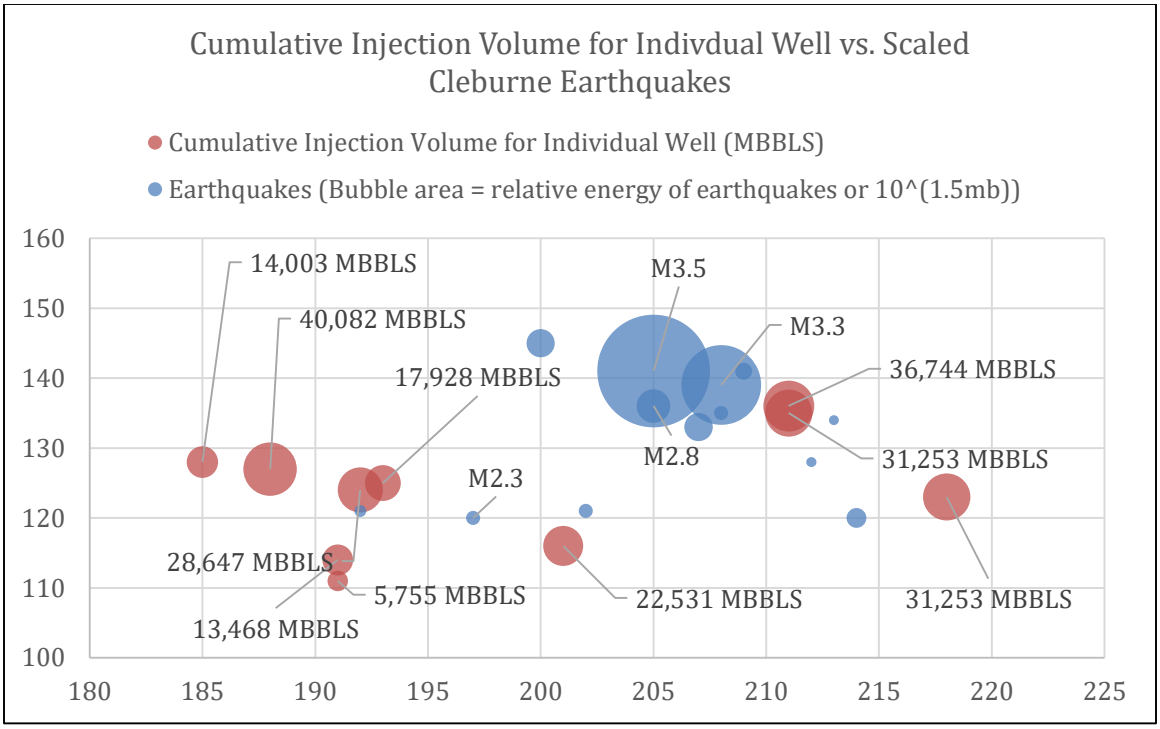

Figure 3.10: Cumulative injection volume for individual wells vs. scaled Cleburne earthquakes.

Another interesting observation to be made is that the earthquake events occurred between two mapped faults instead of along the fault (Figure 3.11). While the USGS database is only accurate to within a few miles, it is unlikely that even with relocation that the earthquakes would fall along the faults. It is more likely that there are other sets of faults in the region that slipped due to the pore pressure increase attributed to wastewater injection, which caused the earthquake sequence.

Based on the analysis, there are spatial and temporal correlations between the seismic events and the area of increased pore pressure. The maximum pore pressure increase associated with the Cleburne earthquakes was approximately 300 psi (2.07 MPa). This level of pore pressure increase is not unusual for the area, since there are other locations with the same level of pore pressure increase without any earthquake

events being observed. This is likely due to the lack of favorably oriented faults or potentially the lack of faults in the areas altogether.

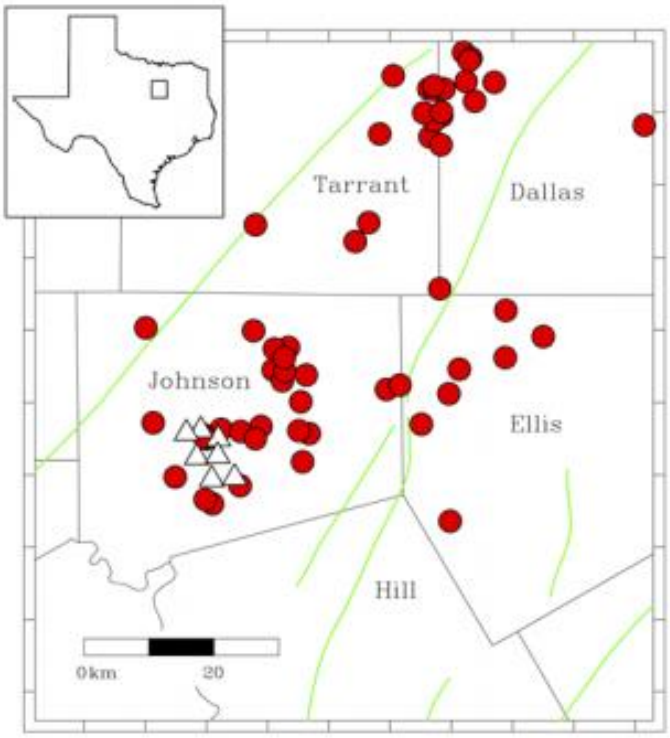

Figure 3.11: Mapped faults (marked by green lines) by Ewing (1990), from Justinic et al. (2013).

3.1.3 Azle Earthquakes

Pore pressure simulation results for the upper Ellenburger and the lower Ellenburger layers on 1 January 2014, end of the Azle earthquake swarm, are presented in Figure 3.a and Figure 3.b respectively. As can be observed from Figure 3., all of the earthquakes occurred in the areas of increase pore pressure. Similar to the previous areas of interest, injection occurred primarily in the lower Ellenburger formation; hence, the layer became the focus of the discussion in this sub-chapter.

From Figure 3.13, it can be observed that most of the Azle earthquakes coincided with areas of pore pressure increase between 50 (0.34 MPa) psi to 80 psi (0.55 MPa), with a few events occurring below and above the pore pressure increase range. Previously, Hornbach et al. (2015) published a study of the Azle earthquakes which include pore pressure modeling. Their simulation utilized 3D groundwater-flow model, with study area that was confined to the vicinity of the earthquake event. The pore pressure simulation included both injectors and producers. Furthermore, water level changes was also assessed, but eventually was deemed inconsequential due to minimal pore pressure increase associated with it. Their simulation resulted in a pore pressure change values of approximately between 40 psi (0.28 MPa) and 80 psi (0.55 MPa), which is consistent with the simulation results of this study for the Azle earthquakes.

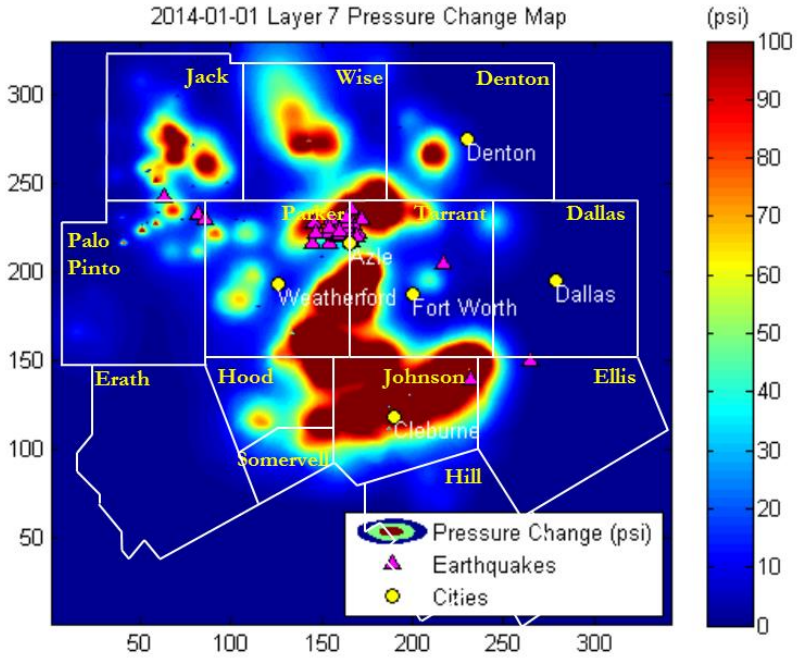

a)

Figure 3.12: a) Azle earthquakes upper Ellenburger pore pressure change plot. b) Azle earthquakes lower Ellenburger pore pressure change plot.

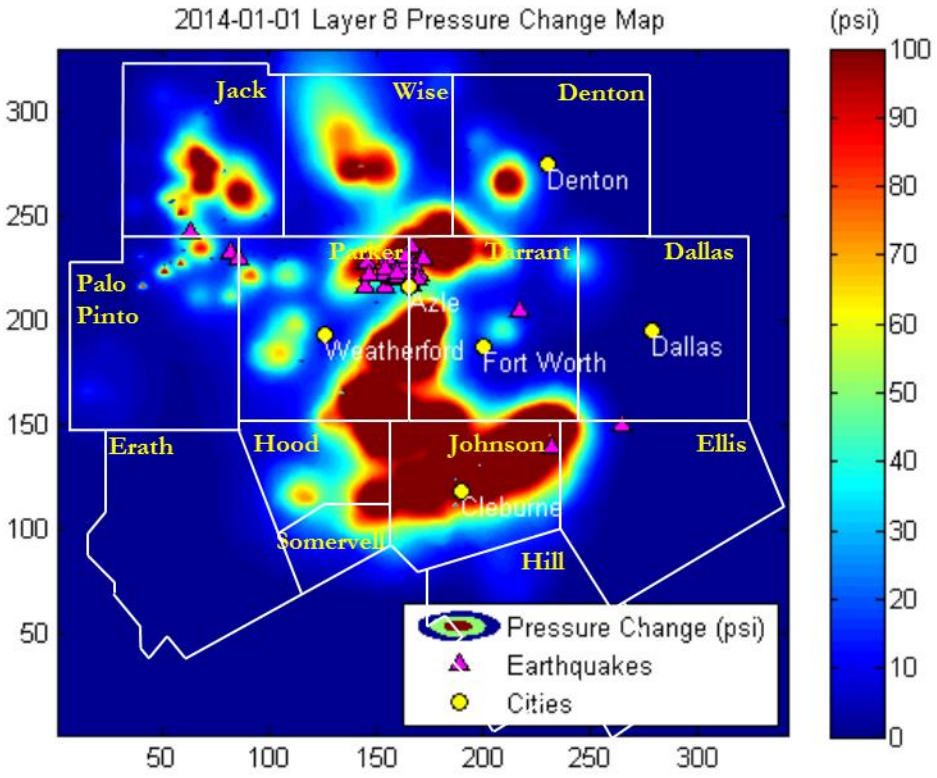

b)

Figure 3.12, cont.

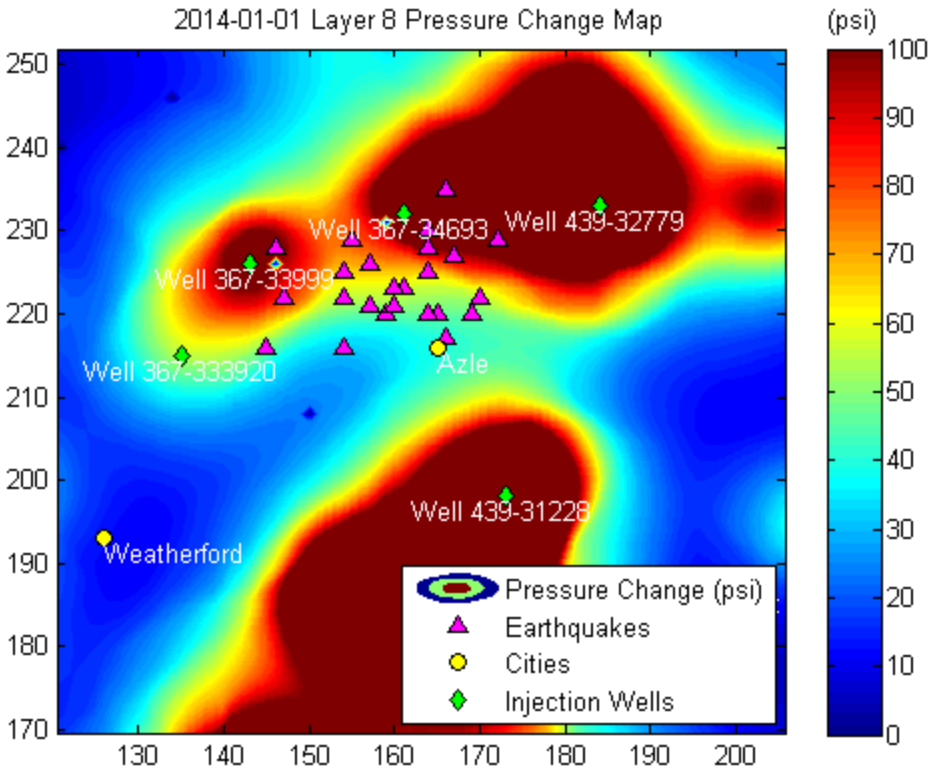

Figure 3.13: Detailed pore pressure change map in the vicinity of the Azle earthquakes' locations.

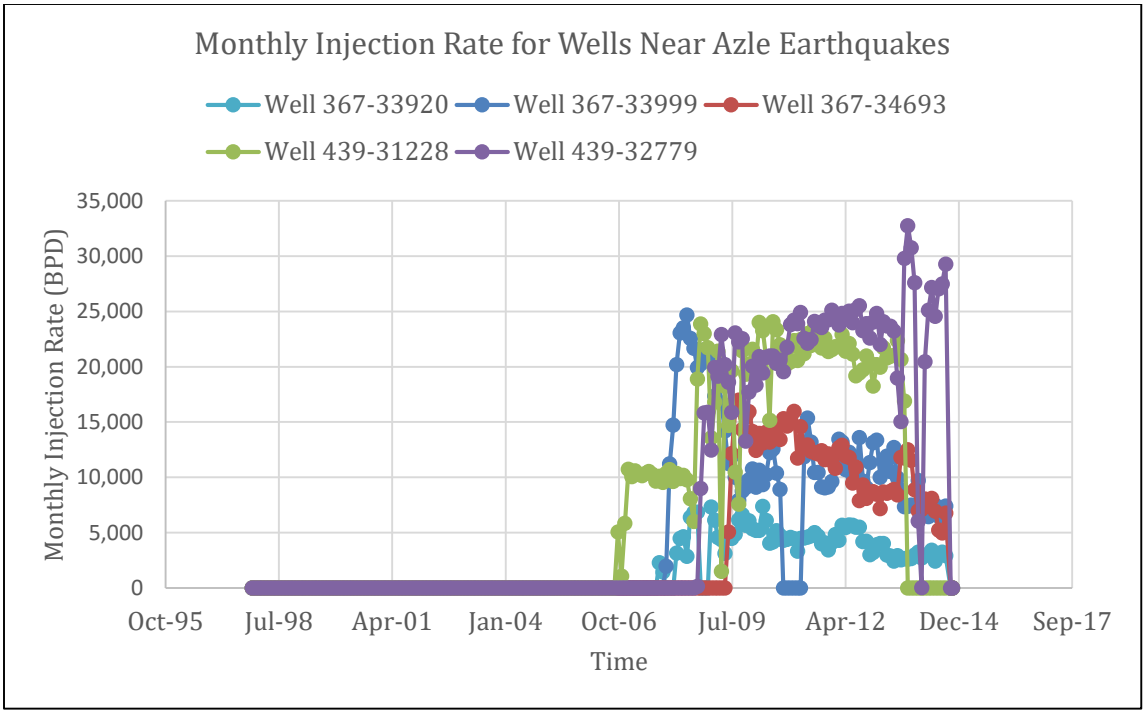

Figure 3.14: Monthly injection rate for wells located near the Azle earthquake swarm.

The five wells located in the vicinity of the Azle earthquake swarm have relatively high injection rates (Figure 3.14). For example, the maximum injection rate for Well 439-32779 is approximately almost 35,000 BPD (5,500 m^3/day). Assuming continuous injection for 30 days, that amounts to more than 1,000,000 BBLS/month (167,000 m^3/month). A case where seismicity was surmised to likely be induced by injection has been reported for wells with much lower injection rate (Kim 2013). It should also be noted that the other two wells in the area, Well 367-33999 and Well 367-34693 have injection rates that have constantly declined since the start of injection. Additionally, there was a short period at which injection was paused for Well 367-33999. Furthermore, since injection activities have continued with little to no breaks, the cumulative injection between the five wells at the end of the injection period amount to approximately 120,000,000 BBLS (19,000,000 m^3) (Figure 3.15). No earthquake events

were observed in the area prior to the Azle earthquake sequence, therefore it is possible that the pressure required to cause slip on fault in the area needs to build-up for a longer period of time.

From Hornbach et al.'s (2015) study, they found that there are two faults in the vicinity of the earthquake sequence (Figure 3.16). The first is a primary normal fault, and the second one is a shallower antithetic normal fault. The second antithetic normal fault is located approximately 1.25 miles (2 km) Southwest of Well 367-34693 (injector #1 in Figure 3.16), and from Figure 3.13, it can be seen that the location of the fault would coincide within the area of pore pressure increase of approximately 90 psi (0.62 MPa).

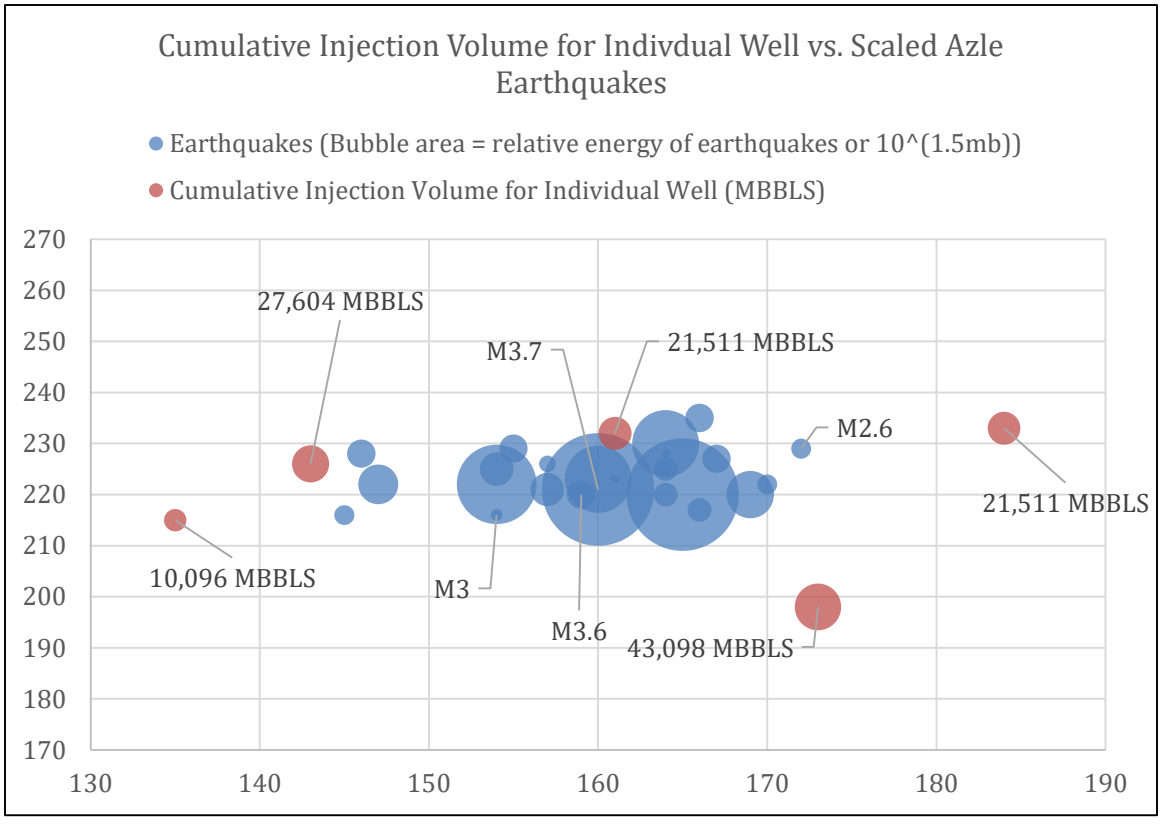

Figure 3.15: Cumulative injection volume for individual wells vs. scaled Azle earthquakes.

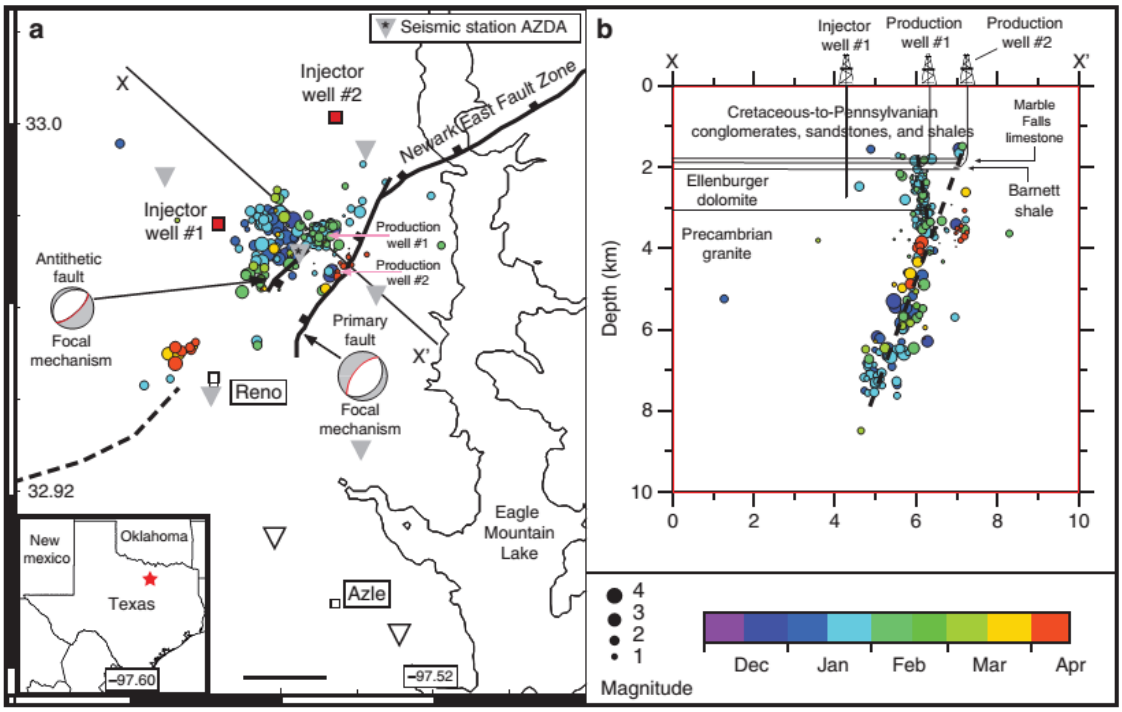

Figure 3.16: Fault locations near the earthquake events, from Hornbach et al. (2015).

Based on the analysis, there is spatial and temporal correlation between the Azle earthquakes and the area of increased pore pressure. The maximum pore pressure increase that corresponds to seismic activity is 120 psi (0.83 MPa). The maximum pore pressure increase from this study is higher than Hornbach et al.'s (2015) study. In their study, they concluded that seismicity was potentially induced not only because of wastewater injection but also by extraction by a well adjacent to the fault. This could potentially be the source of the discrepancy, since production is outside the scope of this study.

3.1.4 Simulation Results for the Basement Layer

The basement is an important aspect of understanding seismicity induced by wastewater injection. This is evident from the study conducted by Hornbach et al. (2015)

where the fault extended down to the basement and the earthquakes focal depths are located in the Precambrian basement (Figure 3.16) even when fluid was injected at a higher interval in the subsurface. Permeability of the basement in the model is very low, and since no flow boundaries (e.g. faults) were included in the simulation, no pore pressure response was observed in the basement layer (Figure 3.17). It should be noted that if a fault is included as part of the simulation of the basement layer, then the pore pressure response would be highly noticeable, since the fault would act as a high permeability channel along itself, while still prohibit flow across the fault.

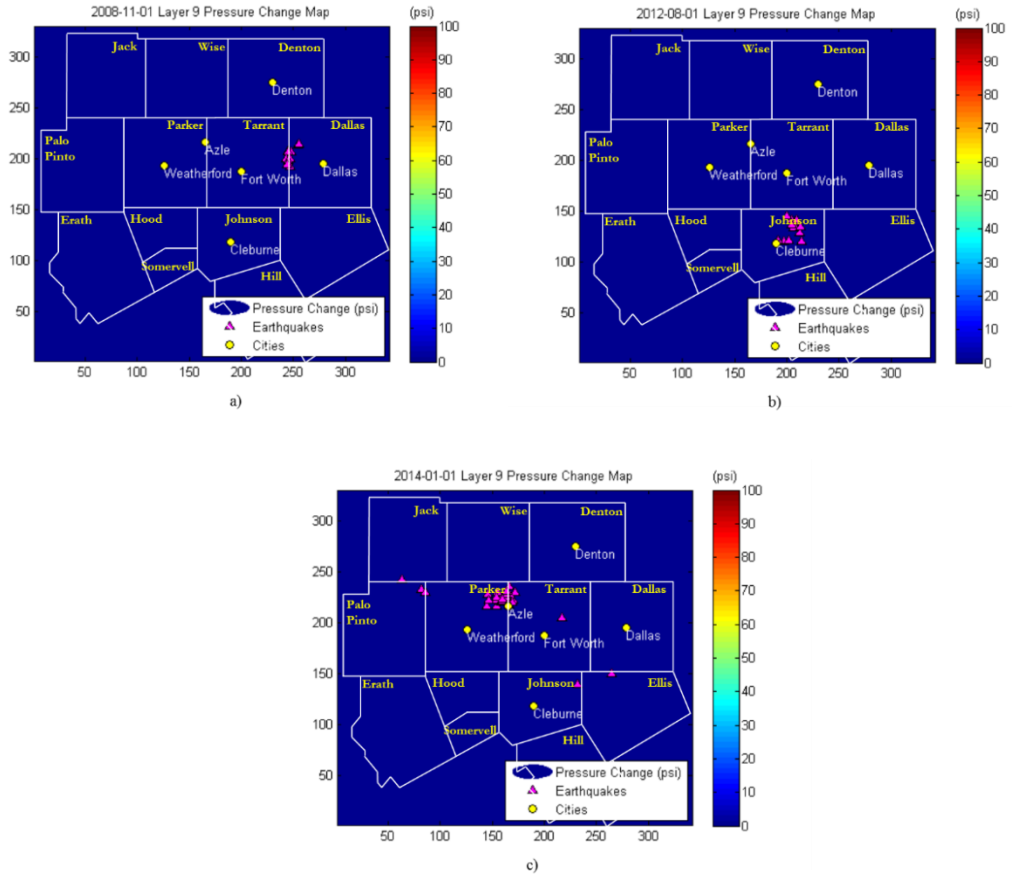

Figure 3.17: a) Basement layer simulation result for the DFW Airport earthquakes. b) Basement layer simulation result for the Cleburne earthquakes. c) Basement Layer simulation result for the Azle earthquakes.

3.1.5 Areas with Increased Pore Pressure but No Earthquakes

While the simulation results showed that there are spatial and temporal correlations between earthquake events and pore pressure increase in all three areas of interest, perhaps the most interesting results from the pore pressure modeling are the areas with elevated pore pressure but no earthquakes were observed throughout the injection duration.

From Figure 3.18 it is apparent that most of the areas with significant pore pressure increase (the dark red zone on the contour maps) does not necessarily always correspond to the location of observed earthquakes. In some instances, for example the location where the Azle earthquakes eventually manifested, at the northeast corner of Parker County and the northwest corner of Tarrant County. These areas have experienced elevated pore pressure since 2008 (Figure 3.18a and Figure 3.18d), yet at that time no earthquakes were recorded. As time progresses, the areas of elevated pore pressure merged as one and created a larger area of increased pore pressure (Figure 3.18b and Figure 3.18e). Finally, when pressure has built up just enough, earthquake events started to occur (Figure 3.18c and f). The same observation also holds true for the area where the Cleburne earthquakes occurred, albeit with a shorter time lag. This observation also hold true for the area in the northeast corner where Palo Pinto County intersects Parker County. Earthquakes were recorded in the area in 2014.

While positive correlation between wastewater injection and induced seismicity are more commonly studied (Keranen et al. 2014; Hornbach et al. 2015; Kim 2013), the negative correlation have yet to be fully understood. An advantage of a basin-wide study is the ability to see what exactly is happening to the pore pressure at a larger scale, even if the resolution of the solution has to be sacrificed. For example, from Figure 3.18, it can

be observed that there are areas of increased pore pressure in both the southeast corner of Jack County and the western-central part of Wise County.

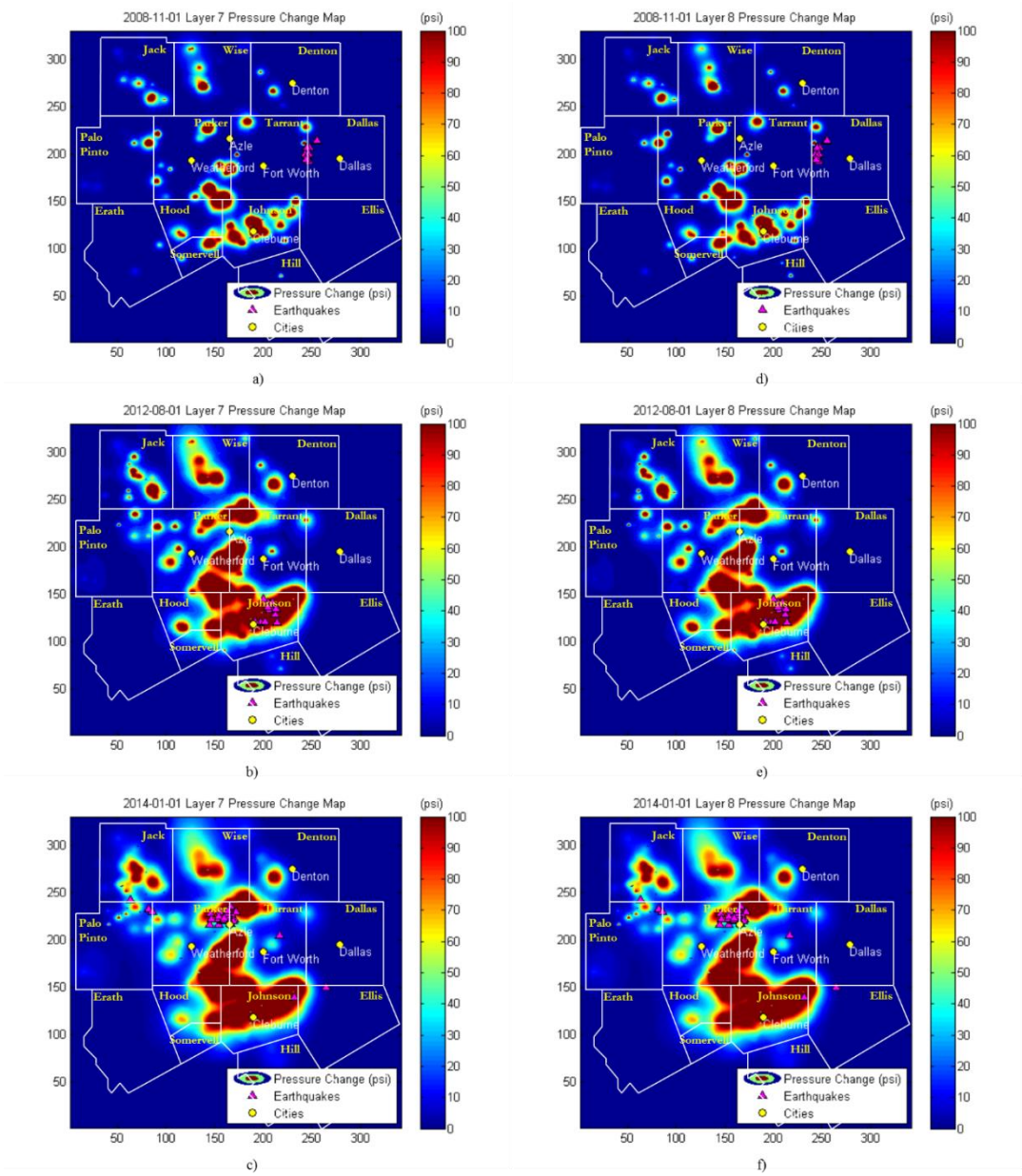

Figure 3.18: a) – c) Upper Ellenburger pore pressure response progression through time from November 2008 to January 2014. d) – f) Lower Ellenburger pore pressure response progression through time from November 2008 to January 2014.

These areas are consistently shown to have high pressures, yet no earthquakes were ever recorded. Based on the Ellenburger structure map (Figure 3.19), there was no major faults in Jack County, therefore one plausible explanation could be that there is no sizable faults in the area that could trigger earthquakes even with the elevated pore pressure.

From the Ellenburger structure map (Figure 3.19), it can be observed that the Mineral Wells fault crosses the southeast corner of Wise County. However, the fault is not in the same direction as the in-situ stress (which trends NE-SW). This unfavorable orientation of the fault may be the reason why while Wise County experience elevated pore pressure upwards of 50 psi (0.34 MPa) in the area where the Mineral Wells fault is located, but no earthquakes were observed.

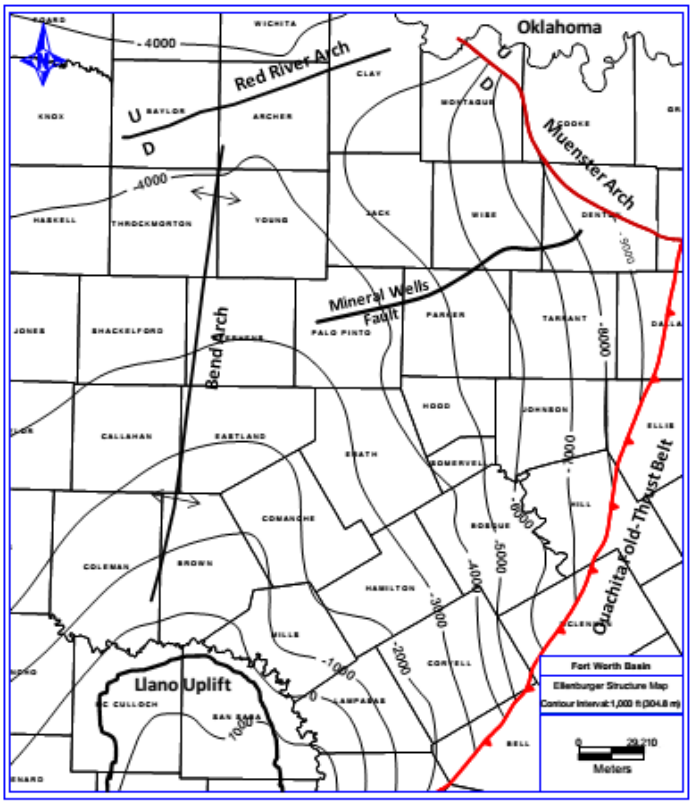

Figure 3.19: Ellenburger Group structure map with fault traces, from Kuhn (2011).

The last area of interest where there is an increase in pore pressure but no earthquake events were observed is at the intersection between Parker County, Tarrant County, Hood County, and Johnson County. As is evident from Figure 3.18, the areal extent of the pore pressure increase for the area increases at every time step. The maximum pore pressure in the area was 500 psi (3.45 MPa). From Figure 3.19, however, it can be seen that there is no mapped fault at the top of the Ellenburger in that region. This could be the primary reason why even with a large increase in pore pressure and pressure build-up in the area, no earthquakes were observed.

3.1.6 Correlation to Cumulative Injection Volume

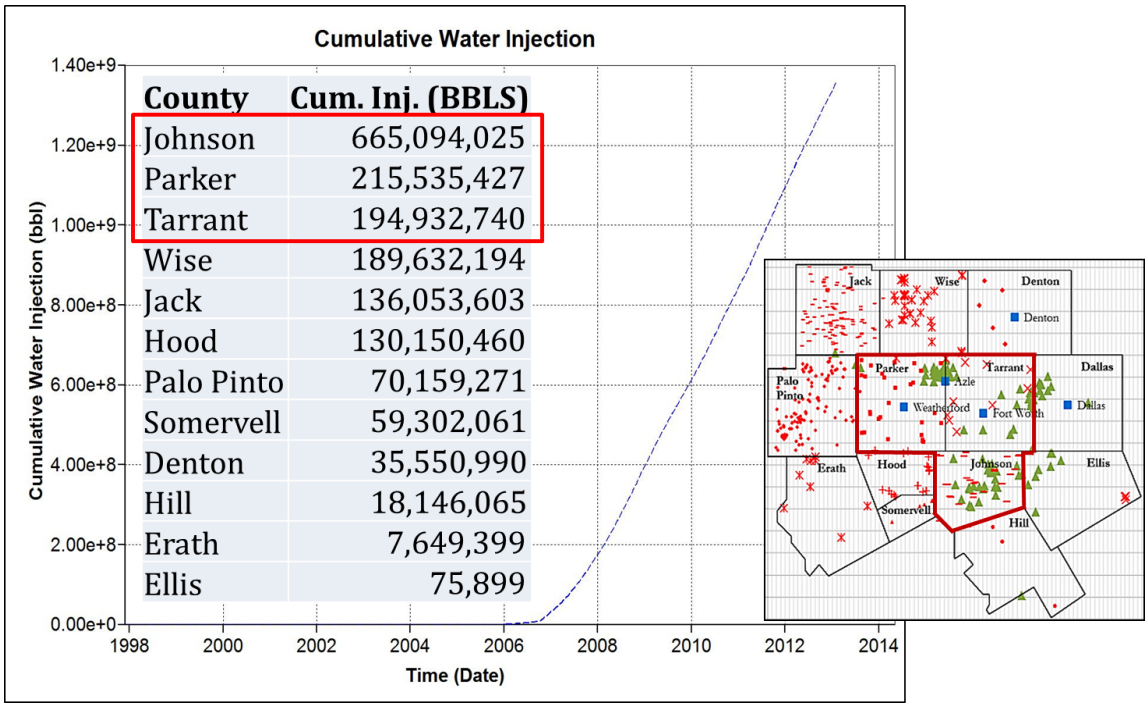

County	Cum. Inj. (BBLS)
Johnson	665,094,025
Parker	215,535,427
Tarrant	194,932,740
Wise	189,632,194
Jack	136,053,603
Hood	130,150,460
Palo Pinto	70,159,271
Somervell	59,302,061
Denton	35,550,990
Hill	18,146,065
Erath	7,649,399
Ellis	75,899

Figure 3.20: Cumulative injection volume by county.

From Figure 3.20, it can be observed that the three counties with the highest cumulative injection are also the same counties where earthquake events are observed.

This correlation is intuitive since seismicity will be induced when pore pressure increases to cause slip on critically stressed faults. For an increase in pore pressure to exist, there has to be an increase in injection volume. Hence, the general correlation between the cumulative injection volume and the counties where earthquake events are observed is in congruent with the physics behind induced seismicity.

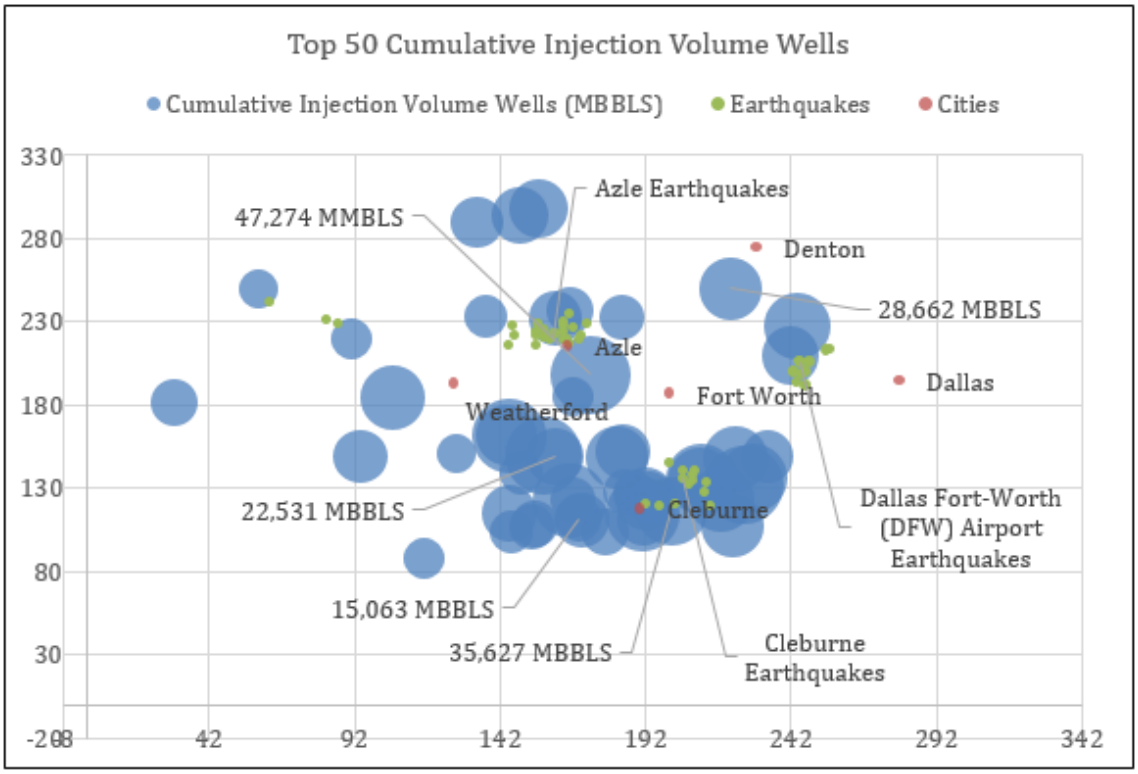

Figure 3.21: Top 50 wells with the highest cumulative injection volume.

From Figure 3.21, it can be observed that most of the high volume wells are concentrated in Johnson County. Out of 50 wells that were plotted, 24 wells are located in Johnson County. 9 of the high volume wells are located in Tarrant County, and 7 are located in Parker County. In Johnson County, an average high volume well inject a cumulative volume of 27,000 MBBLS (4,300,000 m^3), the highest average in comparison to other counties where high volume injection also occurred. While not all areas with

increase pore pressure are associated with earthquake events, however, all areas with earthquakes are associated with elevated pore pressure, and hence large volumes of water injection.

3.2 GEOMECHANICAL ANALYSIS

Frictional analysis for the given stress state to determine the change in pore pressure gradient required to trigger fault slip was performed. The Mohr-Coulomb shear failure equation for a normal faulting stress regime (Equation 2.4) can be solved for the critical pore pressure gradient required for stability. Using values of dS_{hmin}/dz = 0.84 psi/ft (19.00 MPa/km) (Waters et al. 2011) and dS_v/dz = 1.1 psi/ft (24.88 MPa/km) (Rathje & Olson 2007), the critical pore pressure was determined to be 0.72 psi/ft (16.23 MPa/km). Assuming hydrostatic initial pore pressure at 0.433 psi/ft (9.79 MPa/km), an increase of 0.29 psi/ft (6.56 MPa/km) is the amount of pore pressure gradient change needed to induce failure on ideally oriented faults. In this study, it is assumed that S_{hmin} is independent of pore pressure, an oversimplification that resulted in a lower S_{hmin} value. Taking into account the dependence of S_{hmin} on pore pressure, would result in a higher final pore pressure change that is needed to be overcome before slip will occur, which would give a higher tolerance of pore pressure changes, hence it is less likely for earthquakes to occur.

Figure 3.22 shows a plot of pressure with respect to depth for the principal in-situ stresses, initial pore pressure, and pore pressure at Coulomb failure. An increase of ΔP_p in pore pressure is required in order for failure to occur which in turn causes slippage, and hence earthquakes.

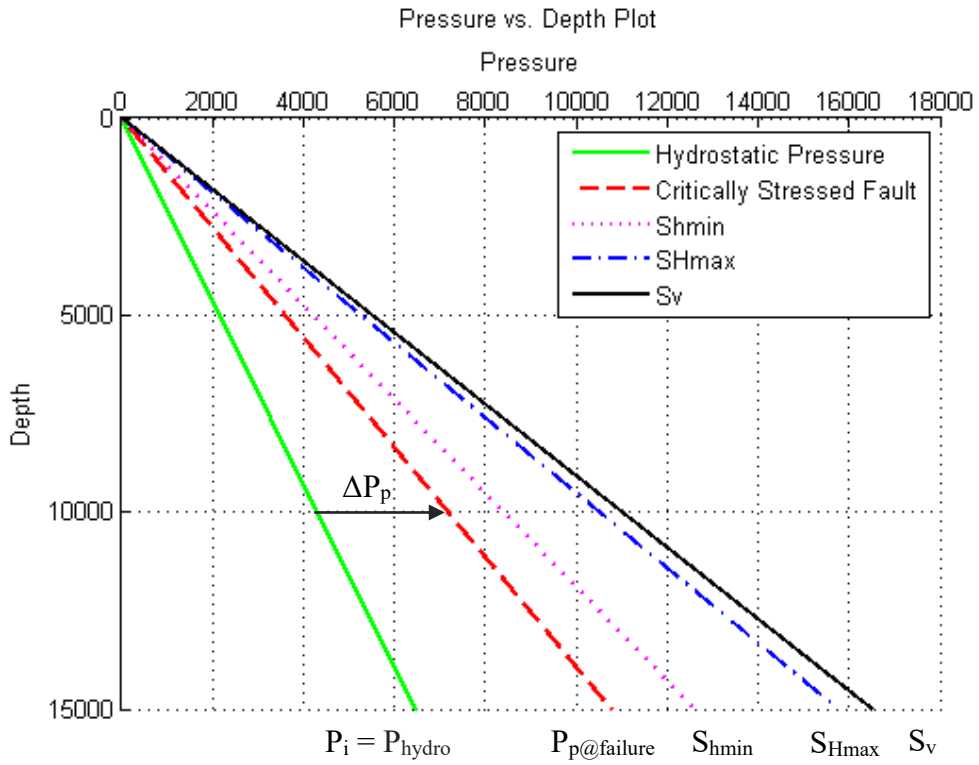

Figure 3.22: Pressure vs. Depth plot of total principal in-situ stresses, initial pore pressure, and pore pressure at Coulomb failure function (CFF).

Analysis of pore pressure increase required to slip favorably oriented faults was performed for both the lower Ellenburger layer and for the basement layer, and the results are plotted in Figure 3.23 and Figure 3.24 respectively. From the figures, it can be observed that the minimum pore pressure change required to cause a favorably oriented fault to slip is approximately 1,100 psi (7.58 MPa) for the lower Ellenburger formation, and approximately 2,200 psi (15.17 MPa) for the basement. However, it was evident from the pore pressure simulation result, as presented in subchapter 3.1, the maximum pore pressure increase that corresponds to an earthquake event was at most 400 psi (2.76 MPa). Based on this result, assuming favorably oriented faults exist in either the

Ellenburger formation or in the basement, the pore pressure increased due to wastewater injection is not sufficient to cause the favorably oriented faults to slip.

On Figure 3.25, a modified Mohr-Coulomb circle is presented to help visualize the gap that exists between the initial pore pressure and the pore pressure of the critically stressed fault. Based on the simulation results, the maximum pore pressure change was 400 psi (2.76 MPa). The critical pore pressure to cause is slip was calculated to be 0.72 psi/ft (16.23 MPa/km). Assuming a depth of 10,000 ft (3.05 km), given the assumptions about S_v and S_{hmin}, then the initial pore pressure required for fault slip to occur is 0.68 psi/ft (15.38 MPa/km). Based upon data from the literature (Bowker 2007), this high of a value for initial pore pressure is not likely. Then, it is possible that there could be localized higher initial pressures, or localized higher pressure changes because of heterogeneous permeability.

Without the assumption that faults are critically stressed, fault slip will only occur when the well pressure gradient reaches the pressure gradient of a critically stressed fault. Many studies (Hornbach et al. 2015; Keranen et al. 2014) assumed that the faults are already critically stressed prior to injection (Zoback & Townend 2001; Townend & Zoback 2000), hence fault slip can be triggered by small amounts of pore pressure changes (Reasenberg & Simpson 1992; Stein 1999). However, in this study, part of the goal is to understand the pore pressure change required to cause non-critically stressed, but favorably oriented faults to slip. Under the assumption that the faults are critically stress, and fault slip can be triggered by small amount of pore pressure change, then the results from the pore pressure simulation are sufficient to cause slippage on critically stressed faults.

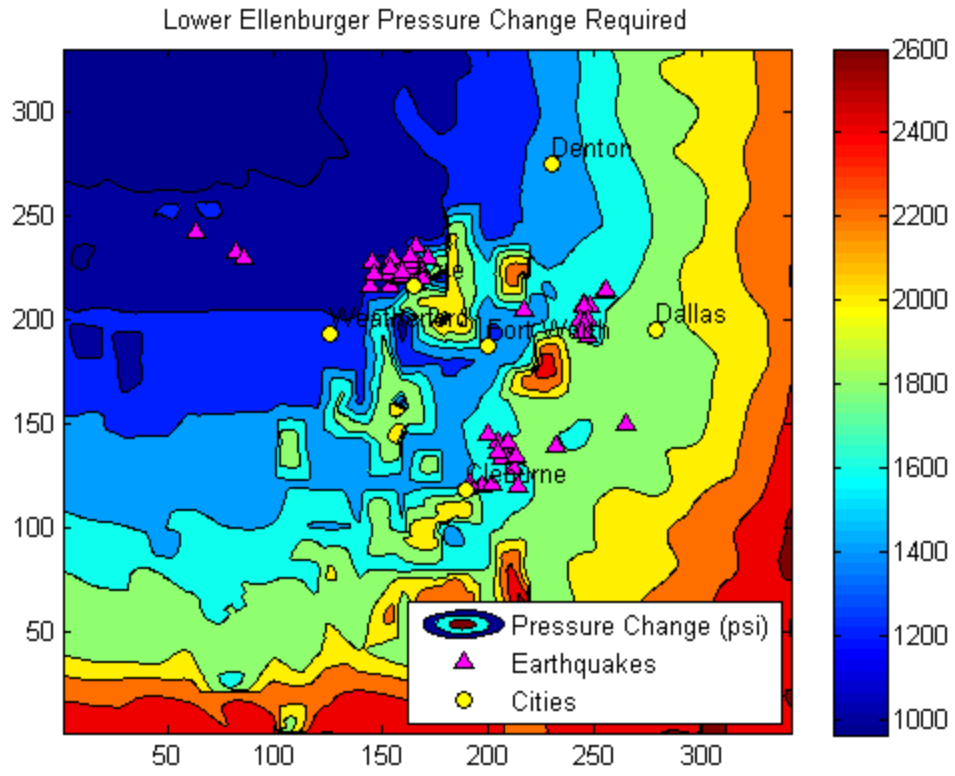

Figure 3.23: Pore pressure change required in the lower Ellenburger layer to cause fault slippage.

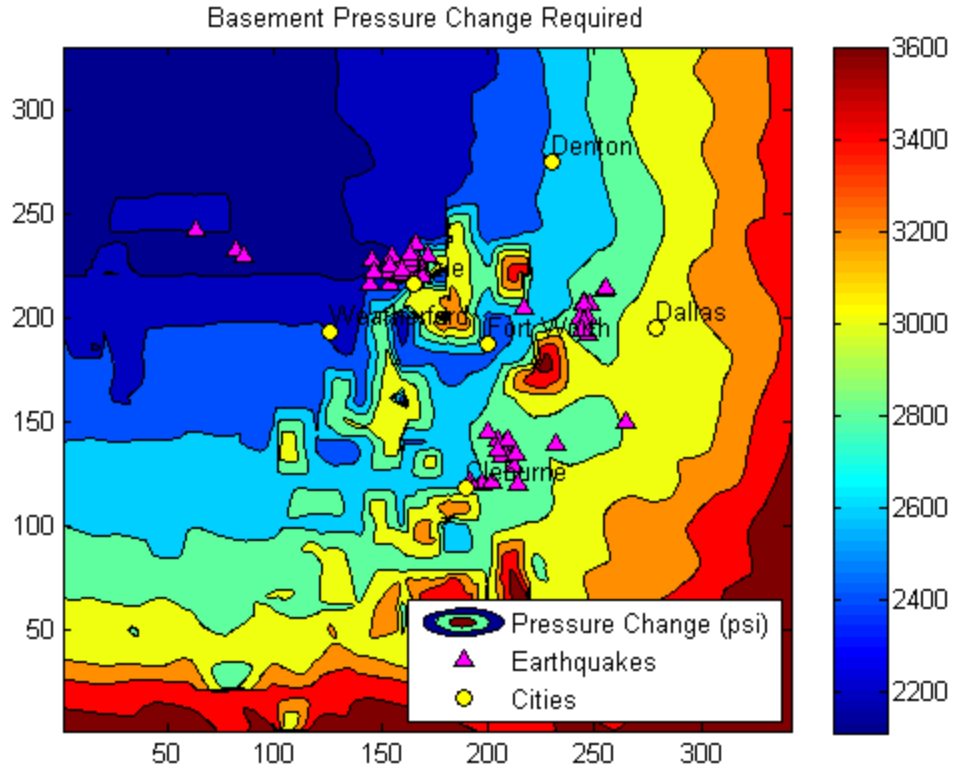

Figure 3.24: Pore pressure change required in the basement layer to cause fault slippage.

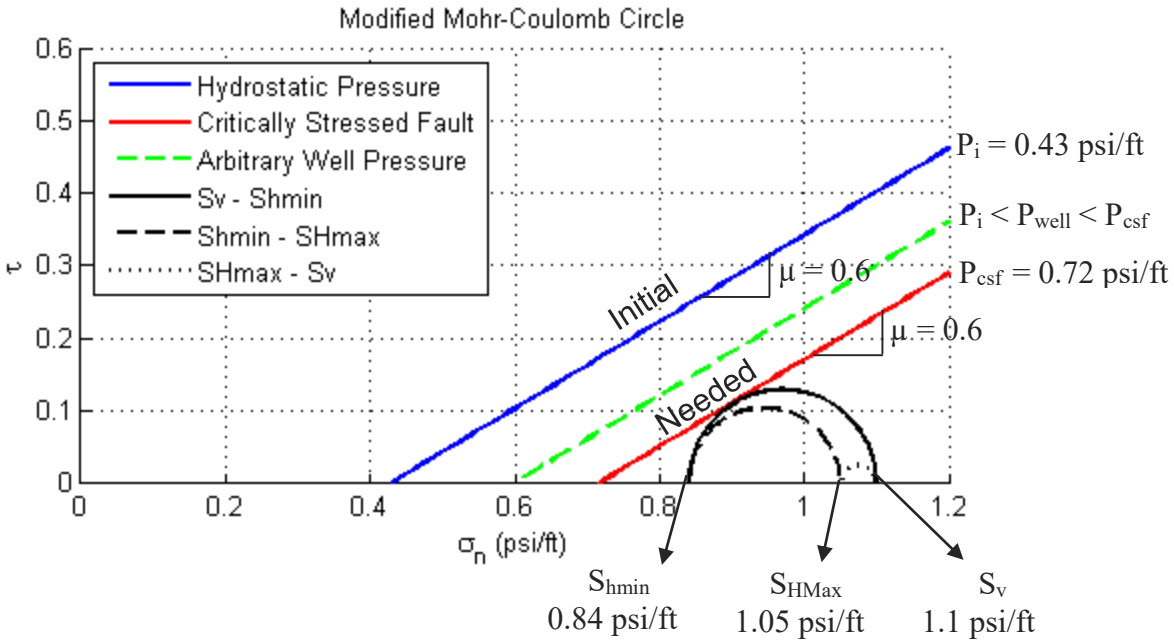

Figure 3.25: Modified Mohr-Coulomb circle.

The disagreement between analyses results lead to re-examination of two of the input data, the formation permeability, *k*, and the value of S_{hmin} used in the pore pressure modeling and the geomechanical analysis respectively. Since spatial and temporal correlation is the strongest for the DFW Airport earthquakes, a more detailed analysis is performed on both of the parameters for this area.

The first data to be re-examined is the permeability input values for the pore pressure modeling in the areas of interest. In theory, since there is some level of uncertainty on the value of thickness, *h*, used for the formation, a re-examination of *kh* should be performed. In this analysis, however, *h*, is assumed to be fixed as given input data and the value of *k* is investigated. Assuming that the in-situ stress data is accurate, the pore pressure required to cause frictional sliding of faults based on the Coulomb failure is given by the plots shown in Figure 3.23 and Figure 3.24 for the lower Ellenburger layer and the basement layer respectively. For the Ellenburger layer, the pore

pressure change required to cause fault slippage is 1,600 psi (11.03 MPa); and for the basement layer, the pore pressure change required to cause fault slippage is 2,800 psi (19.31 MPa). Then, the wellbore pressure response from the simulation can be matched to the pore pressure required to cause fault slippage by varying the *k*.

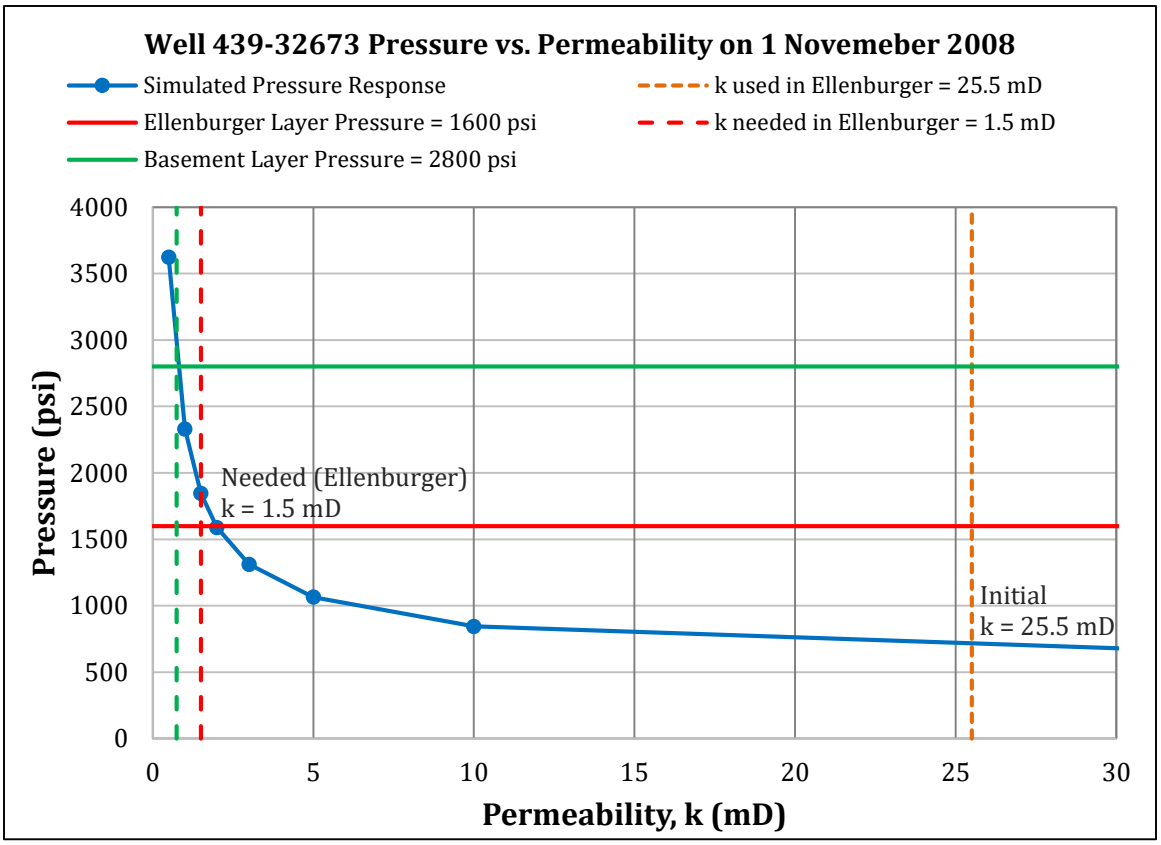

Figure 3.26: Pressure vs. permeability plot for Well 439-32673 on 1 November 2008.

Based on the pressure matching that was already performed as part of the permeability determination for layer 8, the pressure vs. permeability plot is shown in Figure 3.26. The plot shown on Figure 3.26, was developed based on the wellbore pressure response from Well 439-32673 (South Well in DFW Airport earthquakes analysis) located in Tarrant County, where spatial and temporal correlations between the

earthquake swarm and the increased in pore pressure are strongest. As can be seen from the plot, to reach the pore pressure required to initiate slippage on favorably oriented faults in the lower Ellenburger formation, the permeability needed is 1.5 mD, a 10x reduction of the original permeability used in the simulation for the area. Permeability in the pore pressure modeling was assigned by county, and since there are at least 8 other wells spread out throughout Tarrant County, it shows how varied the permeability of the Ellenburger can be within the same county.

The second data to be re-examined is the value for S_{hmin}. Taking the DFW Airport earthquake swarm as the area of interest, based on the simulated pore pressure response at the time of earthquake occurrence, the required S_{hmin} to cause fault slippage can be computed using the equation provided below.

$$\frac{1.1 + 2.1194(P_{presponse} + P_i)}{3.1194} \leq S_{hmin} \tag{3.1}$$

Well 439-32673 was injecting between 10,252 ft (3.12 km) and 13,729 ft (4.18 km). The depth of injection for the determination of S_{hmin} was taken to be 11,991 ft (3.65 km), midway between the injection intervals. Taking the maximum pore pressure response of 400 psi (2.76 MPa) as the simulated pore pressure resulted in pore pressure response gradient of 0.033 psi/ft (0.75 MPa/km) and assuming an initial pore pressure of 0.433 psi/ft (9.79 MPa/km), the pore pressure required in the determination of S_{hmin} is 0.466 psi/ft (10.54 MPa/km). This will result in a critical S_{hmin} value of 0.67 psi/ft (15.16 MPa/km). Therefore, at the depth of 11,991 ft (3.65 km), the S_{hmin} required to cause slip on favorably oriented faults is 8,034 psi (55.39 MPa).

The value of S_{hmin} determined from the analysis is in agreement with S_{hmin} values that reported for the Barnett formation which was between 0.63 psi/ft (14.25 MPa/km) and 0.68 psi/ft (15.38 MPa/km) (Vermylen 2011). For the Ellenburger formation and the

basement, since limited constraint data are available, no other conclusion can be made. However, the results suggest that for the given areas of interest, it is possible that the pore pressure increased introduced by wastewater injection will be sufficient to cause favorably oriented faults to slip. A definite conclusion, however, would be dependent on the available formation properties and in-situ stress data for the areas of interest.

Chapter 4: Conclusions and Future Work

4.1 CONCLUSIONS

Spatial and temporal correlations between seismic activities and the location of pore pressure increase in the areas of interest are evident from the pore pressure modeling results. The level of spatial and temporal correlations varies between locations, however a clear visual spatial correlation can be observed. The pore pressure simulations results are summarized below.

For the DFW Airport earthquakes, based on the simulation results at the beginning of November 2008, areas of pore pressure increase throughout the lower Ellenberger can be observed. Two of the areas in particular, are located very near to the earthquake swarm. However, none of the areas with elevated pore pressure corresponded exactly to the earthquake locations. Upon incorporating the relocated earthquakes' locations in the analysis, it is evident that there is a strong spatial and temporal correlation between DFW airport's earthquake swarm and the area of pore pressure increase. Furthermore, the seismic events can be spatially correlated to a NE-SW trending mapped fault that corresponds to the location of increased pore pressure. The pore pressure change corresponding to the DFW Airport earthquake swarm is confined to an area of roughly 4 miles (6.44 km) by 4 miles (6.44 km). Furthermore, pore pressure change of 50 psi (0.34 MPa) and above is confined to an area of roughly 2 miles (3.22 km) by 2 miles (3.22 km).

For the Cleburne earthquakes, based on the simulation results, there is a strong spatial and temporal correlation between earthquake events and areas of increased pore pressure. The earthquake swarm in the Cleburne area appears to stop and start at a 2-year interval. This suggests that once pressure is released through an earthquake sequence, the pressure build-up has to occur again over a period of time before it reaches a level at

which another earthquake sequence can be triggered. Additionally, the Cleburne earthquakes occurred between two mapped faults instead of along the mapped faults. This suggests that there are other unmapped faults in the locations of the earthquakes. The maximum pore pressure increase associated with the Cleburne earthquakes was approximately 300 psi (2.07 MPa).

For the Azle earthquakes, the simulation results also showed correlations between seismic activities and areas of pore pressure increase. The pore pressure increase associated with the Azle earthquake swarm was approximately between 30 psi (0.20 MPa) and 120 psi (0.83 MPa). The pore pressure increase from the simulation is in the same order of the magnitude as the pore pressure increase from Hornbach et al.'s (2015) simulation. Furthermore, there is a time lag between the start of injection and the onset of the Azle earthquakes. It can be observed rom the results that pressure build-up occurred over time before earthquake events were recorded.

The simulation results for the basement showed no pressure response to injection activities since the permeability of the formation is low. However, it should be noted that faults and fractures in the basement could act as high permeability flow channels.

While correlations exist for all of the earthquake events and the locations of pore pressure increase, it should be noted that for the DFW Airport earthquakes, the correlation only appear once the relocated earthquake locations were compared to the earthquake sequence. The reason behind the lack of immediate correlation is because the USGS database is only accurate to within 1 mile (1.61 km) to 6 miles (9.66 km). The areas of pore pressure change that correspond to seismic activities in all three cases of interest are confined to within the USGS location uncertainty limit, thereby minimizing correlation uncertainty associated to earthquake locations.

The last case is perhaps the most interesting in comparison to the other cases. Analysis was performed on area where there was a significant increase in pore pressure; however, no earthquake events were recorded. One of the reasons why no earthquakes were observed in the areas of increased pore pressure is because there is no sizable fault in the area or perhaps no faults exist in that particular area. Another possibility is that there are faults and fractures, but they are not favorably oriented, hence making it difficult for slip to occur.

The top 50 wells with highest cumulative injection volume were also studied. From this study, it was observed that Johnson County has the highest number of wells injecting at high volume with the highest average cumulative volume by county injected. An interesting observation to be made is that both positive and negative correlation between earthquake events and injection volumes can be made in Johnson County.

From the geomechanical analysis, the pore pressure increase required to cause favorably oriented faults to slip is 0.29 psi/ft (6.56 MPa/km). The simulated pore pressure increase results in both the lower Ellenburger formation and in the basement may not be sufficient to cause favorably oriented faults to slip. However, there are uncertainties involved in the simulation that would affect the results. For example, it is possible that the simulated pore pressure is low because the initial pore pressure gradient was too low. Furthermore, there are uncertainties associated with the formation permeability and the in-situ stress data. To address these uncertainties, re-examination input data for pore pressure modeling and geomechanical analysis was performed.

Two input data for pore pressure modeling and geomechanical analysis, permeability and S_{hmin} respectively, were examined. Analysis for the DFW Airport earthquakes showed that for favorably oriented faults to slip, the permeability in the area where earthquake events occurred has to be lower than 1.5 mD in the lower Ellenburger

formation, a 10x reduction from the original permeability value used in the simulation. Furthermore, the critical S_{hmin} value to cause fault slippage in the area of interest was computed to be 0.67 psi/ft (15.16 MPa/km). With no further constraint data available, these values and analysis are the best that can be achieved for geomechanical analysis of fault slippage.

From the results presented in this study, it can be concluded that there are spatial and temporal correlations between the earthquake sequences of interest and areas of increase pore pressure. Furthermore, it can also be concluded that there are areas where pore pressure increase was observed but no earthquake events were recorded. From the geomechanical analysis, it can be concluded that the pore pressure increase from wastewater injection may be sufficient to cause favorably oriented faults to slip.

4.2 FUTURE WORK

There are many uncertainties associated with the pore pressure simulation and the geomechanical analysis in this study. This is in part due to the lack of publicly available data that can be used to better constrain the model. For future work, inclusion of fault locations, fault orientations, and the focal points of earthquake events would be important in order to further assess the mechanism of induced seismicity due to wastewater injection. Furthermore, accurate in-situ stress values, in particular S_{hmin}, are crucial in the understanding of whether or not an earthquake event is induced by wastewater injection. The inclusions of the data discussed, may be able to help better explain both the positive and negative correlations observed in this study.

Furthermore, a more realistic permeability model should be utilized in the layer of interest. Inclusion of available pressure-matched permeability in a more robust manner would result in a more realistic pore pressure response.

Appendix A: Permeability Pressure Matching Results

Appendix A presents pressure matching plots to determine permeability in the lower Ellenburger formation for all the wells where reasonable pressure data is available. On each plot, the blue curve represents recorded injection pressure data queried from the RRC; the red curve represents the best-matched wellbore pressure response from the simulation and the corresponding permeability (presented in the legend) is used as the basin permeability in the lower Ellenburger layer at that specific location; and the green curves show wellbore pressure response for different permeability for the particular well.

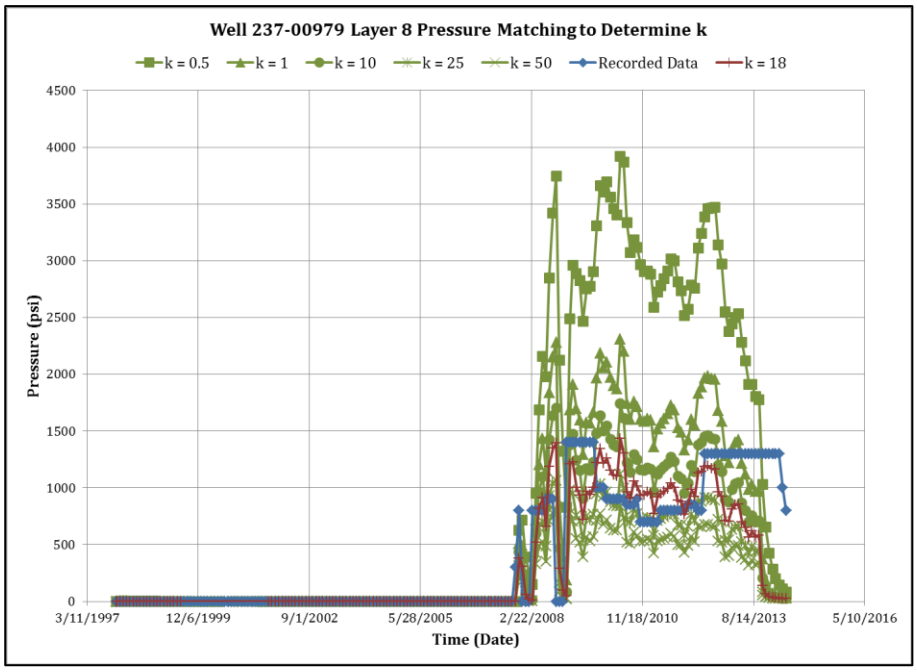

Figure A1: Pressure matching plot if Well 237-00979 to determine k in the lower Ellenburger formation.

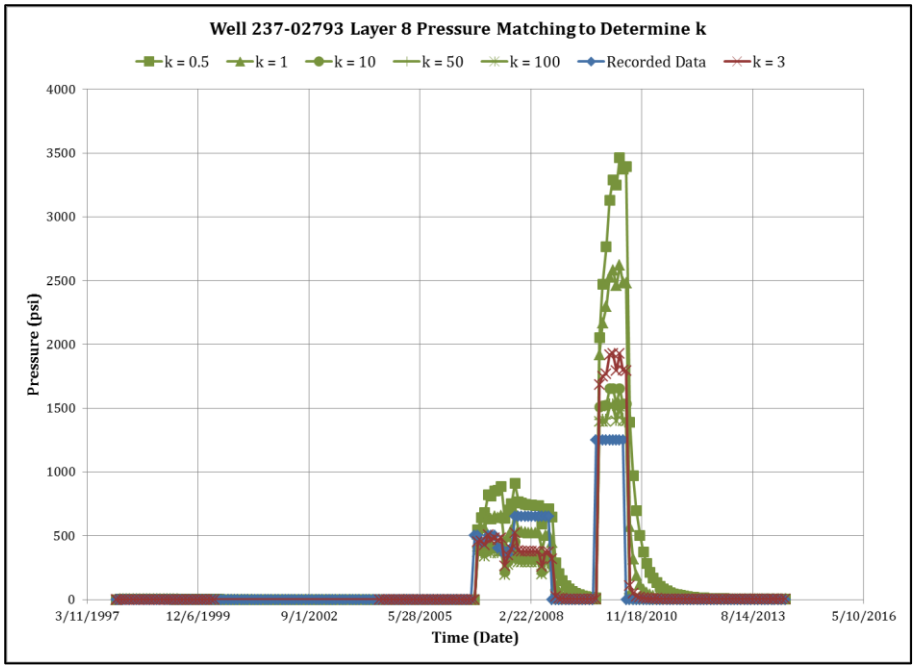

Figure A2: Pressure matching plot if Well 237-02793 to determine k in the lower Ellenburger formation.

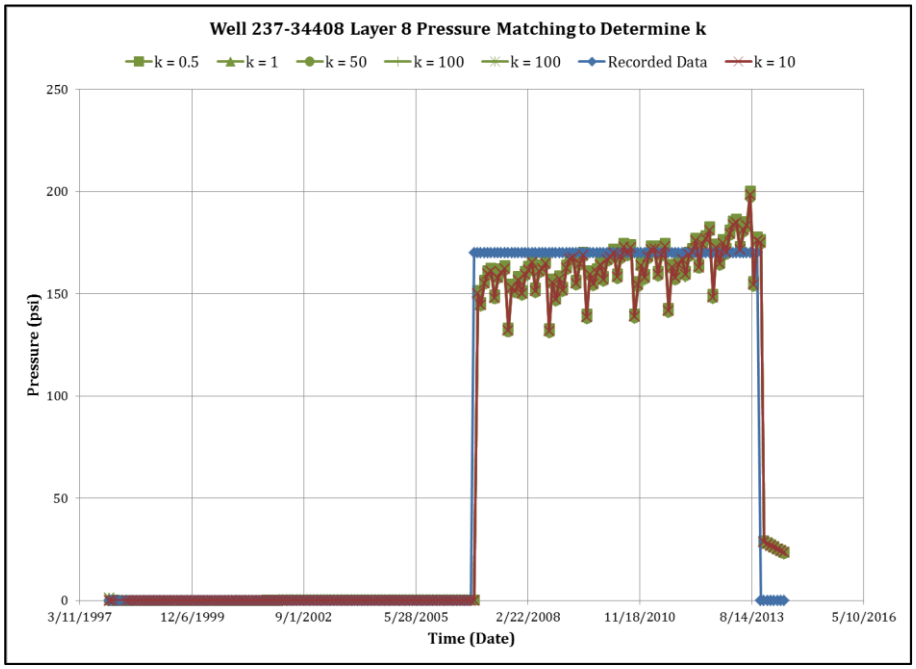

Figure A3: Pressure matching plot if Well 237-34408 to determine k in the lower Ellenburger formation.

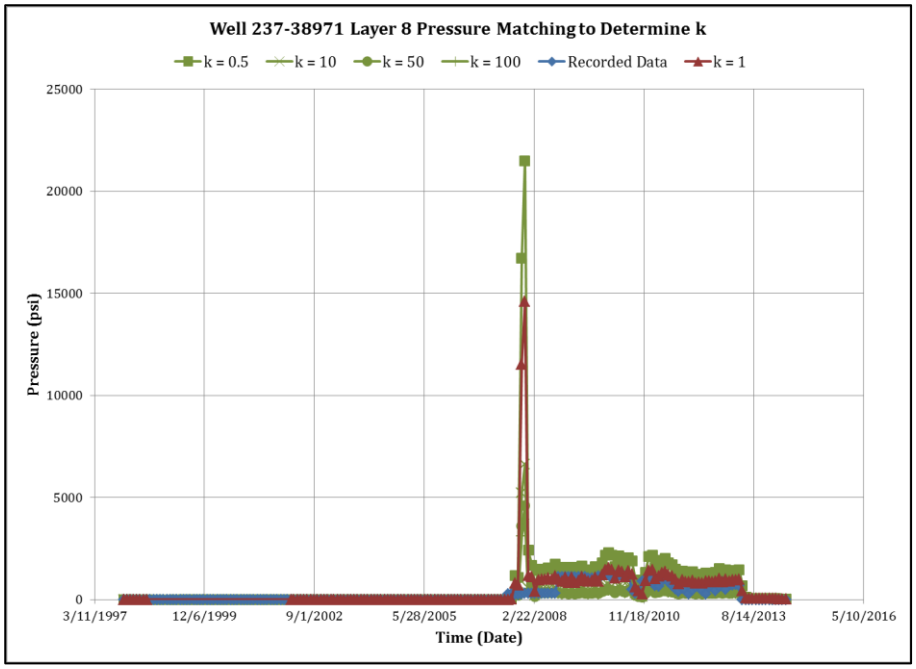

Figure A4: Pressure matching plot if Well 237-38971 to determine k in the lower Ellenburger formation.

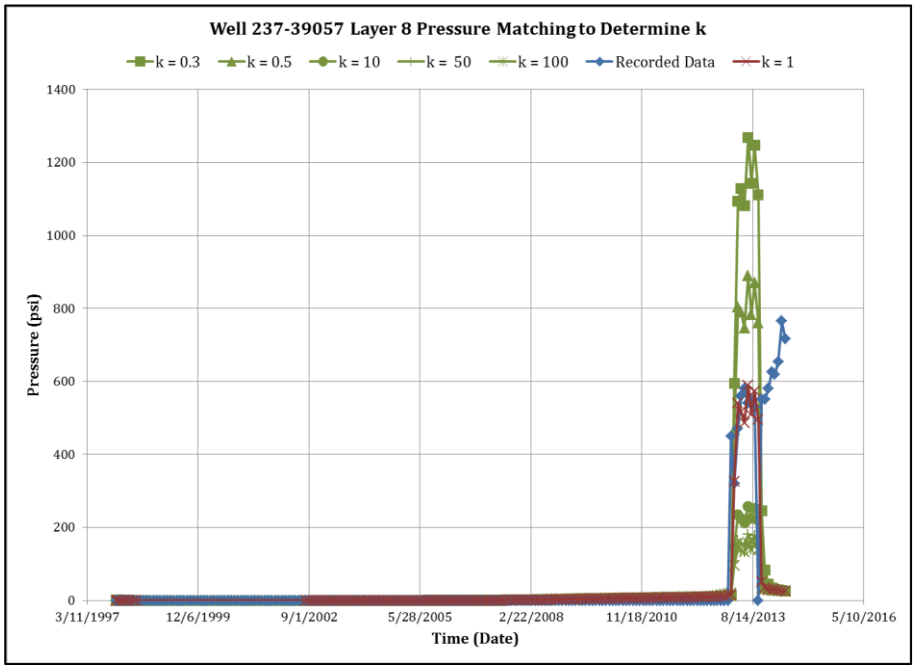

Figure A5: Pressure matching plot if Well 237-39057 to determine k in the lower Ellenburger Formation.

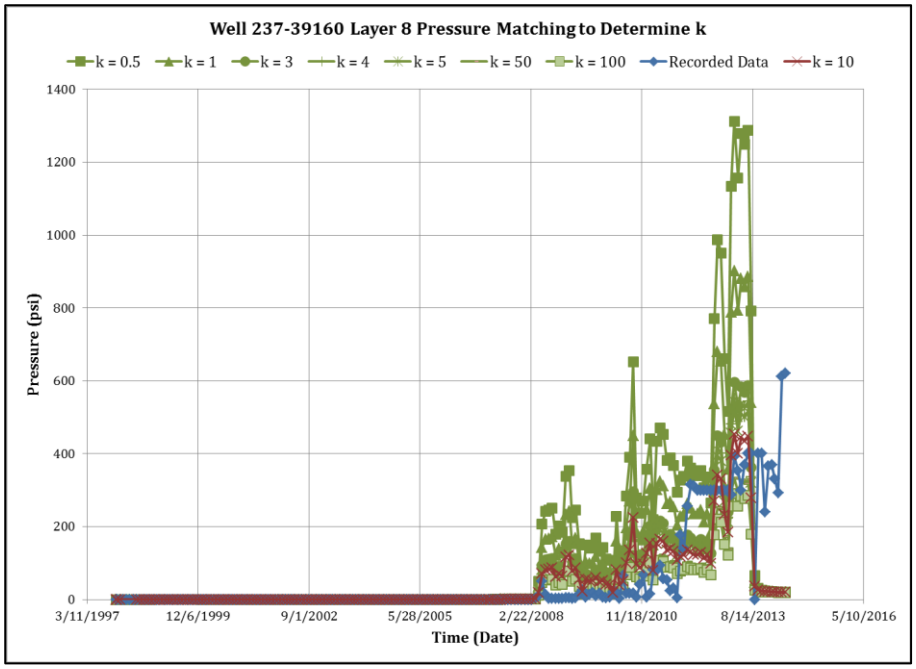

Figure A6: Pressure matching plot if Well 237-39160 to determine k in the lower Ellenburger Formation.

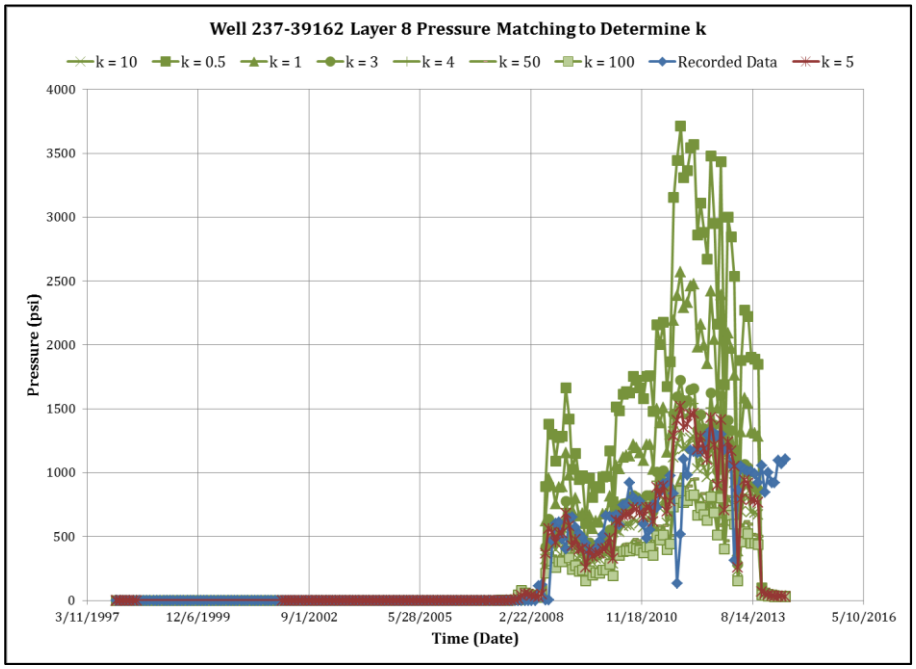

Figure A7: Pressure matching plot if Well 237-39162 to determine k in the lower Ellenburger Formation.

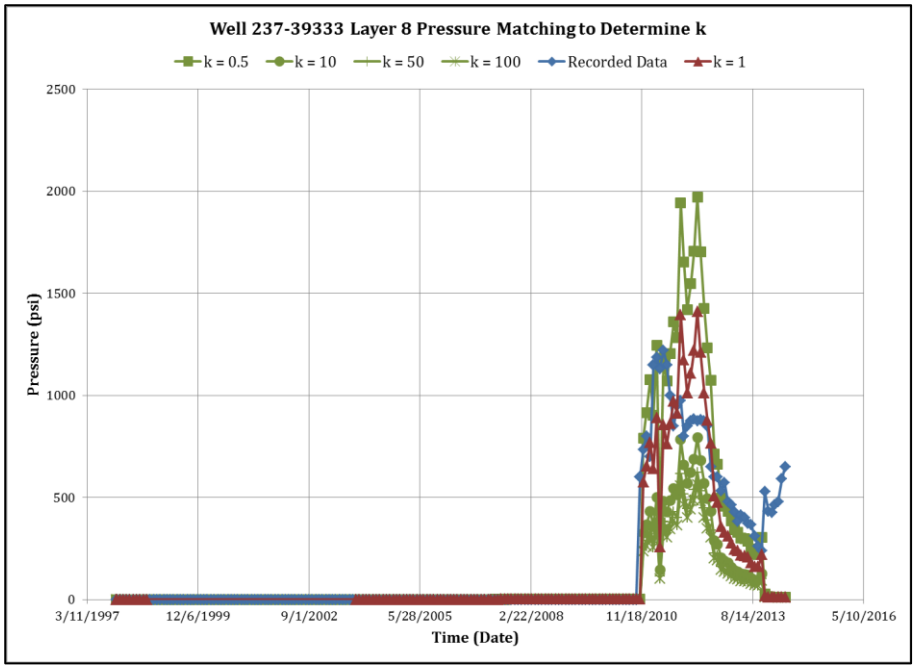

Figure A8: Pressure matching plot if Well 237-39333 to determine k in the lower Ellenburger Formation.

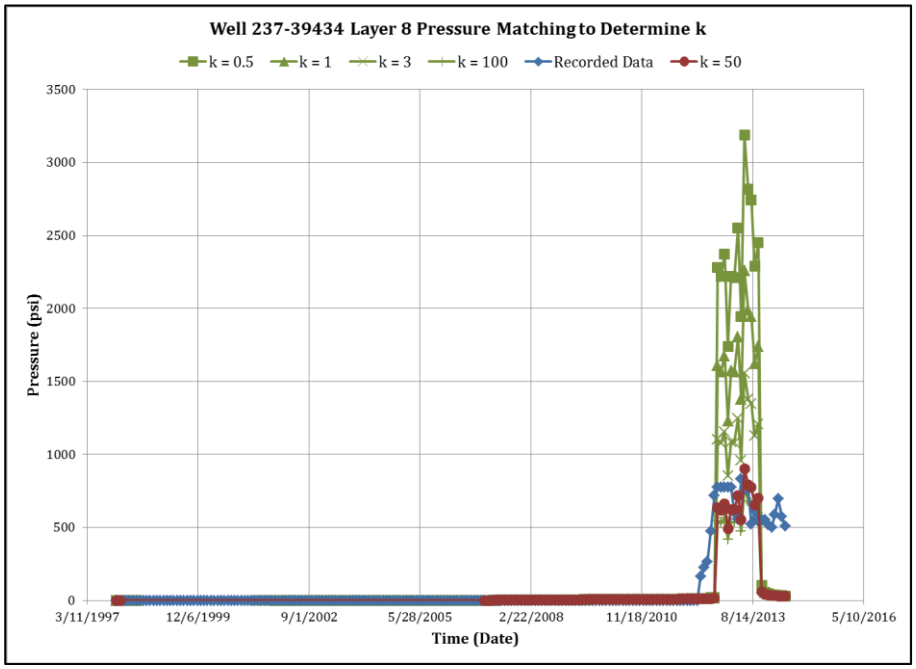

Figure A9: Pressure matching plot if Well 237-39434 to determine k in the lower Ellenburger Formation.

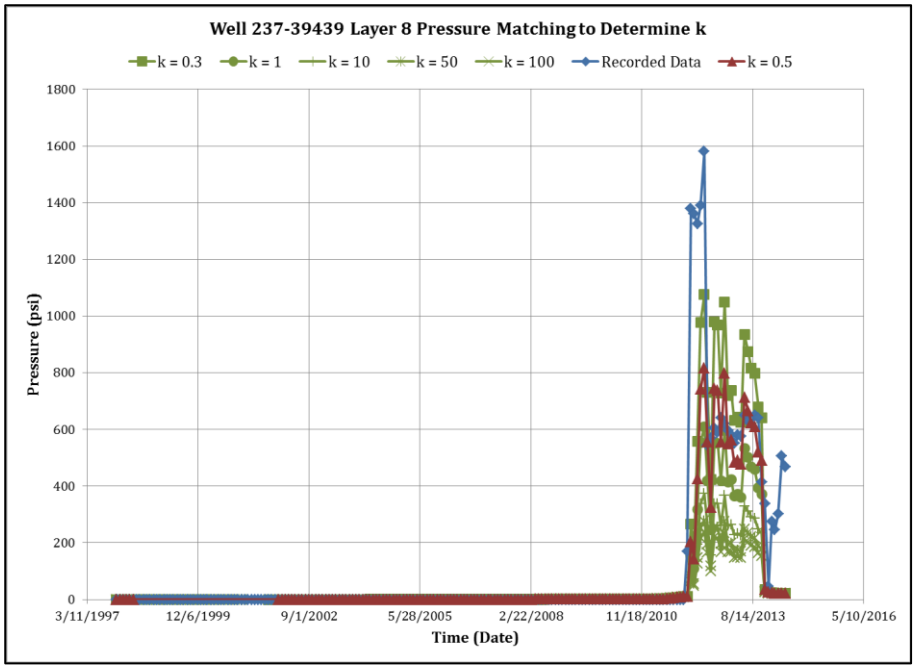

Figure A10: Pressure matching plot if Well 237-39439 to determine k in the lower Ellenburger Formation.

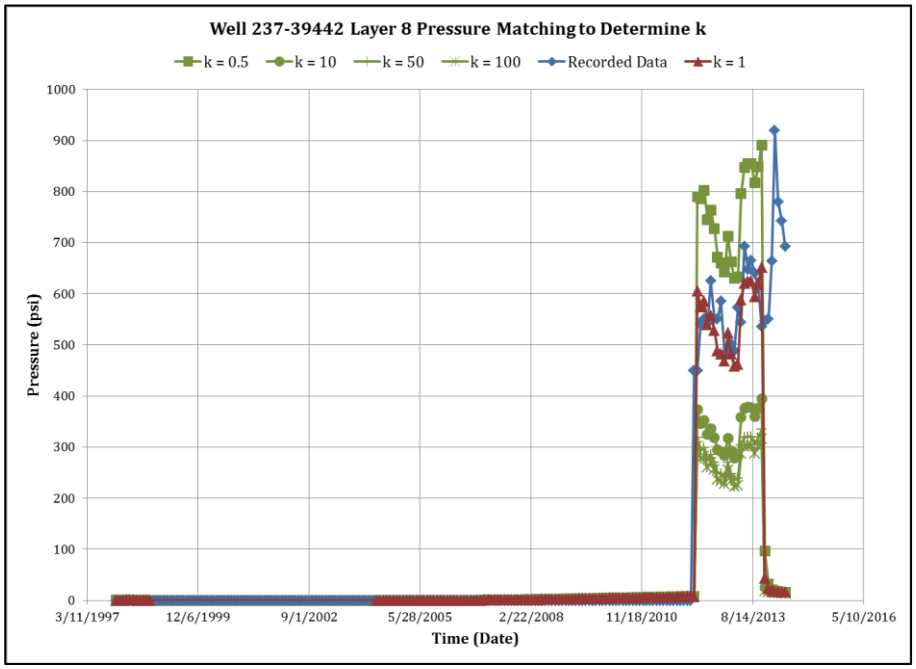

Figure A11: Pressure matching plot if Well 237-39442 to determine k in the lower Ellenburger Formation.

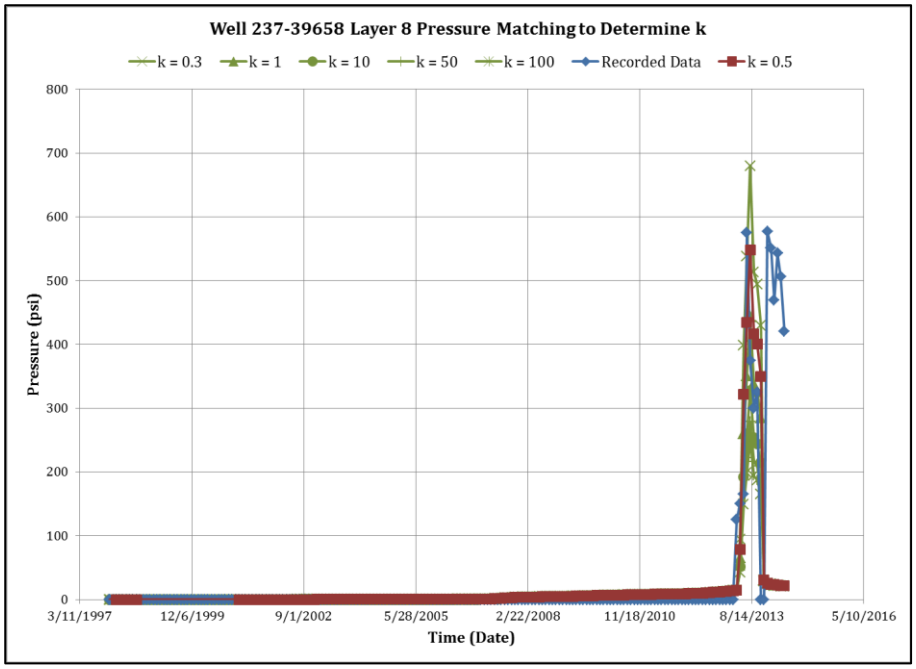

Figure A12: Pressure matching plot if Well 237-39658 to determine k in the lower Ellenburger Formation.

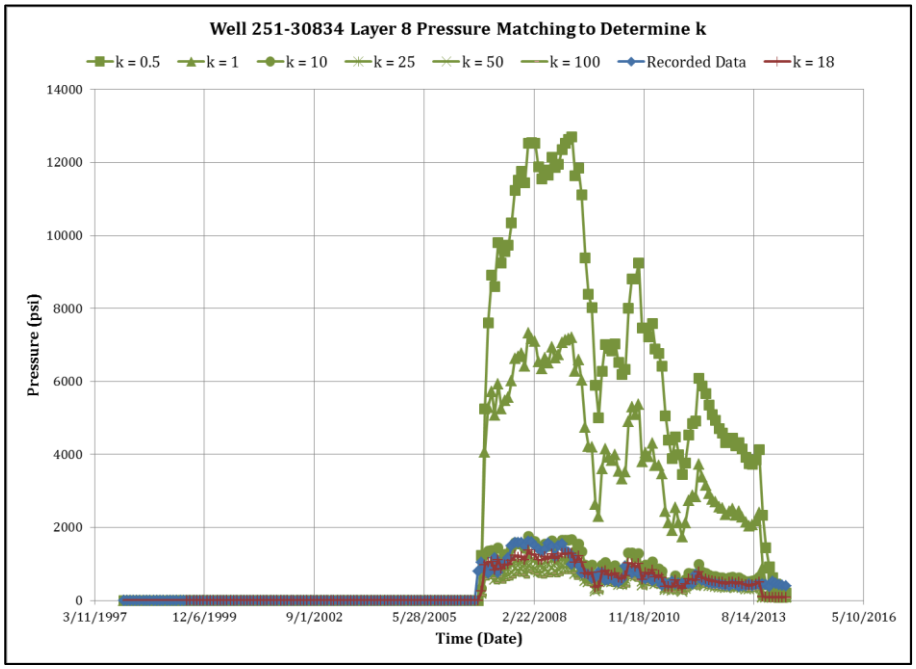

Figure A13: Pressure matching plot if Well 251-30834 to determine k in the lower Ellenburger Formation.

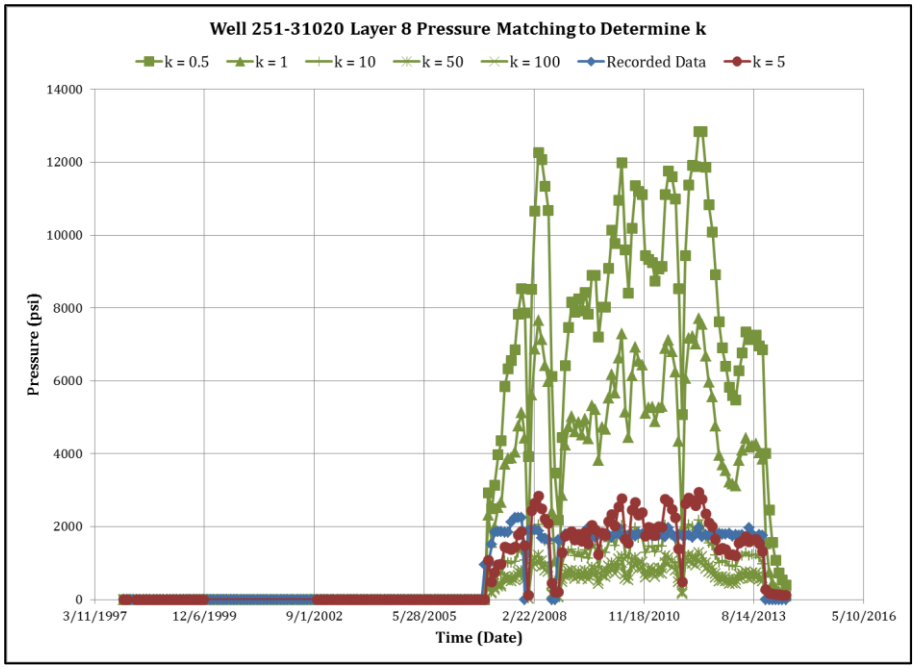

Figure A14: Pressure matching plot if Well 251-31020 to determine k in the lower Ellenburger Formation.

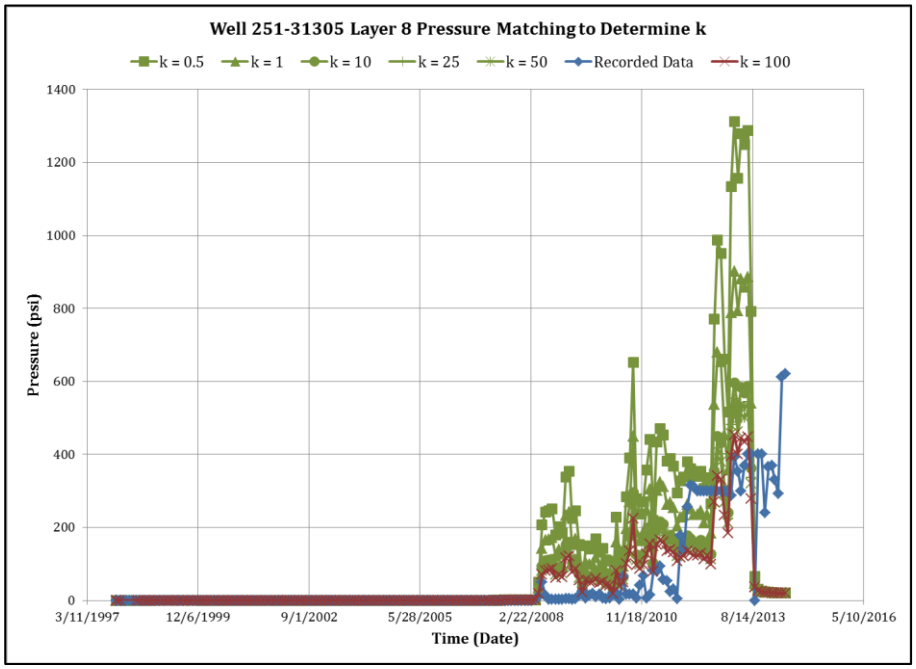

Figure A15: Pressure matching plot if Well 251-31305 to determine k in the lower Ellenburger Formation.

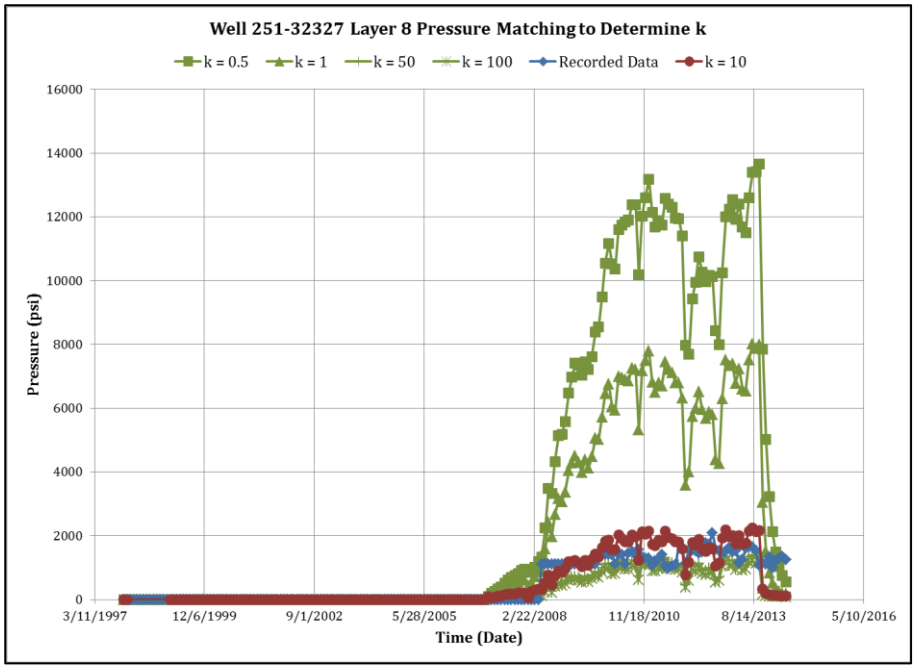

Figure A16: Pressure matching plot if Well 251-32327 to determine k in the lower Ellenburger Formation.

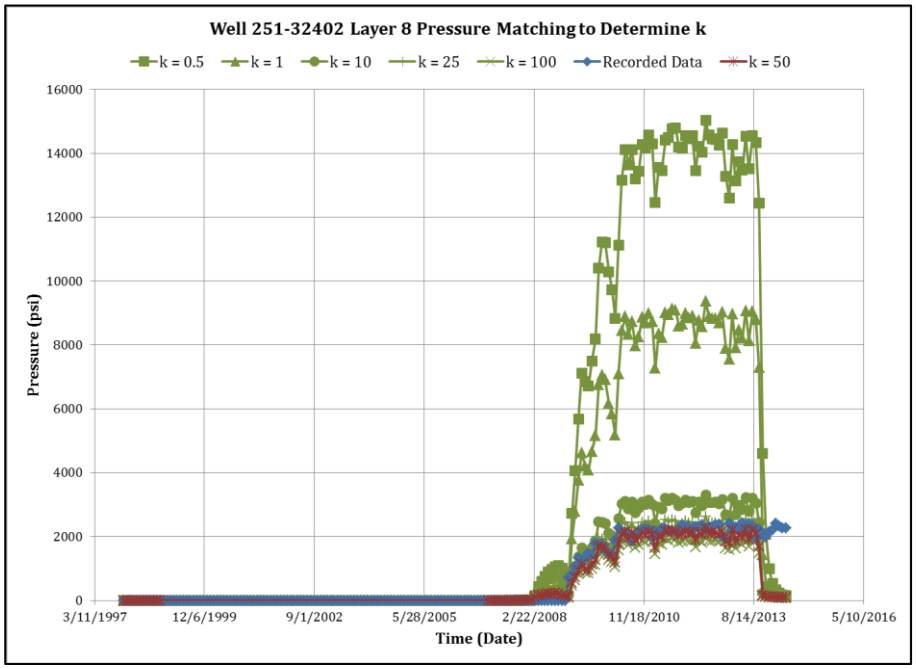

Figure A17: Pressure matching plot if Well 251-32402 to determine k in the lower Ellenburger Formation.

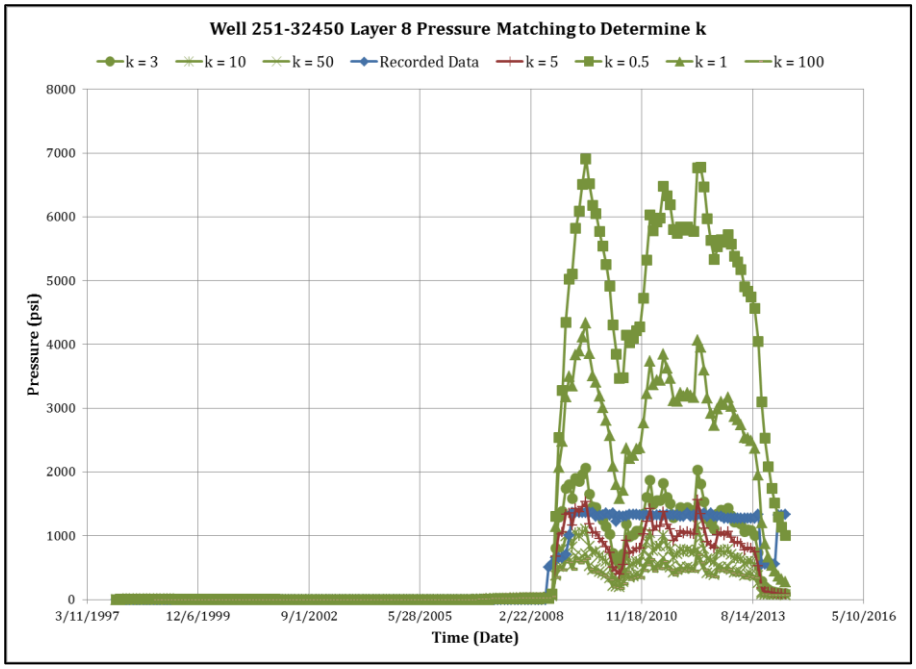

Figure A18: Pressure matching plot if Well 251-32450 to determine k in the lower Ellenburger Formation.

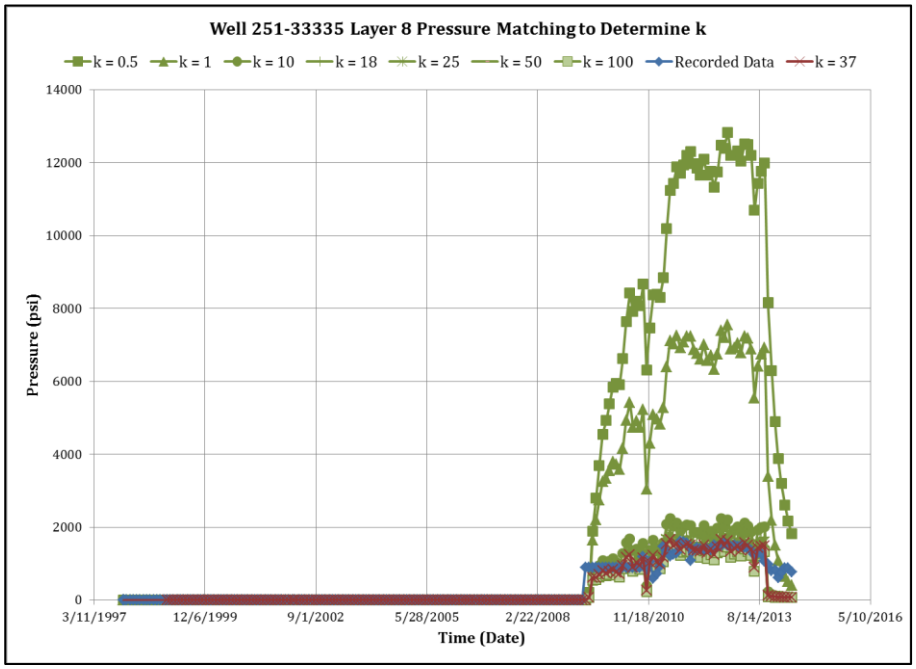

Figure A19: Pressure matching plot if Well 251-33335 to determine k in the lower Ellenburger Formation.

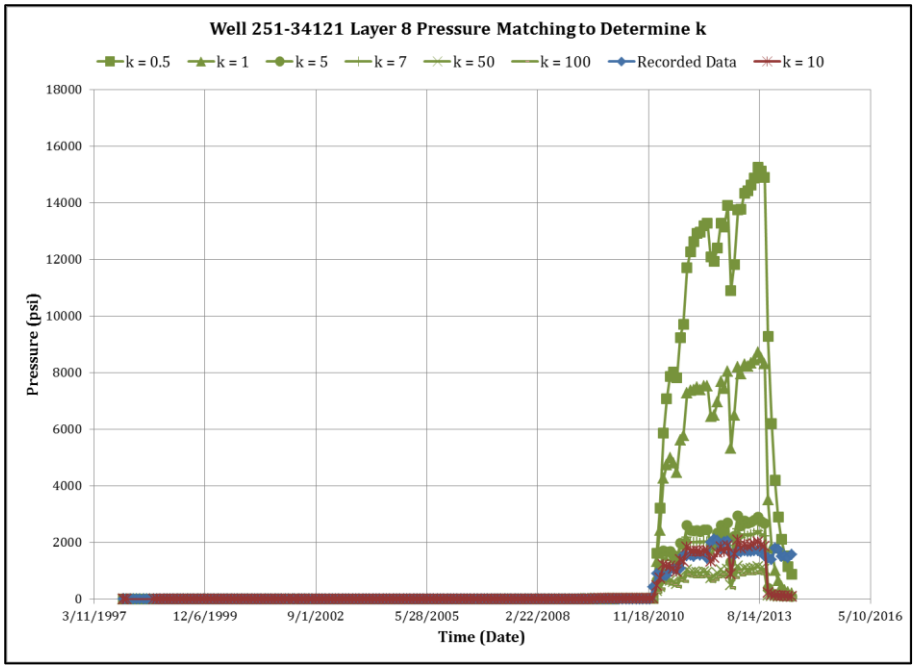

Figure A20: Pressure matching plot if Well 251-34121 to determine k in the lower Ellenburger Formation.

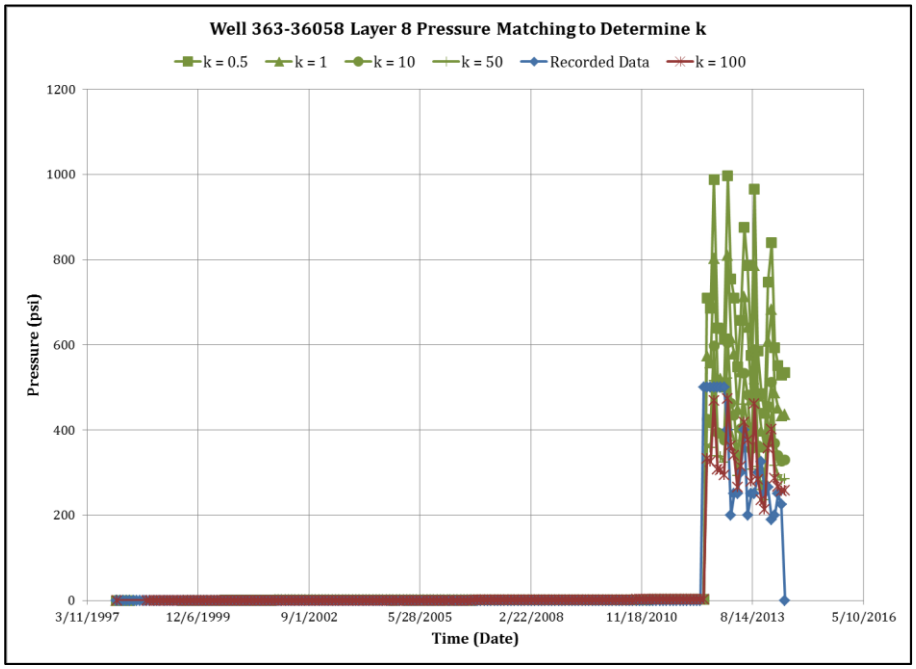

Figure A21: Pressure matching plot if Well 363-36058 to determine k in the lower Ellenburger Formation.

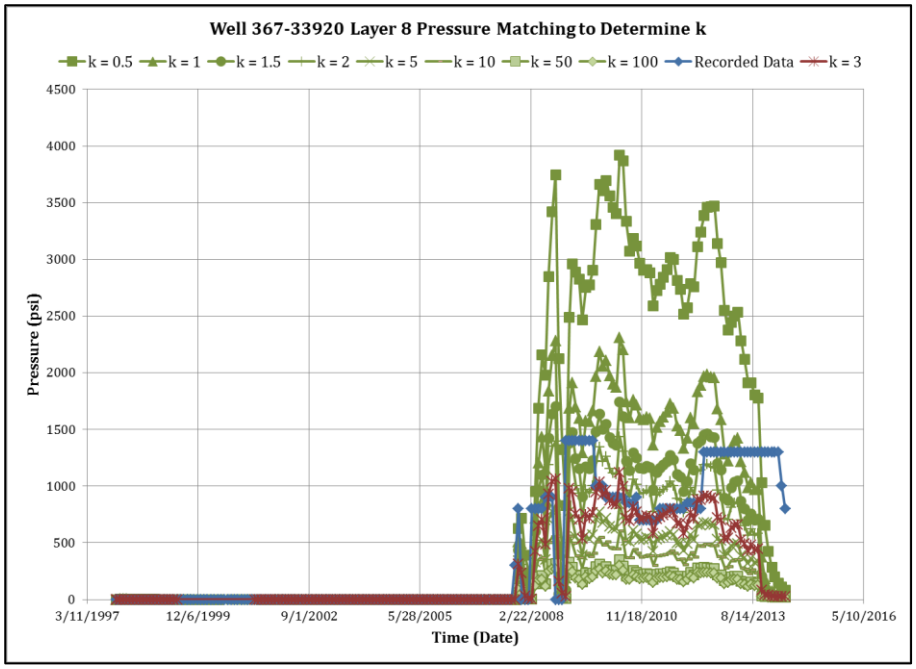

Figure A22: Pressure matching plot if Well 367-33920 to determine k in the lower Ellenburger Formation.

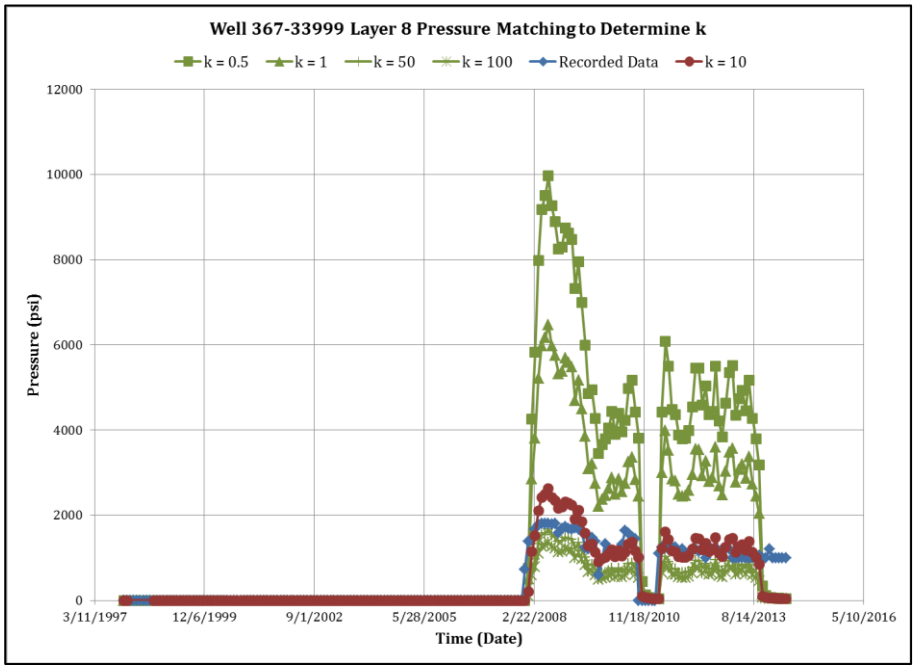

Figure A23: Pressure matching plot if Well 367-33999 to determine k in the lower Ellenburger Formation.

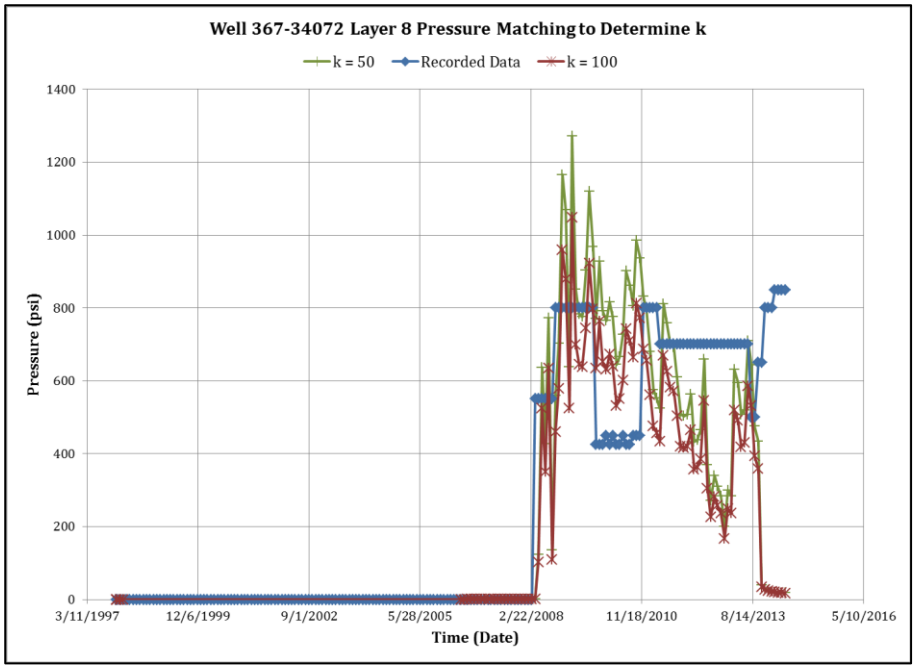

Figure A24: Pressure matching plot if Well 367-34072 to determine k in the lower Ellenburger Formation.

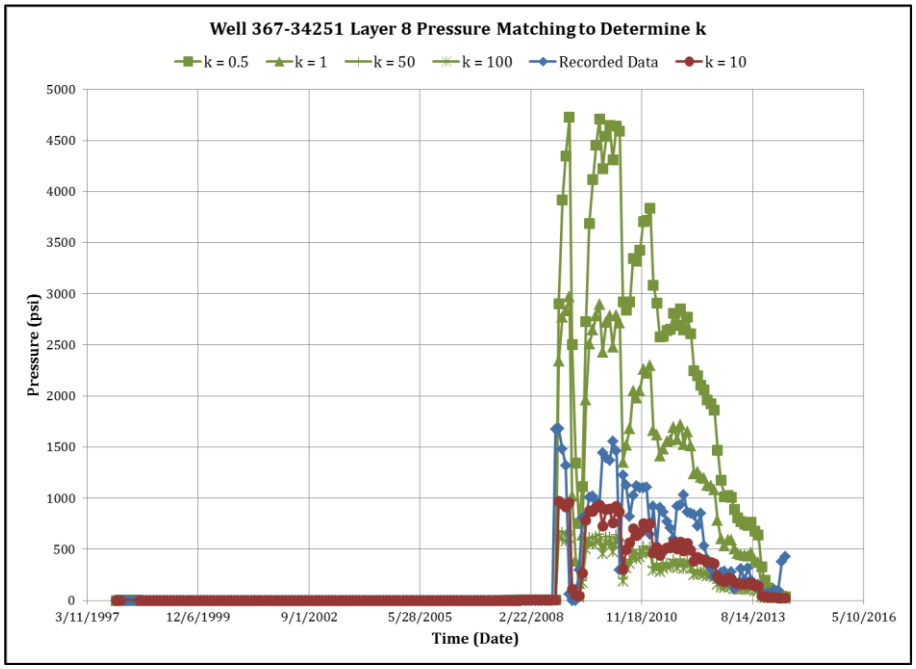

Figure A25: Pressure matching plot if Well 367-34251 to determine k in the lower Ellenburger Formation.

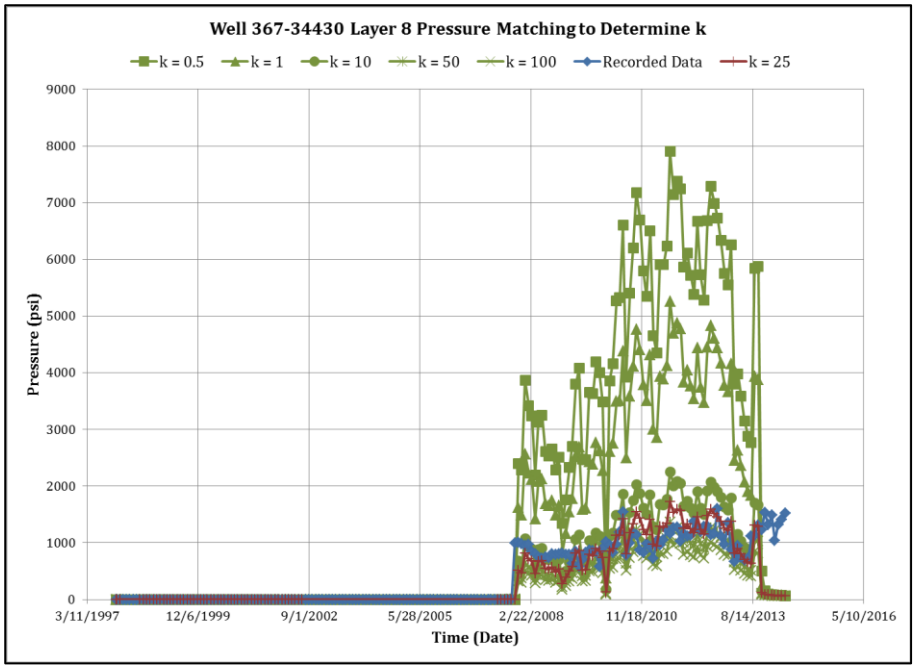

Figure A26: Pressure matching plot if Well 367-34430 to determine k in the lower Ellenburger Formation.

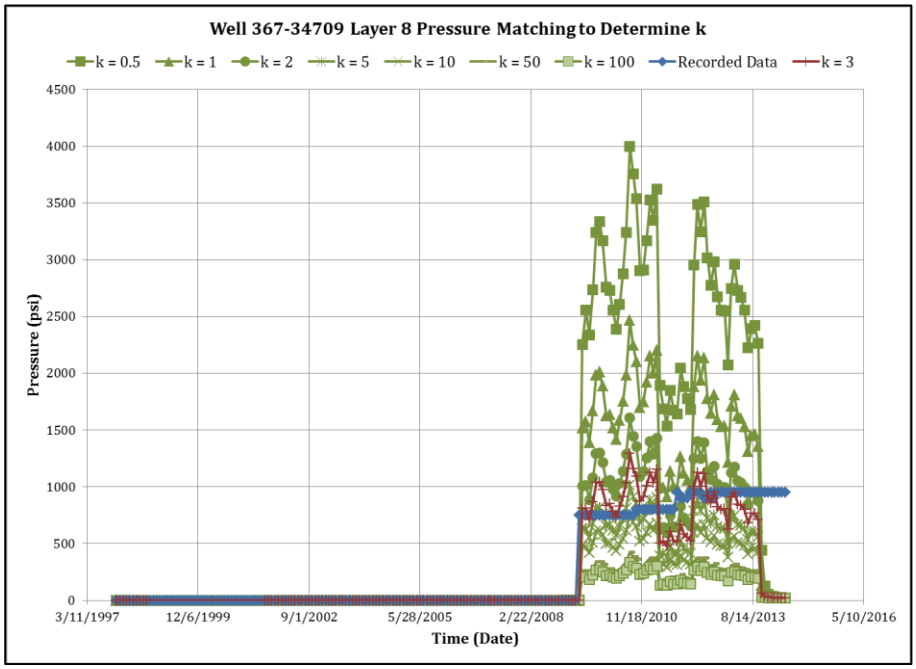

Figure A27: Pressure matching plot if Well 367-34709 to determine k in the lower Ellenburger Formation.

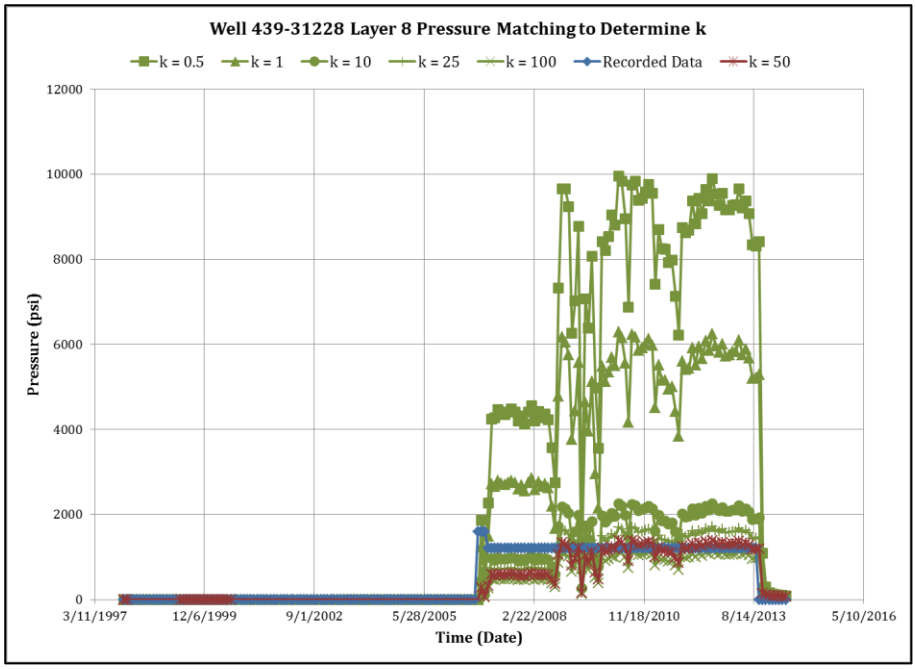

Figure A28: Pressure matching plot if Well 439-31228 to determine k in the lower Ellenburger Formation.

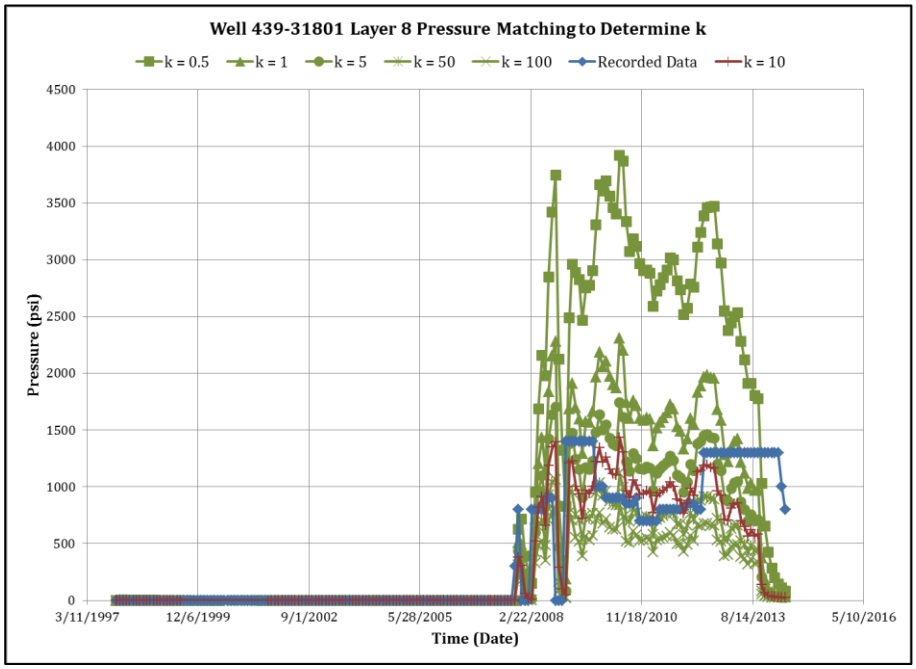

Figure A29: Pressure matching plot if Well 439-31801 to determine k in the lower Ellenburger Formation.

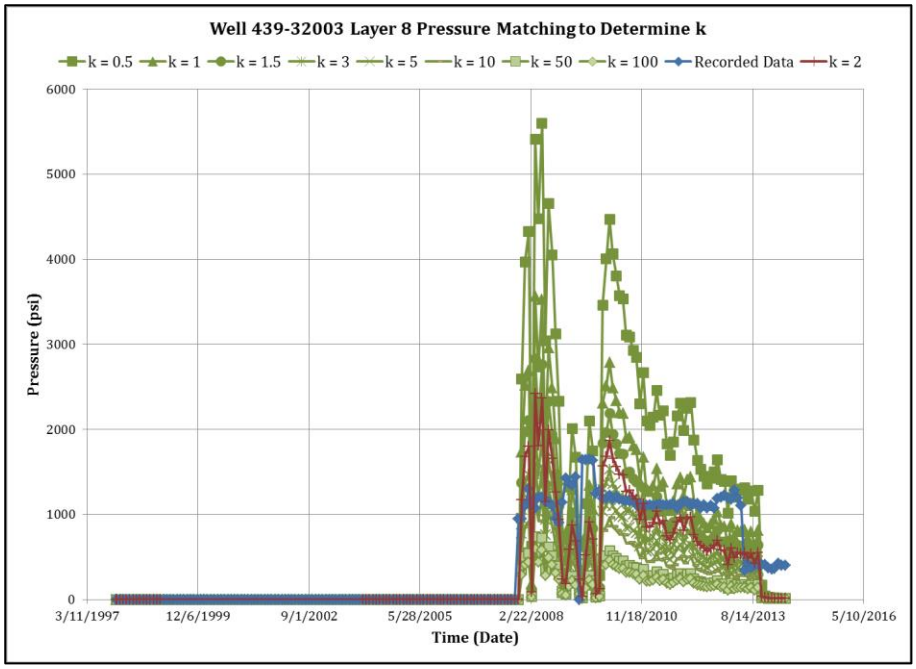

Figure A30: Pressure matching plot if Well 439-32003 to determine k in the lower Ellenburger Formation.

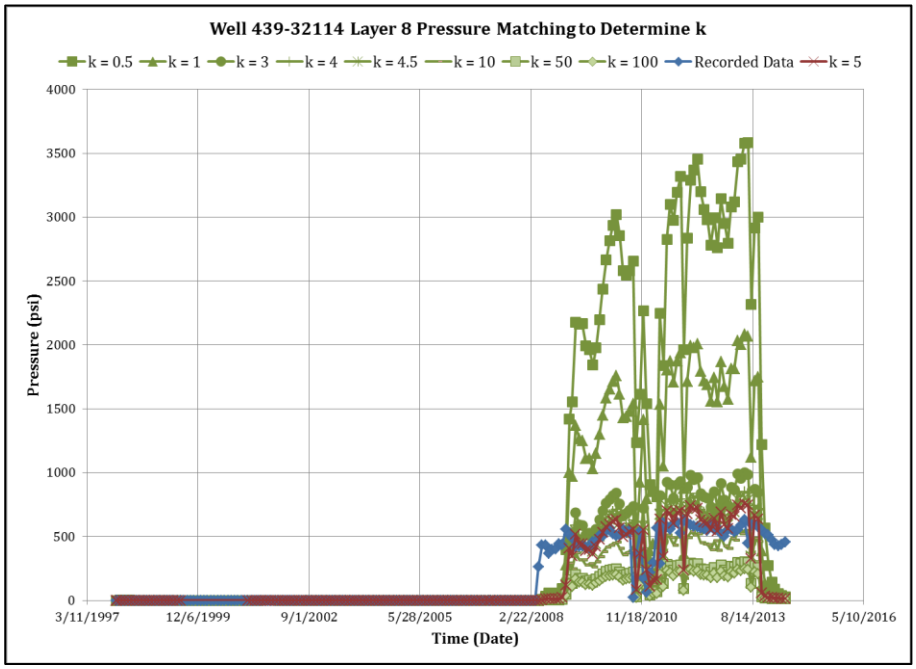

Figure A31: Pressure matching plot if Well 439-32114 to determine k in the lower Ellenburger Formation.

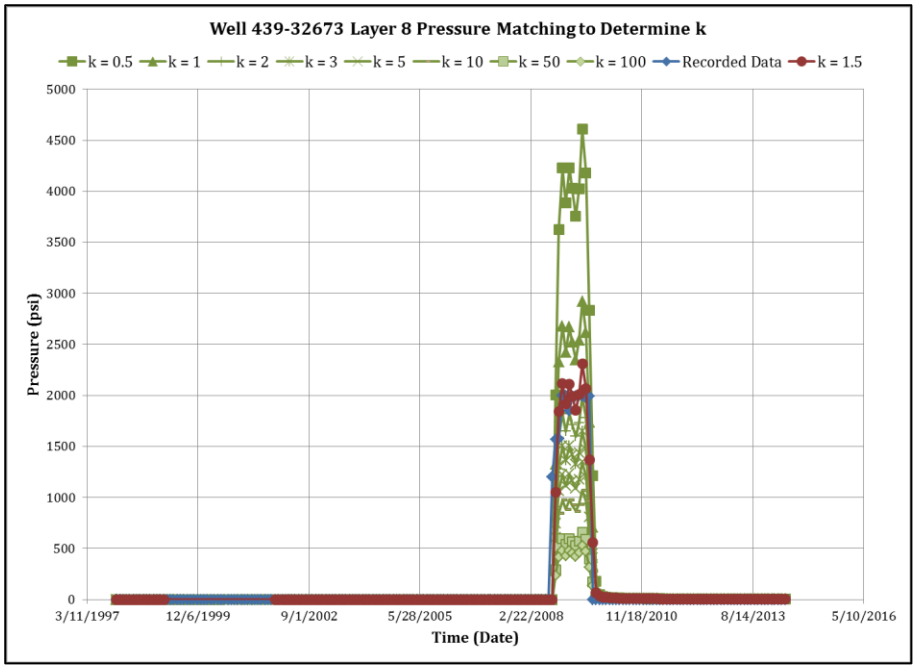

Figure A32: Pressure matching plot if Well 439-32673 to determine k in the lower Ellenburger Formation.

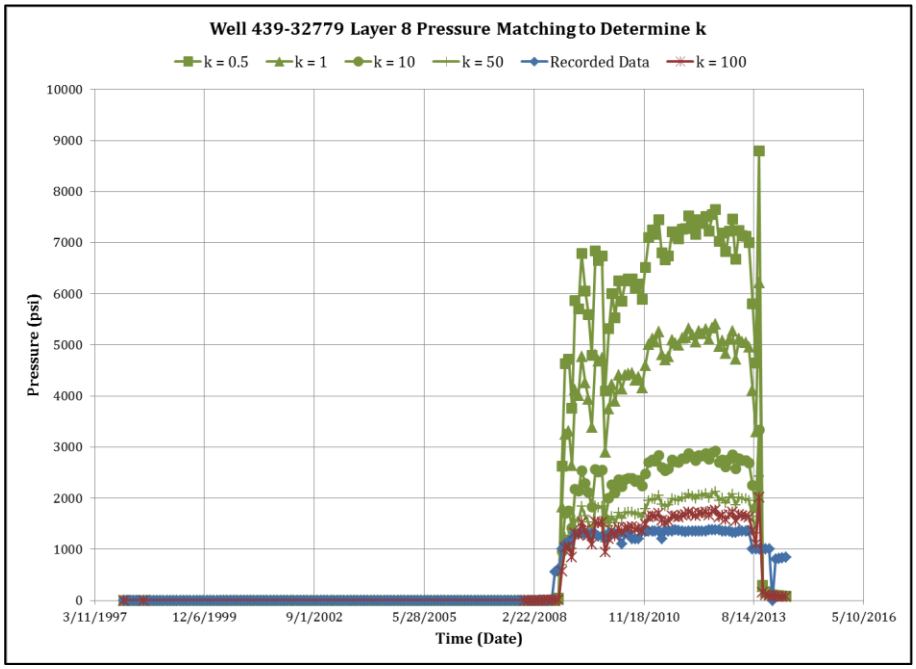

Figure A33: Pressure matching plot if Well 439-32779 to determine k in the lower Ellenburger Formation.

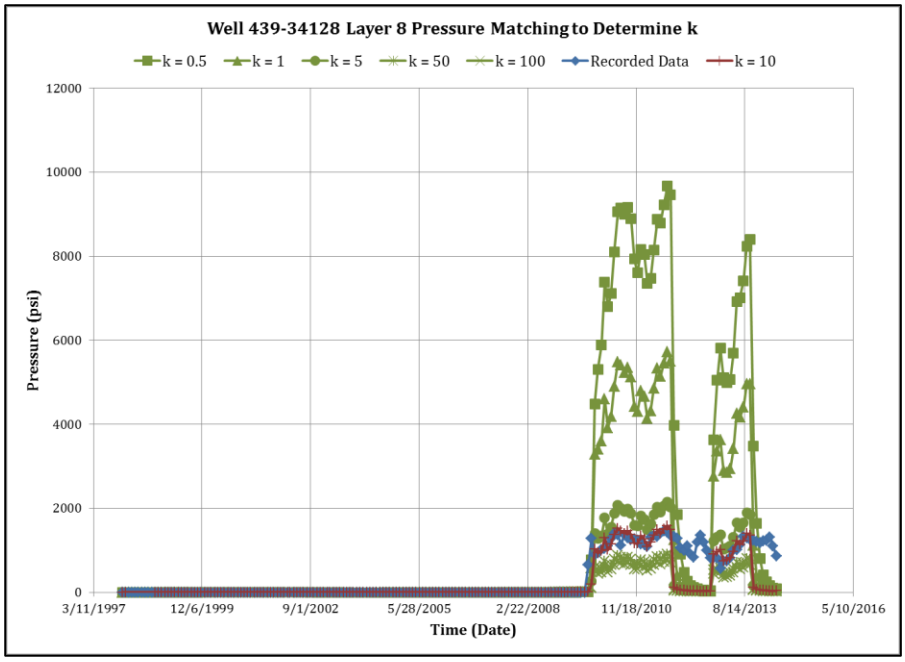

Figure A34: Pressure matching plot if Well 439-34128 to determine k in the lower Ellenburger Formation.

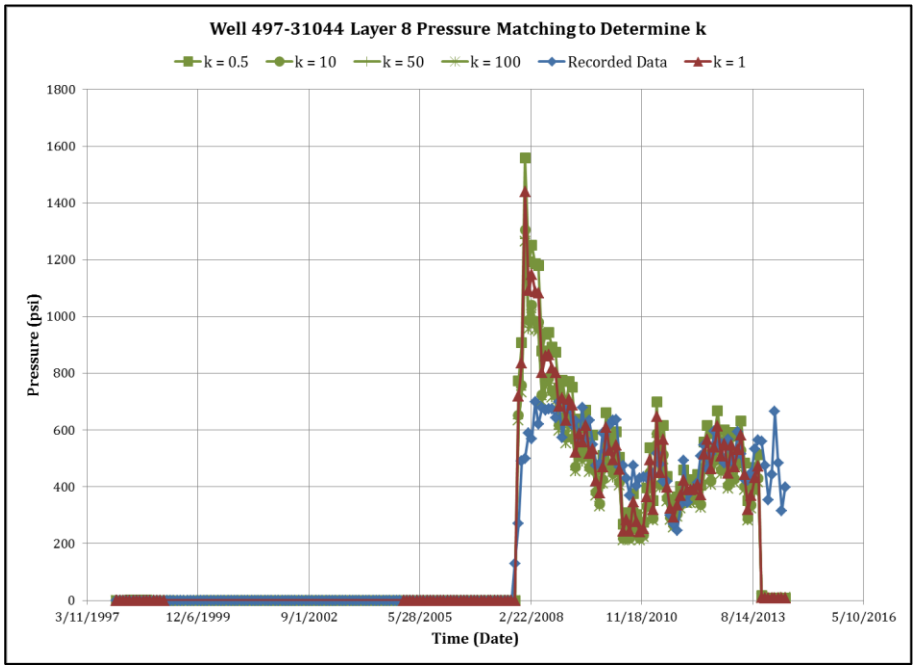

Figure A35: Pressure matching plot if Well 497-31044 to determine k in the lower Ellenburger Formation.

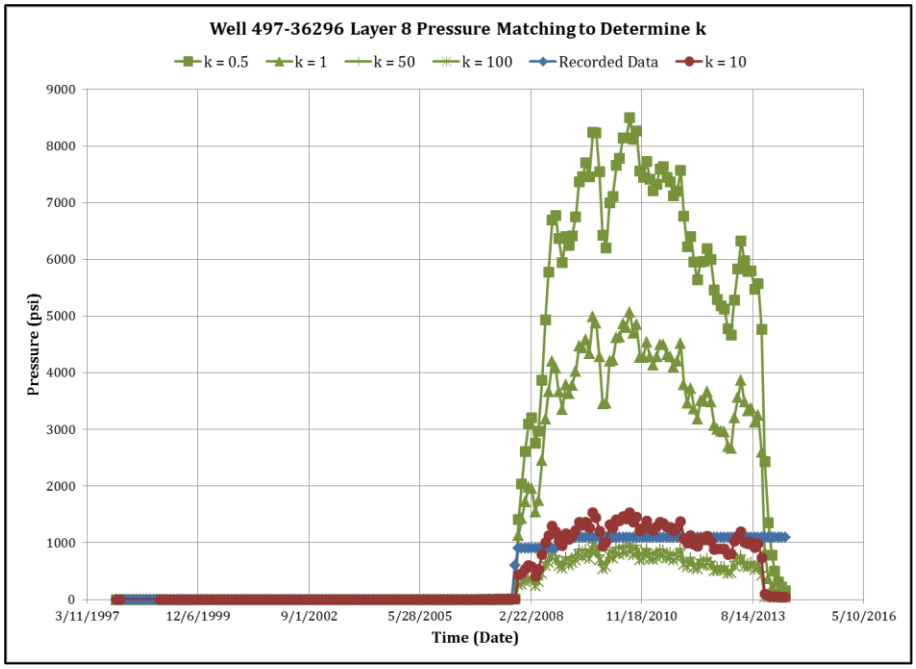

Figure A36: Pressure matching plot if Well 497-36296 to determine k in the lower Ellenburger Formation.

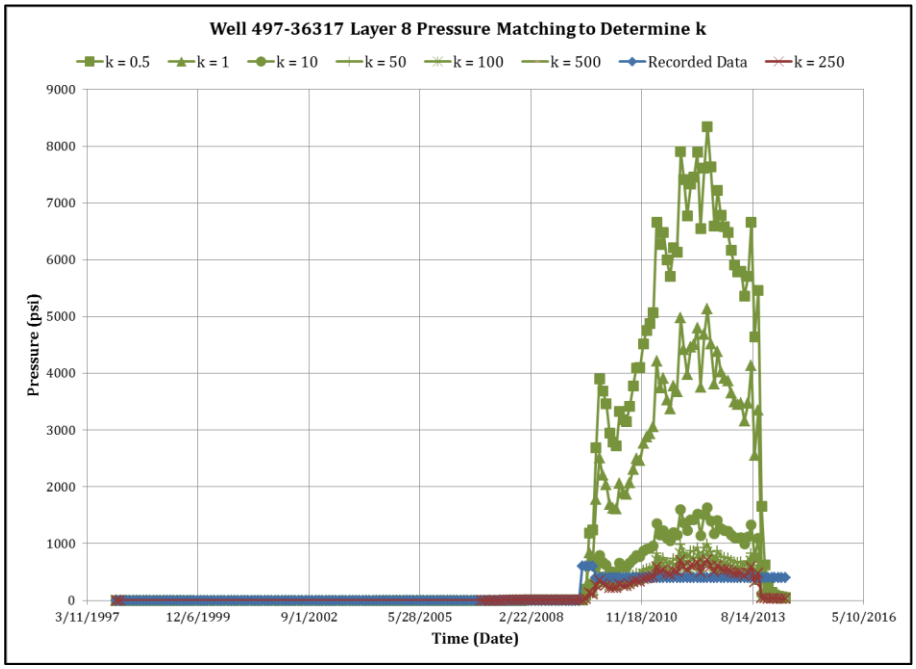

Figure A37: Pressure matching plot if Well 497-36317 to determine k in the lower Ellenburger Formation.

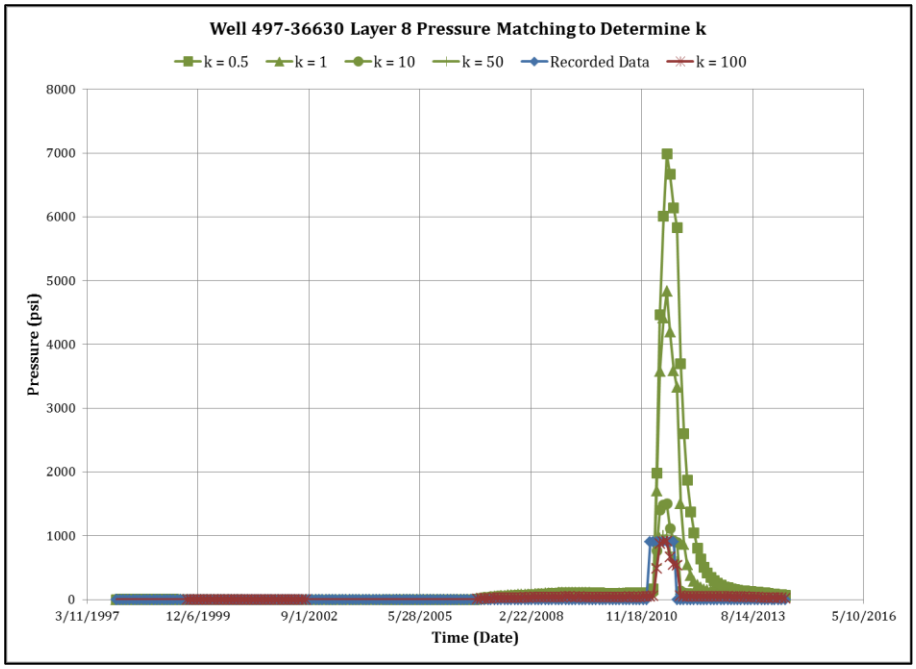

Figure A38: Pressure matching plot if Well 497-36630 to determine k in the lower Ellenburger Formation.

Appendix B: Map View of Pore Pressure Simulation Results

Appendix B presents the complete pore pressure simulation results for all 9 layers in the model for the three areas of interest at the end of each earthquake sequence.

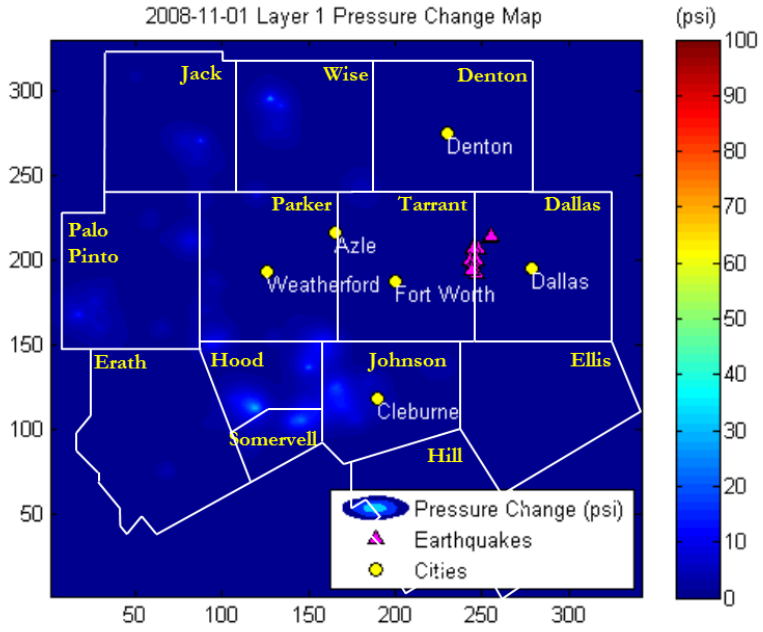

Figure B1: DFW Airport earthquakes Layer 1 pore pressure change plot.

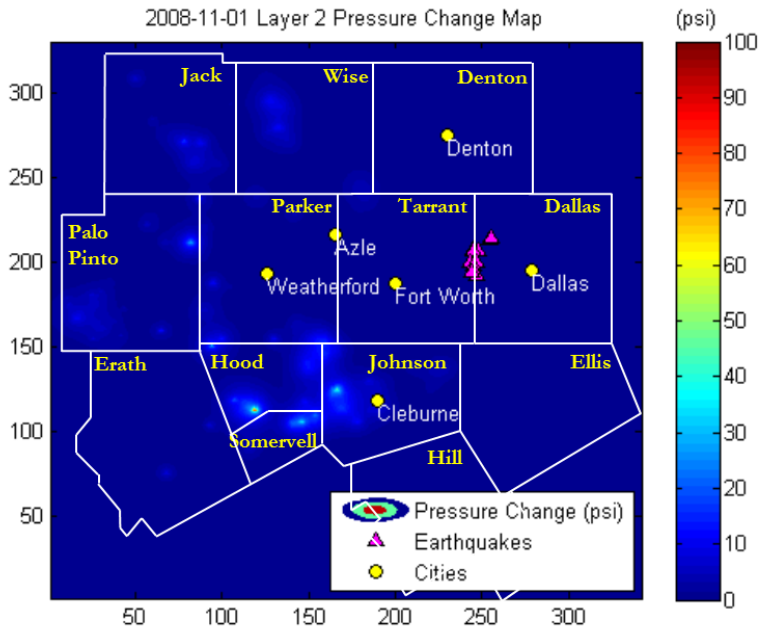

Figure B2: DFW Airport earthquakes Layer 2 pore pressure change plot.

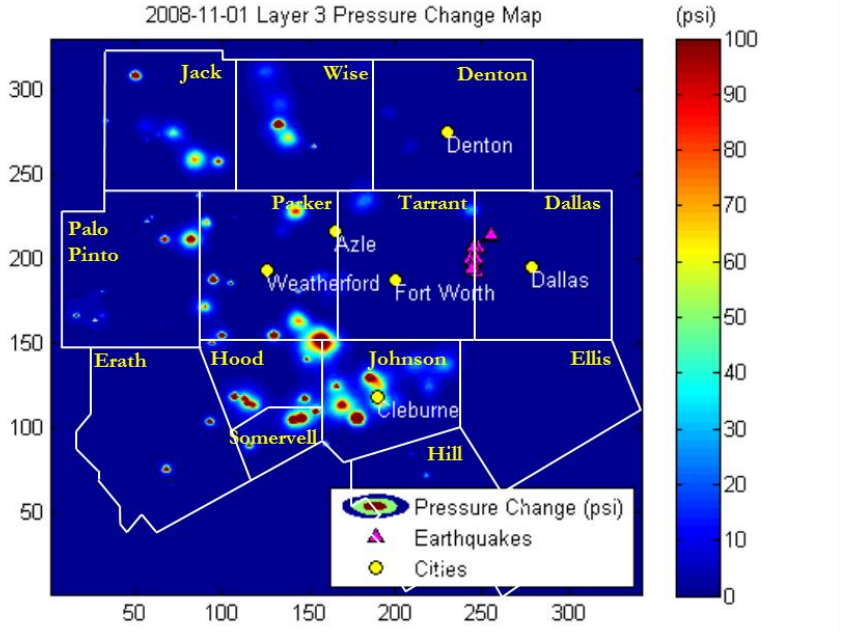

Figure B3: DFW Airport earthquakes Layer 3 pore pressure change plot.

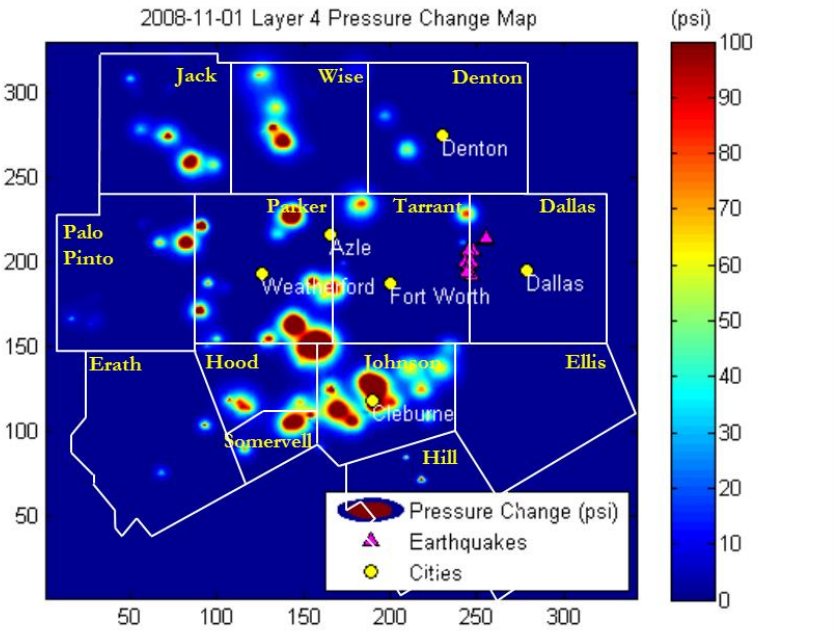

Figure B4: DFW Airport earthquakes Layer 4 pore pressure change plot.

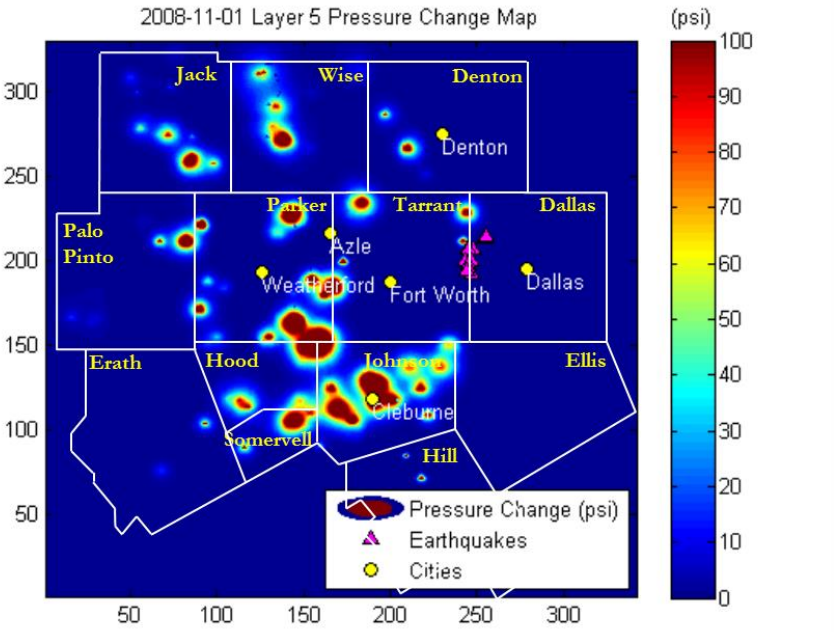

Figure B5: DFW Airport earthquakes Layer 5 pore pressure change plot.

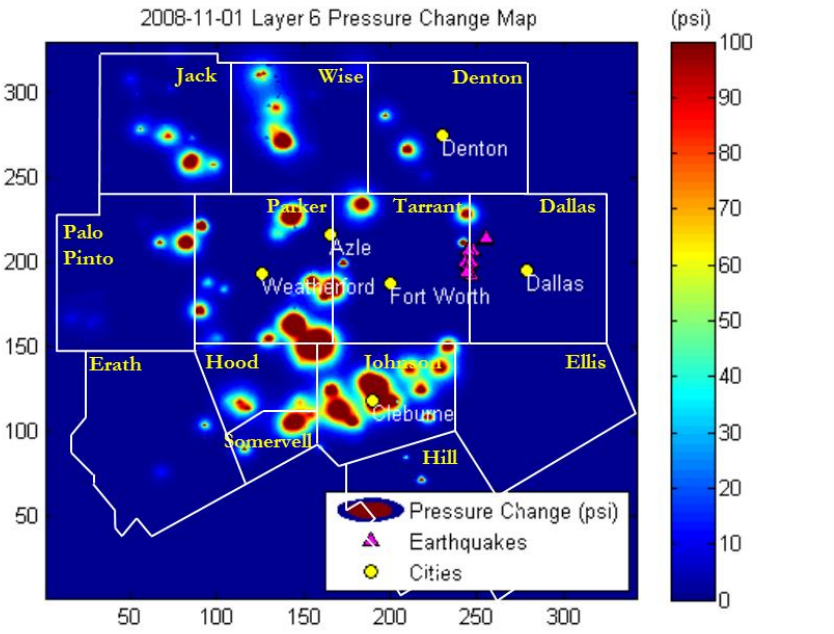

Figure B6: DFW Airport earthquakes Layer 6 pore pressure change plot.

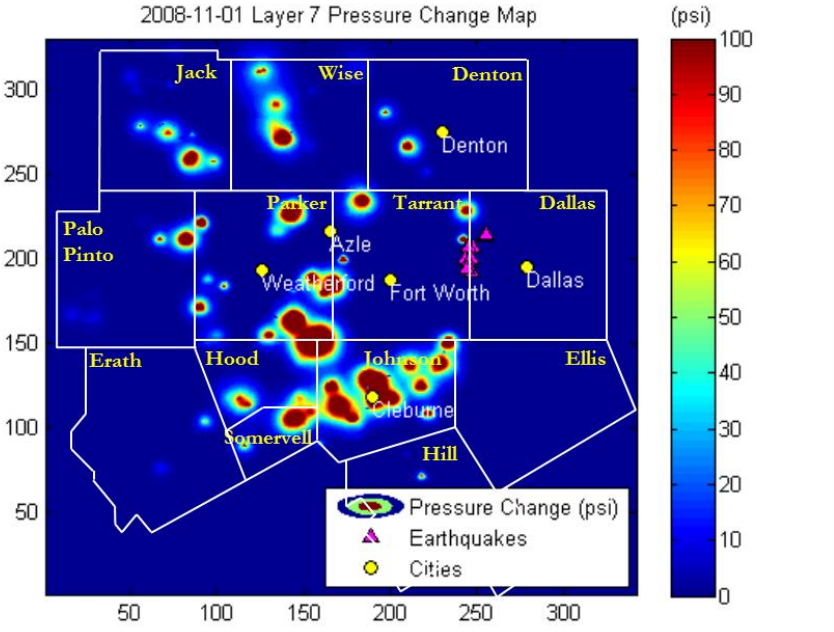

Figure B7: DFW Airport earthquakes Layer 7 pore pressure change plot.

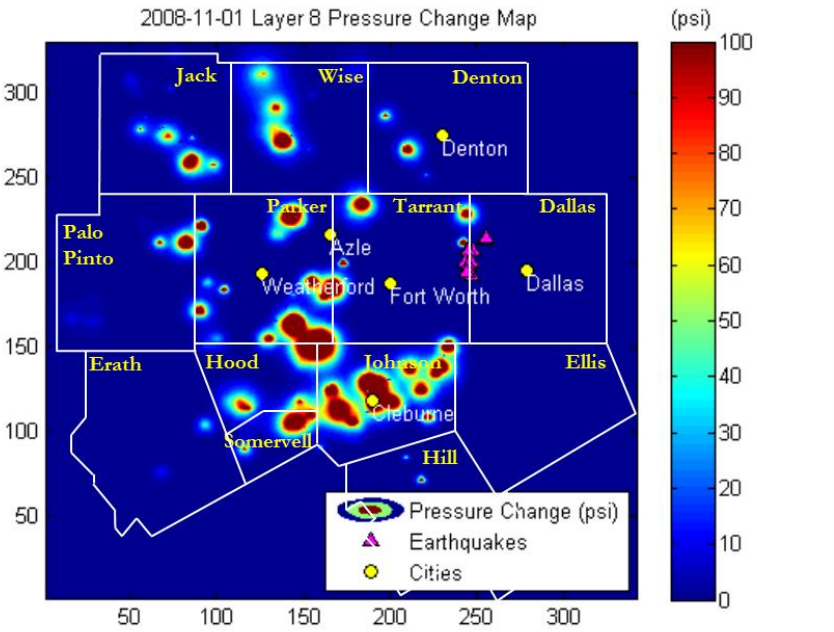

Figure B8: DFW Airport earthquakes Layer 8 pore pressure change plot.

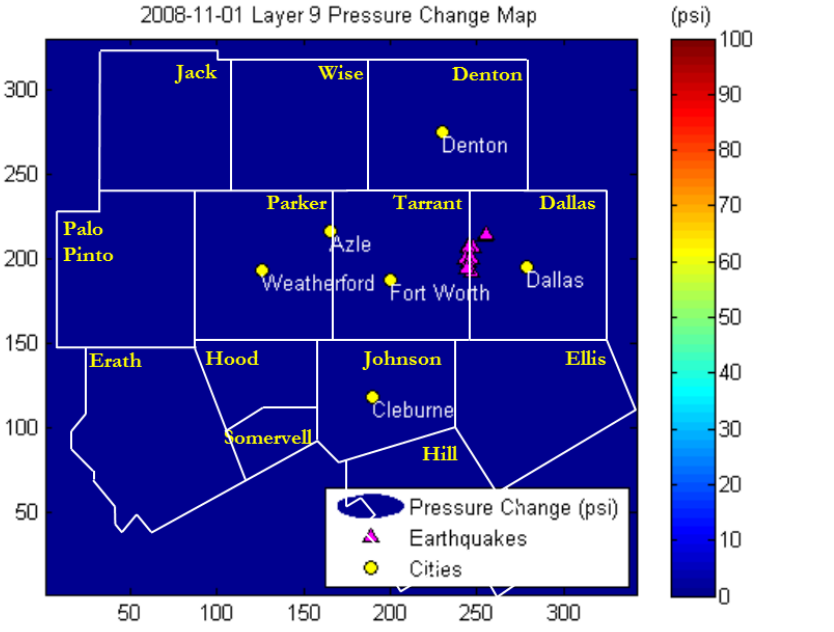

Figure B9: DFW Airport earthquakes Layer 9 pore pressure change plot.

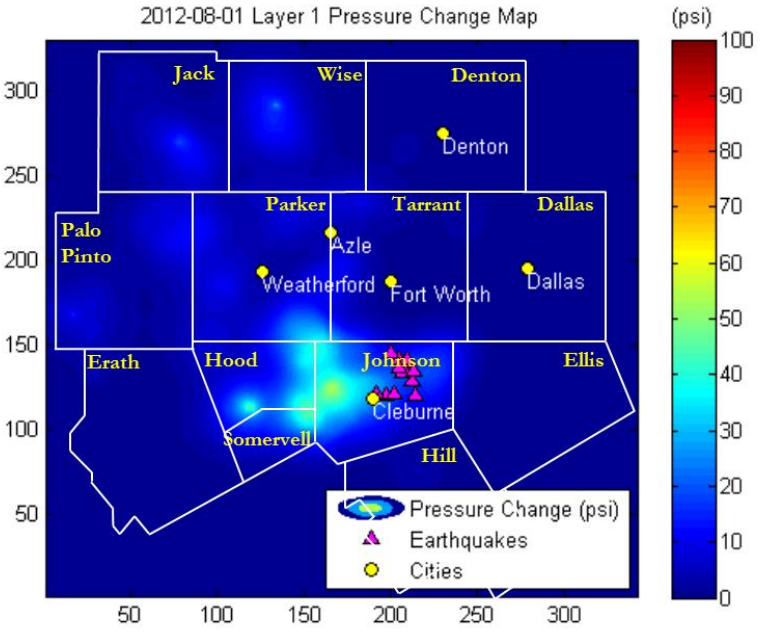

Figure B10: Cleburne earthquakes Layer 1 pore pressure change plot.

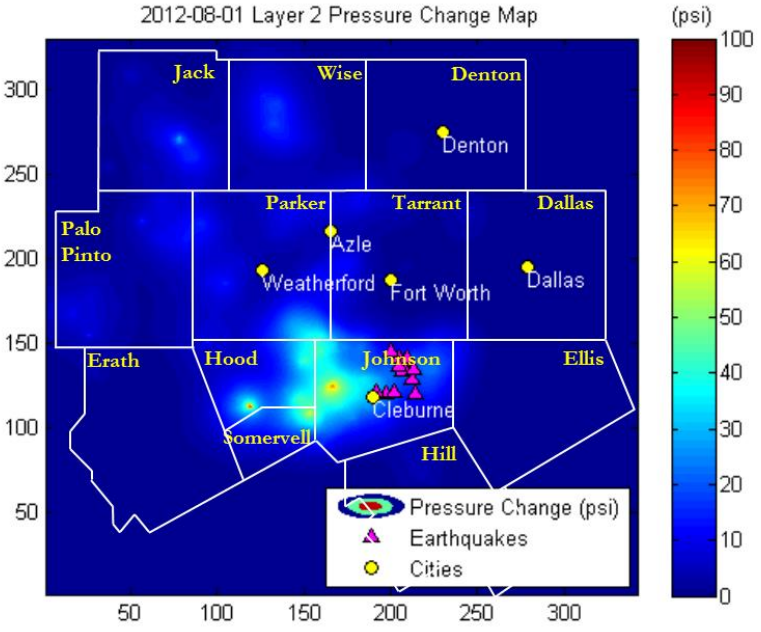

Figure B11: Cleburne earthquakes Layer 2 pore pressure change plot.

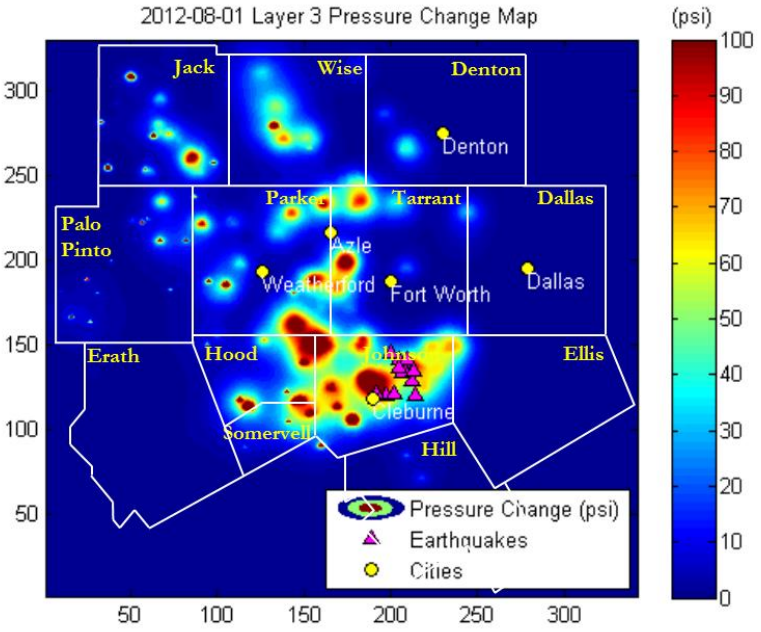

Figure B12: Cleburne earthquakes Layer 3 pore pressure change plot.

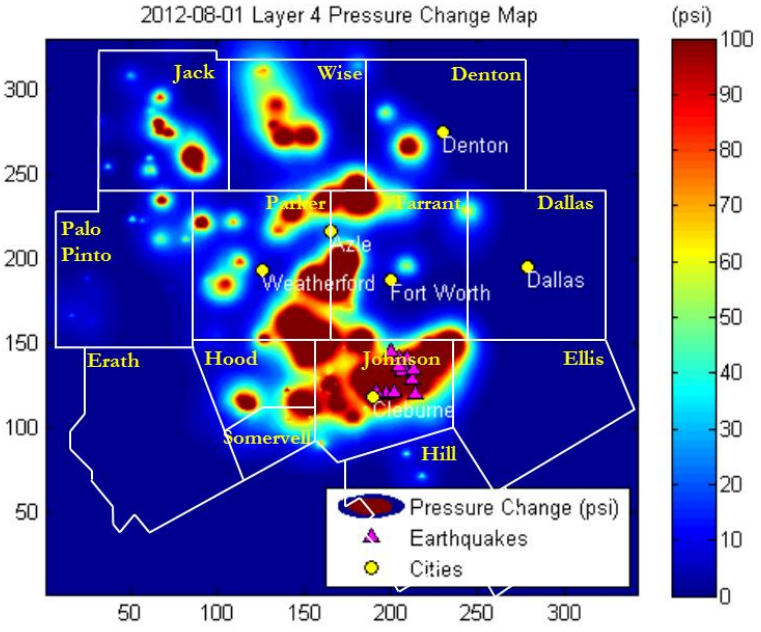

Figure B13: Cleburne earthquakes Layer 4 pore pressure change plot.

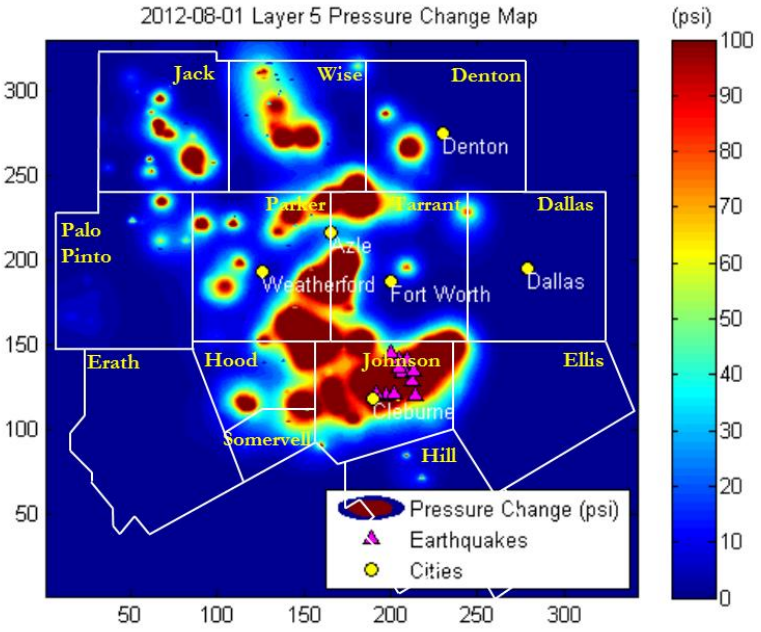

Figure B14: Cleburne earthquakes Layer 5 pore pressure change plot.

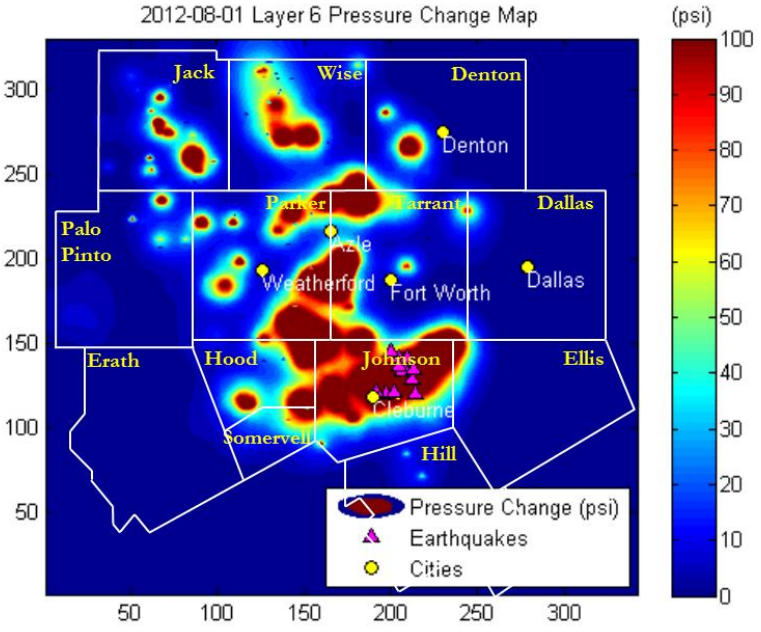

Figure B15: Cleburne earthquakes Layer 6 pore pressure change plot.

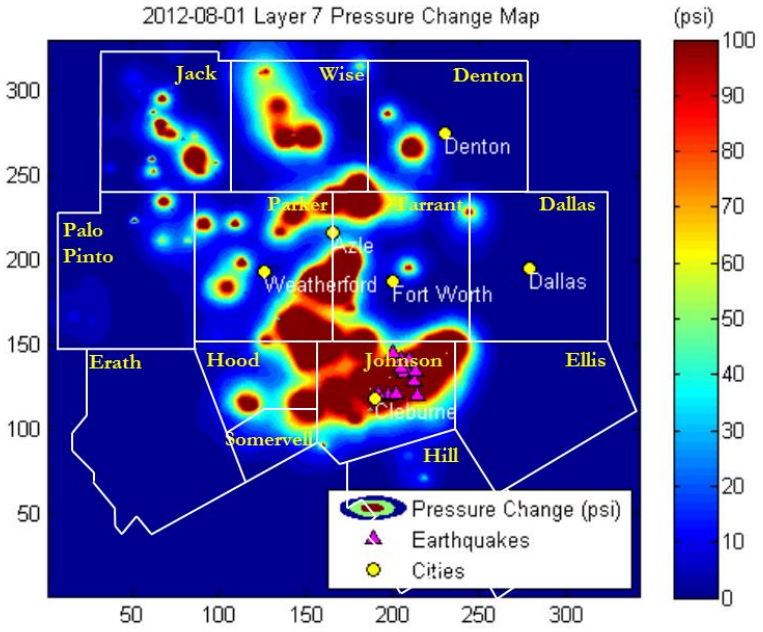

Figure B16: Cleburne earthquakes Layer 7 pore pressure change plot.

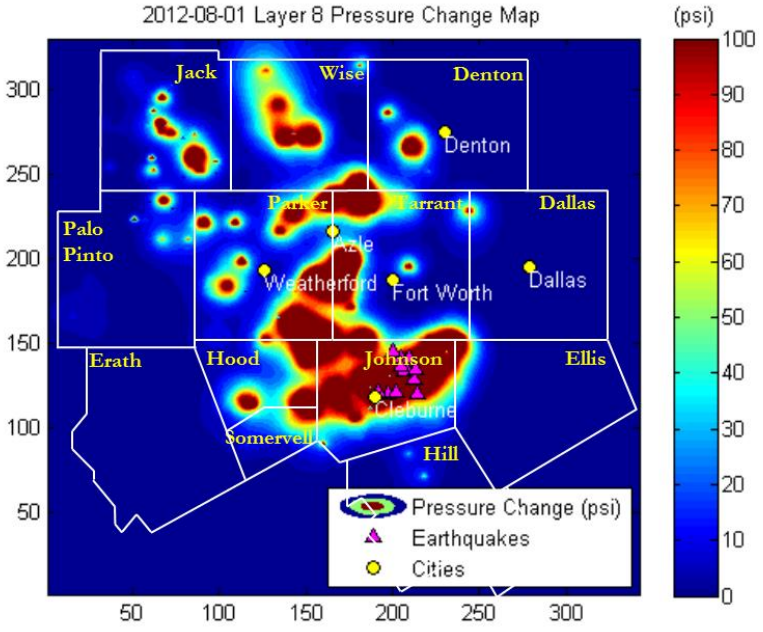

Figure B17: Cleburne earthquakes Layer 8 pore pressure change plot.

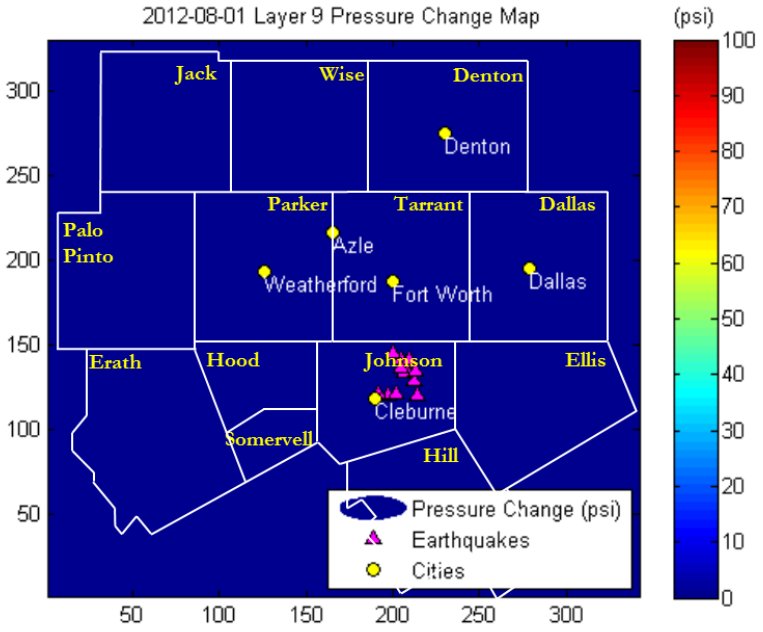

Figure B18: Cleburne earthquakes Layer 9 pore pressure change plot.

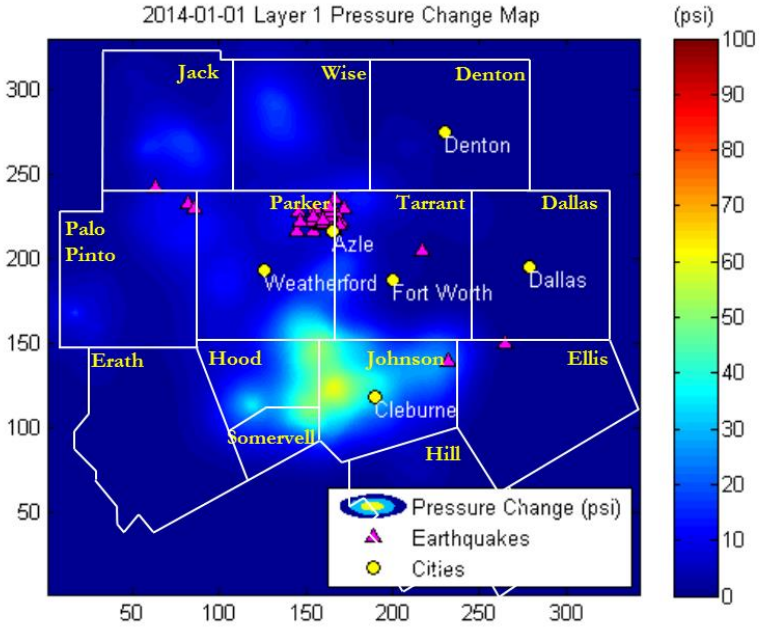

Figure B19: Azle earthquakes Layer 1 pore pressure change plot.

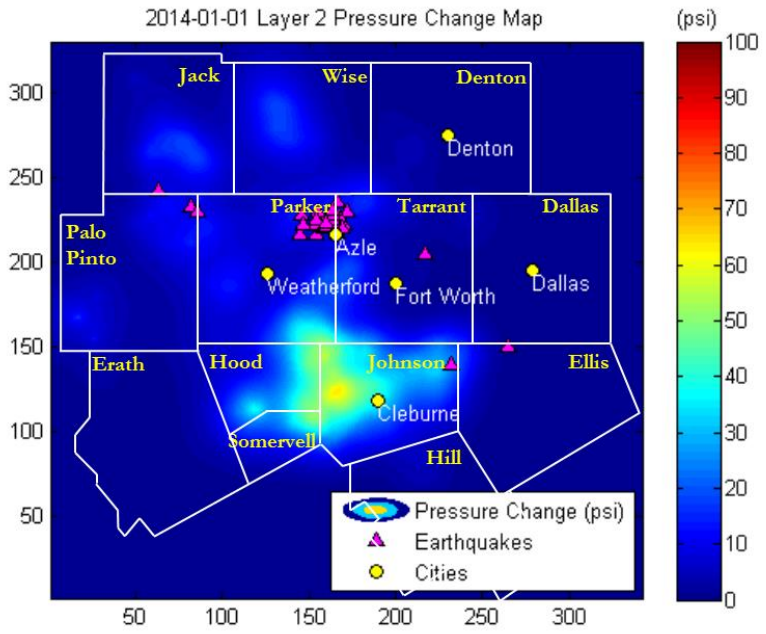

Figure B20: Azle earthquakes Layer 2 pore pressure change plot.

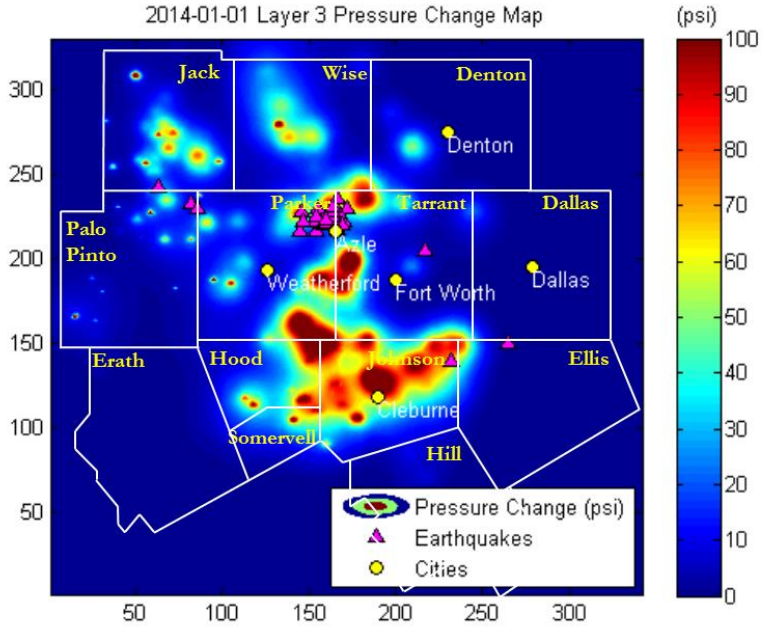

Figure B21: Azle earthquakes Layer 3 pore pressure change plot.

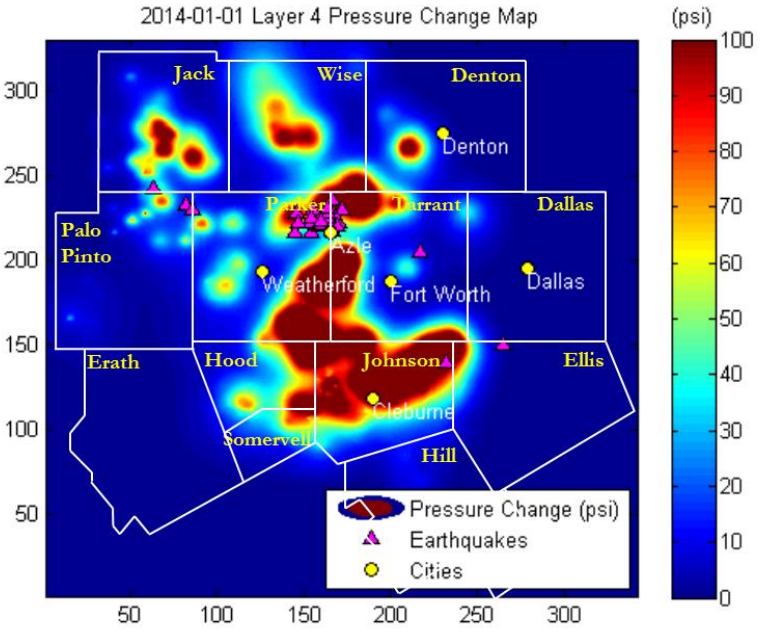

Figure B22: Azle earthquakes Layer 4 pore pressure change plot.

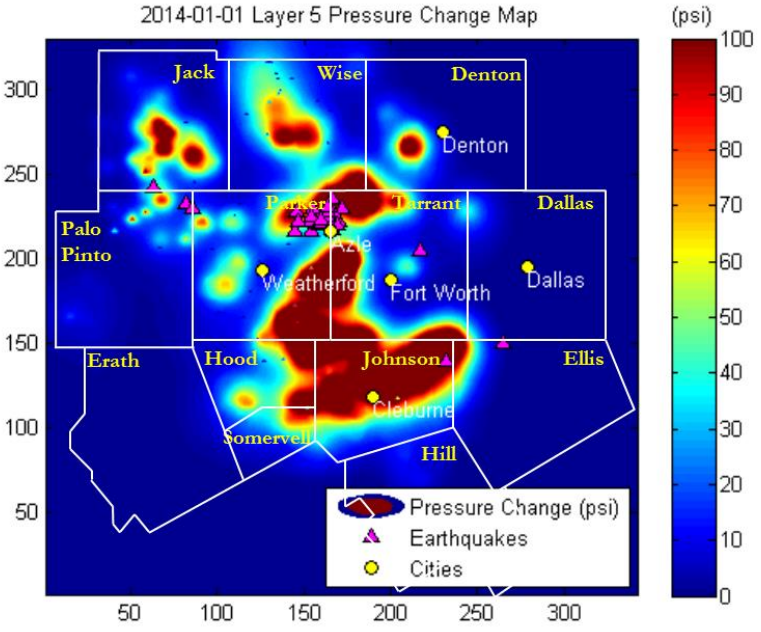

Figure B23: Azle earthquakes Layer 5 pore pressure change plot.

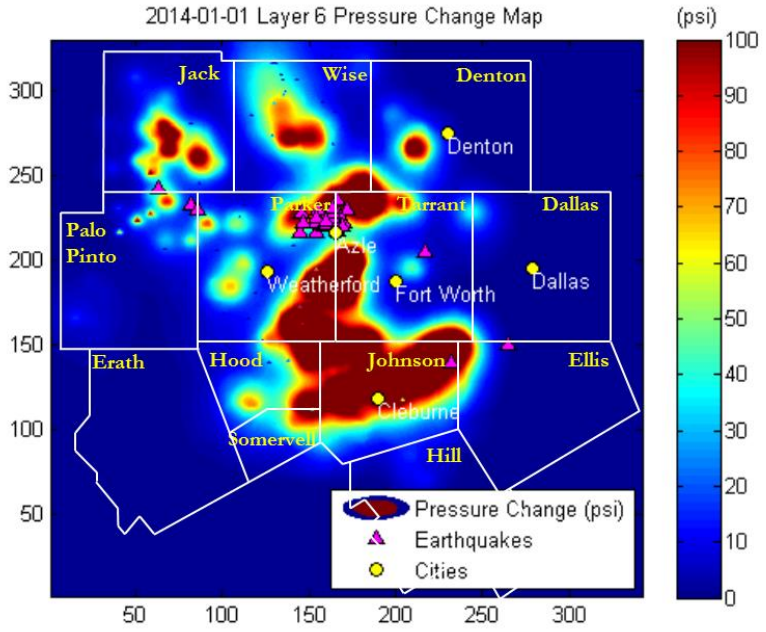

Figure B24: Azle earthquakes Layer 6 pore pressure change plot.

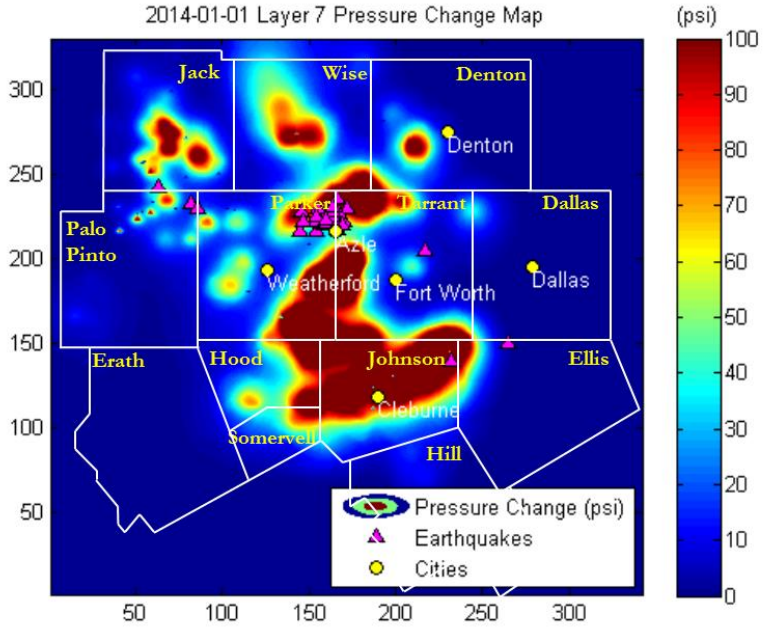

Figure B25: Azle earthquakes Layer 7 pore pressure change plot.

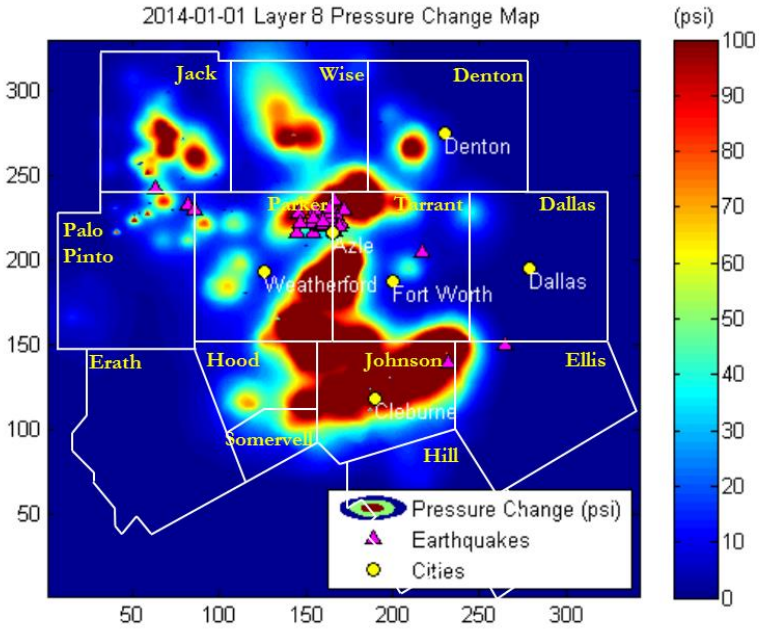

Figure B26: Azle earthquakes Layer 8 pore pressure change plot.

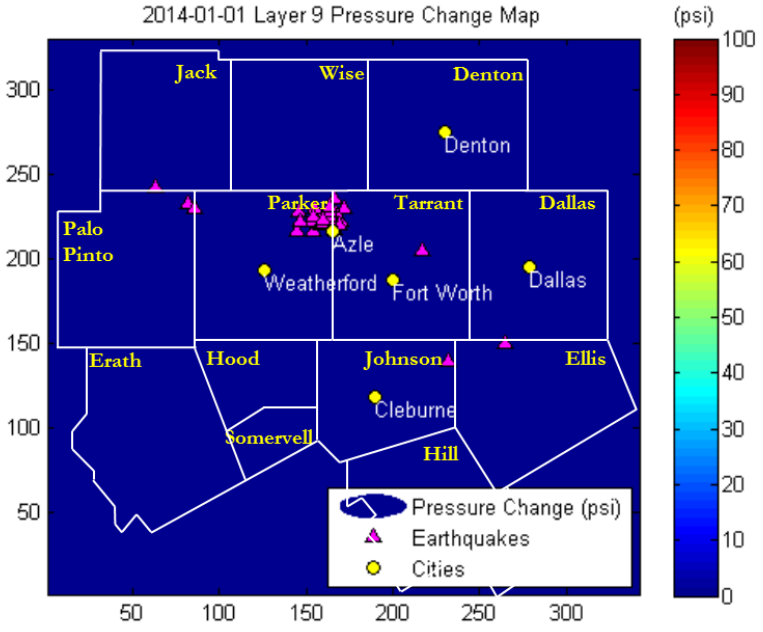

Figure B27: Azle earthquakes Layer 9 pore pressure change plot.

References

Baker, T., 2015. *Corporation Commission*, Oklahoma City, OK.

Ball, B.M.M. & Perry, W.J., 1990. Bend Arch-Fort Worth Basin Province. , (045), pp.1–11.

Baruch, E., Elebiju, O.O. & Perez, R., 2008. Geophysical Evidence of Basement Controlled Faulting in the Ellenburger Group and Viola Limestone , Fort Worth Basin , Texas. *SEG Houston*.

Baruch, E.T., Slatt, R.M. & Marfurt, K.J., 2012. Seismic Stratigraphic Analysis of the Barnett Shale and Ellenburger Unconformity Southwest of the Core Area of the Newark East Field, Fort Worth Basin, Texas. *AAPG Memoir 97: Shale Reservoirs—Giant Resources for the 21st Century*, pp.403–418.

Bowker, K.A., 2007. Barnett Shale Gas Production, Fort Worth Basin: Issues and Discussion. *AAPG Bulletin*, 91(4), pp.523–533. Available at: http://search.datapages.com/data/doi/10.1306/06190606018.

Clark, C. & Veil, J., 2009. Produced Water Volumes and Management Practices in the United States. *Argonne National Laboratory Report*, p.64pp.

Coppersmith, K.J. et al., 2012. *Project Plan : Central and Eastern United States Seismic Source Characterization for Nuclear Facilities*, Palo Alto, CA, Washington DC.

Davis, S.D. & Frohlich, C., 1993. Did (or Will) Fluid Injection Cause Earthquakes? - Criteria for a Rational Assessment. *Seismologial Research Letter*, 64, pp.207–224.

Davis, S.D. & Pennington, W., 1989. Induced Seismic Deformation in the Cogdell Oil Field of West Texas. *Bulletin of the Seismological Society of ...*, 79(5), pp.1477–1494. Available at: http://www.bssaonline.org/content/79/5/1477.short.

Elebiju, O.O., Keller, G.R. & Marfurt, K.J., 2010. Investigation of Links Between Precambrian Basement Structure and Paleozoic Strata in the Fort Worth Basin, Texas, U.S.A., Using High-Resolution Aeromagnetic (HRAM) Data and Seismic Attributes. *Geophysics*, 75(4), p.B157.

Elfenbein, C., Husby, Ø. & Ringrose, P., 2005. Geologically-based Estimation of kv/kh Ratios: An Example From the Garn Formation, Tyrihans Field, Mid-Norway. *Geological Society, London*, pp.537–543. Available at: http://www.geomodeling.com/PDF/PA_SBED_GeologicalBaseEstimationkvkhratios_2005.pdf.

Environmental Protection Agency, 2015. Underground Injection Control Classes of Injection Wells. *Environmental Protection Agency*, pp.1–2. Available at: water.epa.gov/type/groundwater/uic/wells.cfm [Accessed July 24, 2015].

Frohlich, C., 2012a. A Survey of Earthquakes and Injection Well Locations in the Barnett Shale, Texas. *The Leading Edge*, 31(12), pp.1446–1451. Available at: http://tle.geoscienceworld.org/content/31/12/1446\nhttp://tle.geoscienceworld.org.pallas2.tcl.sc.edu/content/31/12/1446.abstract\nhttp://tle.geoscienceworld.org.pallas2.tcl.sc.edu/content/31/12/1446.full.pdf.

Frohlich, C. et al., 2010. Dallas-Fort Worth Earthquakes Coincident with Activity Associated with Natural Gas Production. *The Leading Edge*, 29(3), p.270.

Frohlich, C. et al., 2011. The Dallas-Fort Worth Earthquake Sequence: October 2008 through May 2009. *Bulletin of the Seismological Society of America*, 101(1), pp.327–340.

Frohlich, C., 2012b. Two-year Survey Comparing Earthquake Activity and Injection-well Locations in the Barnett Shale, Texas. *Proceedings of the National Academy of Sciences*, 109(35), pp.13934–13938.

Fu, Q. et al., 2015. Log-derived Thickness and Porosity of the Barnett Shale, Fort Worth basin, Texas: Implications for Assessment of Gas Shale Resources. *AAPG Bulletin*, 99(1), pp.119–141. Available at: http://search.datapages.com/data/doi/10.1306/07171413018.

Galchen, R., 2015. Weather Underground. *The New Yorker*.

Grinberg, A., 2014. *In The Pits: Oil and Gas Wastewater Disposal into Open Unlined Pits and the Threat to California's Water and Air*,

Healy, J.H. et al., 1968. The Denver Earthquakes. *Science*, 161, pp.1301–1310.

Hentz, T.F., Ambrose, W. a. & Carr, D.L., 2012. Reservoir Systems of the Pennsylvanian Lower Atoka Group (Bend Conglomerate), Northern Fort Worth Basin, Texas: High-resolution Fades Distribution, Structural Controls on Sedimentation, and Production Trends. *AAPG Bulletin*, 96(7), pp.1301–1332.

Herkommer, M.A. & Denke, G.W., 1982. Stratigraphy and Hydrocarbons, Parker County, Texas. *Dallas Geological Society*, pp.97 – 127.

Holtz, M.H. & Kerans, C., 1992. Characterization and Categorization of West Texas Ellenburger Reservoirs. *Permain Basin Section SEPM Publications*, 92(33), pp.31–44.

Hornbach, M.J. et al., 2015. Causal Factors for Seismicity Near Azle, Texas. *Nature Communications*, 6(6728), pp.1–11. Available at: http://dx.doi.org/10.1038/ncomms7728.

Hsieh, P. a. & Bredehoeft, J.D., 1981. A Reservoir Analysis of The Denver Earthquakes: A case of Induced Seismicity. *Journal of Geophysical Research*, 86(B2), p.903.

Hubbert, M.K. & Rubey, W.W., 1959. Role of fluid Pressure in Mechanics of Overthrust Faulting: I. Mechanics of Fluid-filled Porous Solids and Its Application to

Overthrust Faulting. *Bulletin of the Geological Society of America*, 70(2), pp.115–166.

Justinic, A.H. et al., 2013. Analysis of the Cleburne, Texas, Earthquake Sequence from June 2009 to June 2010. *Bulletin of the Seismological Society of America*, 103(6), pp.3083–3093.

Kasap, E., 2001. Estimating kv/kh Ratio for Conductive and Nonconductive Shales and Mudstones. *Society of Petroleum Engineer*.

KCC, 2013. *Induced Seismicity and The O&G Industry*, Wichita, KS.

Kemp, J., 2014. Water is the Biggest Output of US Oil and Gas Wells. *Reuters*.

Keranen, K.M. et al., 2014. Sharp Increase in Central Oklahoma Seismicity Since 2008 Induced by Massive Wastewater Injection. *Science*, 345(6195), pp.448–451.

Kim, W.Y., 2013. Induced Seismicity Associated With Fluid Injection into a Deep Well in Youngstown, Ohio. *Journal of Geophysical Research: Solid Earth*, 118(7), pp.3506–3518.

Lin II, R.-G., Schleuss, J. & Lauder, T.S., 2015. Man-made Earthquakes Increasing in Central and Eastern US, Study Finds. *The Los Angeles Times*.

McDonnell, A., Loucks, R.G. & Dooley, T., 2007. Quantifying the Origin and Geometry of Circular Sag Structures in Northern Fort Worth Basin, Texas: Paleocave Collapse, Pull-apart Fault Systems, or Hydrothermal Alteration? *AAPG Bulletin*, 91(9), pp.1295–1318.

McGarr, B.A. et al., 2015. Coping With Earthquakes Induced by Fluid Injection. *Science*, 347(6224), pp.1830–1831.

Miller, S.A., Nur, A. & Olgaard, D.L., 1996. Earthquakes as a Coupled Shear Stress - High Pore Pressure Dynamical System. *Geophysical Research Letters*, 23(2), pp.197–200.

Perez-Pena, R., 2015. US Maps Pinpoint Earthquakes Linked to Quest for Oil and Gas. *The New York Times*.

Pollastro, R.M. et al., 2003. Assessing Undiscovered Resources of the Barnett-Paleozoic Total Petroleum System , Bend Arch – Fort Worth Basin Province , Texas. *Assessment*, 10034, p.#10034.

Pollastro, R.M. et al., 2007. Geologic framework of the Mississippian Barnett Shale, Barnett-Paleozoic total petroleum system, Bend arch–Fort Worth Basin, Texas. *AAPG Bulletin*, 91(4), pp.405–436. Available at: http://search.datapages.com/data/doi/10.1306/10300606008.

Raleigh, C.B., Healy, J.H. & Bredehoeft, J.D., 1976. An Experiment in Earthquake Control at Rangely, Colorado. *Science (New York, N.Y.)*, 191(4233), pp.1230–1237.

Rathje, E.M. & Olson, J.E., 2007. Technical Issues Related to Hydraulic Fracturing and Fluid Extraction / Injection near the Comanche Peak Nuclear Facility in Texas WLA Project Number 1908 Project Number : 1908 - Comanche Peak MHI COLA Title : Technical Issues Related to Hydraulic Fractur. , pp.10–18.

Reasenberg, P. a & Simpson, R.W., 1992. Response of regional seismicity to the static stress change produced by the loma prieta earthquake. *Science (New York, N.Y.)*, 255(5052), pp.1687–1690.

Shapiro, S. a. et al., 2006. Fluid Induced Seismicity Guided by a Continental Fault: Injection Experiment of 2004/2005 at the German Deep Drilling Site (KTB). *Geophysical Research Letters*, 33(1), pp.2–5.

Stein, R.S., 1999. The Role of Stress Transfer in Earthquake Occurrence. *Nature*, 402(6762), pp.605–609. Available at: http://dx.doi.org/10.1038/45144.

Texas RRC, 2014. Railroad Commission Adopts Disposal Well Rule Amendments Today. Available at: http://www.rrc.state.tx.us/all-news/102814b/ [Accessed November 15, 2015].

The Mathworks Inc., 2013. MATLAB.

Townend, J. & Zoback, M.D., 2000. How Faulting Keeps The Crust Strong. *Geology*, 28(5), pp.399–402.

Vermylen, J.P., 2011. Geomechanical studies of the Barnett shale, Texas, USA. , 125(May), p.143pp. Available at: http://books.google.com/books?hl=en&lr=&id=gcTa8B0OTvMC&oi=fnd&pg=PR12&dq=GEOMECHANICAL+STUDIES+OF+THE+BARNETT+SHALE+,+TEXAS+,+USA&ots=kwr8jKWbrV&sig=JERNg8wcMQHlj_4i4SjseSrSmO4.

Walsh, F.R. & Zoback, M.D., 2015. Oklahoma's Recent Earthqaukes and Saltwater Disposal. *Science Advances*, (June), pp.1–9.

Waters, G. a, Lewis, R.E. & Bentley, D.C., 2011. The Effect of Mechanical Properties Anisotropy in the Generation of Hydraulic Fractures in Organic Shales. *SPE Annual Technical Conference and Exhibition*, (Fig 1), pp.1–25.

Weingarten, M. et al., 2015. High-rate injection is associated with the increase in U.S. mid-continent seismicity. *Science*, 348(6241), pp.1336–1340.

Zoback, M.D., 2012. Managing the seismic risk posed by wastewater disposal. *Earth*, (April), pp.38–43. Available at: http://wwvv.armarocks.org/documents/newsletters/2012_02_02_spring.pdf.

Zoback, M.D., 2007. *Reservoir Geomehanics* 1st ed., New York, NY: Cambridge University Press.

Zoback, M.D. & Healy, J.H., 1984. Friction, Faulting, and In-Situ Stress. , 2(6), pp.689–698.

Zoback, M.D. & Townend, J., 2001. Implications of Hydrostatic Pore Pressures and High Crustal Strength for The Deformation of Intraplate Lithosphere. *Tectonophysics*, 336(1-4), pp.19–30.